

---

[All ETDs from UAB](#)

[UAB Theses & Dissertations](#)

---

2005

## Characterization of a rod photoreceptor cGMP -gated cation channel beta-subunit knockout mouse.

Youwen Zhang  
*University of Alabama at Birmingham*

Follow this and additional works at: <https://digitalcommons.library.uab.edu/etd-collection>

---

### Recommended Citation

Zhang, Youwen, "Characterization of a rod photoreceptor cGMP -gated cation channel beta-subunit knockout mouse." (2005). *All ETDs from UAB*. 5484.  
<https://digitalcommons.library.uab.edu/etd-collection/5484>

This content has been accepted for inclusion by an authorized administrator of the UAB Digital Commons, and is provided as a free open access item. All inquiries regarding this item or the UAB Digital Commons should be directed to the [UAB Libraries Office of Scholarly Communication](#).

# NOTE TO USERS

This reproduction is the best copy available.

**UMI**<sup>®</sup>



CHARACTERIZATION OF A ROD PHOTORECEPTOR cGMP-GATED CATION  
CHANNEL BETA-SUBUNIT KNOCKOUT MOUSE

by

YOUWEN ZHANG

A DISSERTATION

Submitted to the graduate faculty of The University of Alabama at Birmingham,  
in partial fulfillment of the requirements for the degree of  
Doctor of Philosophy

BIRMINGHAM, ALABAMA

2005

UMI Number: 3201191

### INFORMATION TO USERS

The quality of this reproduction is dependent upon the quality of the copy submitted. Broken or indistinct print, colored or poor quality illustrations and photographs, print bleed-through, substandard margins, and improper alignment can adversely affect reproduction.

In the unlikely event that the author did not send a complete manuscript and there are missing pages, these will be noted. Also, if unauthorized copyright material had to be removed, a note will indicate the deletion.

**UMI**<sup>®</sup>

---

UMI Microform 3201191

Copyright 2006 by ProQuest Information and Learning Company.

All rights reserved. This microform edition is protected against unauthorized copying under Title 17, United States Code.

ProQuest Information and Learning Company  
300 North Zeeb Road  
P.O. Box 1346  
Ann Arbor, MI 48106-1346

ABSTRACT OF DISSERTATION  
GRADUATE SCHOOL, UNIVERSITY OF ALABAMA AT BIRMINGHAM

Degree Ph.D. Program Vision Science

Name of Candidate Youwen Zhang

Committee Chair Shu-Zhen Wang

Title Characterization of a cGMP-gated Cation Channel Beta-Subunit Knockout Mouse

Cation flow into the rod photoreceptor outer segment is regulated by a cGMP-gated channel (CNGC1) consisting of two subunit types,  $\alpha$  and  $\beta$ . The CNGC1 has a stoichiometry of  $3\alpha:1\beta$ . The cyclic nucleotide-gated cation channel B1 subunit (*Cngb1*) locus encodes the channel  $\beta$ -subunit located at the plasma membrane and two soluble glutamic- acid-rich proteins (GARP), GARP-1 and GARP-2. A *Cngb1* knockout mouse has been created by targeted deletion of an N-terminal region common to all three gene products. Absence of the three proteins also led to a significant reduction of the channel  $\alpha$ -subunit without affecting the levels of several other rod outer segment (ROS) disk and plasma membrane proteins, indicating that the channel  $\beta$ -subunit or GARPs are required to target the  $\alpha$ -subunit to its appropriate location. ROS in the knockout mouse are shorter at maturation, and some disks in each rod examined were misaligned and abnormally elongated. However, the rod electroretinogram (ERG) was readily measurable in 30-day-old knockout mice (KO), and some mice showed b-wave response amplitudes approaching that of wild type (WT). In dark-adapted condition, the maximal averaged b-wave amplitude of the KO is 1/2 that of WT; however, the KO a-wave amplitude is only 1/8 that of WT; the threshold intensity is 2.8 log units increased in KO, consistent with the degeneration of rod photoreceptors. Both b-wave amplitudes under light- and dark-adapted conditions are decreased over the first 4 months postnatal, but cone response is relatively

increased, suggesting a slower degeneration of cone circuitry. The *Cngbl* *-/-* mice showed a 27-fold reduction in rod sensitivity ( $I_{1/2}$ ) to light in 1-month-olds, which was maintained at 2 months, indicating impaired function beginning at 1-month. The recovery of *Cngbl* *-/-* mice is not delayed and may actually be faster than wild type. In contrast to results from heterologous expression studies of the channel  $\alpha$ -subunit, the  $\beta$ -subunit is required for normal channel activity in ROS, and the  $\beta$ -subunit and/or GARPs are also necessary to maintain the structural integrity of the rod photoreceptor and ROS disks. Remarkably, phototransduction, albeit attenuated, occurred only when trace levels of homomeric  $\alpha$ -subunit channels were present in ROS.

## DEDICATION

This dissertation is dedicated to my wife, Lan Ge, and to my parents, Fu Zhang and Suzhen Zhu, for their love, support, and patience during my Ph.D. studies.

The dedication also goes to my Birmingham-born sons, Lele and Huanhuan; they are the inspiration for me to complete my studies.

## ACKNOWLEDGMENTS

First and foremost, I wish to express my most sincere gratitude to my mentor, Dr. Steven J. Pittler, for giving me such an important project, encouraging me to learn ERG, providing excellent guidance in research, having patience with my language barrier, and securing financial support during my tenure in his laboratory.

I am also very grateful to Dr. Timothy W. Kraft for teaching me ERG, opening his lab resources to me, helping me to set up the ERG research plan, and for offering excellent instruction and invaluable advice during my academic career.

I also thank my other committee members, Drs. Shu-Zhen Wang, Kent T. Keyser, and Franklin R. Amthor, for their time, advice, and encouragement. I also thank Dr. Stuart Mangle, a former committee member, for his help and guidance prior to his departure from UAB.

Many thanks to Dr. Michael Loop for spending several hours in calculating fiber optic illuminance values.

I also appreciate Dr. Kent T. Keyser, Director of the Vision Science Graduate Program, for his responsible attitude to my academic career when I was hesitating regarding my choice of a primary lab.

I extend my thanks to my labmates in Dr. Pittler's lab, Marcel Ionita, Shanta Sarfare, Suxia Yao, Telisha Swain, and Jeff Messinger, for their technical help, advice, and discussion. Marcel and Shanta also read and helped correct some of the thesis writing. In Dr. Kraft's lab, I thank Diana Niculescu for teaching me basic ERG analysis techniques.

I thank Glen Rubin for grammar consultation and Yuquen Wen for taking pictures of electrodes.

I also thank the people who taught me in my rotations in Dr. Shu-Zhen Wang's lab, Dr. Christine Curcio's lab and Dr. Richard Mayne's lab. I also thank the program administrators, Kay Johnston, Nan Travis, and Ramona Hart, for their assistance in my studies.

I extend my thanks to the faculty and staff in the Department of Vision Sciences for teaching me and providing assistance in many ways.

I also thank my friends Zhuo Zhang and Gong Feng, for providing me protocols of Northern and Western and for demonstrating each technique in their labs.

Finally, thanks go to all of my friends who have been watching my progress, wishing me well, and providing help to my family. Special thanks go to a couple from Hunter Street Baptist Church, Chimei Lee and C.N. Wei, who really helped my family a lot and saved me time for study.

## TABLE OF CONTENTS

	<i>Page</i>
ABSTRACT.....	ii
DEDICATION.....	iv
ACKNOWLEDGMENTS.....	v
LIST OF TABLES.....	xi
LIST OF FIGURES.....	xii
LIST OF ABBREVIATIONS.....	xiv
INTRODUCTION.....	1
Photoransduction.....	1
General Mechanism of Phototransduction.....	1
Phototransduction Initiator—Rhodopsin.....	2
Photoisomerized Rhodopsin Deactivation.....	4
Recoverin.....	5
Arrestin Translocation.....	6
Protein Phosphatase 2A (PP2A).....	6
Photoexcitation Steps in Transducin and PDE6.....	7
Phosducin Modifying G Protein Function.....	8
Complex of T $\alpha$ -GTP-PDE6 $\gamma$ and RGS9-1-G $\beta$ 5L-R9AP.....	9
PDE6.....	10
Guanylate Cyclase (GC) and GC Activating Proteins (GCAPs).....	11
A Brief Review of Mammalian Retina.....	13
General Information.....	13
Visual Pigment Renewal in RPE.....	14
CNGB1.....	16
Cyclic Nucleotide-Gated (CNG) Channel.....	16
Rod CNG Channel Has Two Homologous Subunits.....	17
B1 and A1 Isoforms Distribution.....	18
CNGB1 Gene Location, Structure, and Expression.....	19
Stoichiometry of CNGB1.....	21
Transmembrane Topography.....	22
GARPs.....	23

## TABLE OF CONTENTS (Continued)

	<i>Page</i>
Relation to NCKX1.....	25
Electrical Physiology Properties and B1's Modulation Function.....	26
Interaction Between A1 and B1 Subunit .....	30
Rim Proteins and Plasma Membrane Proteins.....	32
Channel Subunit-Related Mutations and Knockout Models .....	34
Effects of Genetic Modifiers on Human Disease and Mouse Gene Knockout Model.....	35
Technologies to Produce Genetically Altered Animal .....	36
ERG History and Major Components Origin .....	37
History of ERG .....	37
The a-wave Originates in Photoreceptors .....	38
The b-wave's Origin .....	38
The c-wave Originates in Retinal Pigment Epithelium (RPE) Cells .....	40
Other Minor ERG Components' Origin .....	41
Dark Current and Channels on Photoreceptors.....	42
Isolating Rod- and Cone-Mediated Responses from Mouse .....	43
Sensitivity of Rod Photoreceptor .....	46
Photoreceptor Degeneration, Equivalent-Light Hypothesis, and Recovery Kinetics .....	48
Hypothesis.....	50
 METHODOLOGY .....	 52
Generation of <i>Cngb1</i> Knockout Mouse .....	52
Genomic PCR for Genotyping.....	54
RT-PCR Analysis of Transcription Level of <i>Cngb1</i> , <i>Neo</i> , and Other Genes .....	54
Sequencing of RT-PCR Products.....	57
Northern Blot of <i>Cngb1</i> Transcripts by Probing N-terminal GARP Region.....	58
ROS Isolation and Western Analysis of ROS Proteins .....	59
Immunocytochemistry Analysis of ROS Proteins .....	59
Light and Electron Microscopy .....	60
Basic ERG Response Recording.....	60
Isolation Cone Photoreceptor Response Under Dark-Adapted Conditions .....	61
Sensitivity of ERG Rod b-wave.....	62
Recovery of ERG b-wave by Multiple Flashes .....	63
 RESULTS .....	 65
Genotyping Mice by Genomic DNA Multiple PCR.....	65
General Phenotype of Our <i>Cngb1</i> Knockout Mouse .....	66
Structure of the Complete Murine <i>Cngb1</i> Gene .....	66
Incomplete <i>Cngb1</i> Gene Transcription in mRNA Level .....	68

TABLE OF CONTENTS (Continued)

	<i>Page</i>
<i>Cngb1</i> Gene Products Are not Detectable in the KO Mouse Retina .....	70
The cGMP-gated Cation Channel $\alpha$ -Subunit Is Diminished or Absent in the KO Mouse ROS .....	71
Channel Subunits Are not Mislocalized in the Retina .....	71
Morphology of the KO Mouse Retina .....	72
Dark-Adapted ERG a- and b-wave Show Significant Differences Between WT and KO Mice in 1-Month-Old Results .....	72
Light-Adapted ERG b-wave Amplitudes Do not Show Significant Differences Between WT and KO Mice in 1-Month-Old Results.....	74
ERG Threshold Intensity of 1-Month-Old KO Mice Is 2.8 Log Units Higher Than That of WT Mice .....	74
Rod b-wave Sensitivity ( $I_{1/2}$ ) of KO Mice Is 1.41 Log Units Higher Than That of WT Mice at 1-Month-Old .....	75
The b-wave Recovery of 1-Month-Old KO Mice Under Multiple Flashes Is Faster Than That of WT Mice.....	76
Dark-Adapted b-wave Amplitude Declines Faster Than Light-Adapted b-wave Amplitude for KO Mice During a 4-Month Period .....	77
The b-wave Implicit Time of KO Mice Under Dark-Adapted Conditions Is Delayed at all Ages Tested.....	80
Over 1- to 4-Month-Old a-wave Amplitudes Under Light-Adapted Conditions Continuously Decrease.....	81
Rod b-wave Sensitivities Did not Change in 2-Month-Old Mice .....	81
Multiple Flash Responses Recorded Over Different Ages .....	82
 CONCLUSION AND DISCUSSION .....	 109
 <i>Cngb1</i> Gene Knockout Does not Affect Neighboring Genes .....	 109
The Effect of N-terminal Gene Knockout on <i>Cngb1b</i> .....	110
Complete <i>Cngb1</i> cDNA Sequence and Translated Protein Sequence Provide Basis for Further Study of <i>Cngb1</i> -Related Project .....	111
Structure of Murine <i>Cngb1</i> Transcripts Exemplifies the Diversity of Transcription.....	111
Functional PGK Promoter for Part of <i>Cngb1</i> Gene Expression Can Be Avoided in Future Knockout Model Design.....	112
Molecular Biology and Proteomics Confirm That Our Mouse Model Is a True $\beta$ -Subunit and GARPs Knockout Model .....	112
The Channel $\beta$ -Subunit Is Required for $\alpha$ -Subunit Transport to ROS.....	113
The $\beta$ -Subunit Does not Play a Critical Role in ROS Morphogenesis but Has a Structure Role .....	114
Electrophysiological Change in 1-Month-Old KO Mice.....	116
1- to 4-Month-Old ERG Changes and Retinal Degeneration .....	119
Recovery Kinetics and Retinal Degeneration .....	121

TABLE OF CONTENTS (Continued)

	<i>Page</i>
Comparison of the 3' and Our 5' <i>Cngb1</i> Knockout Mouse Models.....	122
Retinal Degeneration Model .....	125
LIST OF REFERENCES.....	126
APPENDIX: INSTITUTIONAL ANIMAL CARE AND USE COMMITTEE APPROVAL FORM .....	157

## LIST OF TABLES

<i>Table</i>	<i>Page</i>
1 PCR and Sequencing Primers Designed and Used .....	55
2 Body Weight of WT and KO Mice.....	67
3 1-Month-Old Mice ERG Under Dark-Adapted and Light-Adapted Conditions .....	73
4 ERG Thresholds of Three Genotypes .....	75
5 1-Month-Old Rod b-wave Sensitivities ( $I_{1/2}$ ) of Three Genotypes .....	76
6 1-Month-Old b-wave Recovery Under Multiple Flashes .....	77
7 1- to 4-Month-Old b-wave Amplitudes Under Dark-Adapted Conditions.....	78
8 1- to 4-Month-Old b-wave Amplitudes Under Light-Adapted Conditions .....	78
9 1- to 4-Month-Old b-wave Amplitude Ratios of Light- Over Dark-Adapted Conditions .....	79
10 1- to 4-Month-Old b-wave Implicit Times Under Dark-Adapted Conditions.....	80
11 1- to 4-Month-Old a-wave Amplitudes Under Light-Adapted Conditions .....	81
12 1- and 2-Month-Old Rod b-wave Sensitivities .....	82
13 The b-wave Recoveries During a 4-Month Period .....	83

## LIST OF FIGURES

<i>Figure</i>	<i>Page</i>
1 Schematic of genome deletion strategy .....	53
2 PCR amplification of mouse genomic DNA .....	85
3 <i>Cngb1</i> gene in murine chromosome 8 .....	86
4 Complete murine <i>Cngb1</i> cDNA and protein sequences .....	87
5 Map of <i>Cngb1</i> gene exons and alternative transcripts .....	88
6 RT-PCR analysis of <i>Cngb1</i> and other photoreceptor loci .....	89
7 A Neo/ <i>Cngb1</i> hybrid mRNA is produced in <i>Cngb1</i> -KO mice .....	90
8 Northern blot analysis of <i>Cngb1</i> -KO and wild-type littermate total RNA .....	91
9 Expression of photoreceptor proteins in the <i>Cngb1</i> knockout mouse .....	92
10 Immunolocalization of ROS proteins .....	93
11 Morphology of <i>Cngb1</i> -KO mouse retina .....	94
12 The b-wave amplitude and implicit time in 1-month-old mice .....	95
13 The a-wave amplitude and implicit time in 1-month-old mice .....	96
14 1-month-old dark-adapted ERG .....	97
15 Intensity-response curve fitting in 1-month-old mice .....	98
16 Dark-adapted ERG recovery under multiple flashes .....	99
17 1-month-old b-wave recovery by multiple flashes .....	100
18 Normalized dark-adapted 1- to 4-month-old b-wave amplitudes .....	101
19 Normalized light-adapted 1-4 month-old b-wave amplitudes .....	102

LIST OF FIGURES (Continued)

<i>Figure</i>		<i>Page</i>
20	Light-/dark-adapted b-wave amplitude over ageings .....	103
21	1- to 4-month-old b-wave implicit times under dark-adapted conditions.....	104
22	1- to 4-month-old a-wave amplitudes under dark-adapted conditions .....	105
23	1- and 2-month-old rod b-wave sensitivities (Log $I_{1/2}$ ).....	106
24	All 4-month b-wave recoveries by multiple flashes .....	107
25	All 4-month HT and KO b-wave recoveries by multiple flashes .....	108
26	A structural role for GARP-2 and the $\beta$ -subunit in ROS .....	124

## LIST OF ABBREVIATIONS

A1	CNGA1, rod CNG channel $\alpha$ subunit
A3	CNGA3, cone CNG channel $\alpha$ subunit
ABCA4, ABCR	ATP binding cassette transporter
ATP	adenosine triphosphate
B1	CNGB1, rod CNG channel $\beta$ subunit
B3	CNGB3, cone CNG channel $\beta$ subunit
bp	base pair
CaM	calmodulin
cAMP	cyclic adenosine monophosphate
cDNA	complementary DNA
cGMP	cyclic guanosine monophosphate
CNG	cyclic nucleotide-gated
CNGA1	cyclic nucleotide-gated cation channel $\alpha$ subunit
CNGB1	cyclic nucleotide-gated cation channel $\beta$ subunit
CNGB1a	rod cyclic nucleotide-gated cation channel $\beta$ subunit
CNGB1b	olfactory cyclic nucleotide-gated cation channel $\beta$ subunit
CNGC1	rod cyclic nucleotide-gated cation channel
DNA	deoxyribonucleic acid
ERG	electroretinogram
GARP	glutamic acid rich protein

## LIST OF ABBREVIATIONS (Continued)

G $\beta$ 5L	long splice variant of type 5 G-protein $\beta$ -subunit
GC	guanylate cyclase
GCAP	guanylate cyclase activating protein
GTP	guanosine triphosphate
HT	heterozygote
I <sub>1/2</sub>	half-maximal stimulus intensity
ISI	interstimulus interval
kDa	kilo Dalton
kifc3	kinesin family member c3
KO	knockout
Meta	photoisomerized states of rhodopsin
mRNA	messenger ribonucleic acid
NCBI	national center for biotechnology information
NCKX	sodium, calcium, potassium exchanger
ND	neutral density
Neo	neomycin phosphotransferase, neomycin resistance
PDE	phosphodiesterase
PGK	phosphoglycerate kinase
PP2A	Protein Phosphatase 2A
R*	activated rhodopsin
R9AP	RGS9-1-anchor protein
RGS	regulators of G-protein signaling, 9, splicing variant 1

LIST OF ABBREVIATIONS (Continued)

RK	Rhodopsin Kinase
RNA	ribonucleic acid
ROS	rod outer segment
RIS	rod inner segment
PCR	polymerase chain reaction
RP	retinitis pigmentosa
RPE	retinal pigment epithelium
RT	reverse transcription
SEM	standard error of mean
STDEV	standard deviation
T	Transducin
T <sub>α</sub>	transductin α
TEPP	testis/prostate/placenta-expressed protein
WT	wild-type

## INTRODUCTION

### Phototransduction

#### *General Mechanism of Phototransduction*

Light triggers a phototransduction cascade in the retina initiated by rhodopsin. The retinal rod photoreceptor is extremely sensitive to light, with the ability to detect even a single photon (Baylor, Lamb, & Yau, 1979). Rhodopsin is a member of the G protein coupled receptor family (GPCR) in a complex with the covalently attached chromophore *11-cis*-retinal. Upon absorbing light, rhodopsin is photoisomerized to a photo-excited form R\* [metarhodopsin (Meta) II] generating *all-trans*-retinal. R\* activates a heterotrimeric membrane-binding G-protein transducin (T) by catalyzing the exchange of guanosine 5'-triphosphate (GTP) for bound guanosine 5'-diphosphate (GDP) on the transducin  $\alpha$ -subunit ( $T_\alpha$ ). Activated  $T_\alpha$ -GTP disassociates from transducin  $\beta\gamma$  subunits ( $T_{\beta\gamma}$ ) and binds to a photoreceptor-specific phosphodiesterase (PDE6) consisting of two catalytic subunits ( $\alpha$  and  $\beta$ ) and two identical inhibitory  $\gamma$  subunits. PDE6 is activated by removal of the  $\gamma$  inhibition by  $T_\alpha$  and rapidly hydrolyzes free cyclic guanosine monophosphate (cGMP) in the cytoplasm. A cGMP-gated cation channel (CNGC1) in the plasma membrane closes due to PDE6-mediated reduction of cGMP. Closure of this channel reduces the inward dark current carried by  $\text{Na}^+$  and  $\text{Ca}^{2+}$ , resulting in rod cell hyperpolarization and inhibiting glutamate release at the synapse, thereby generating a neural signal that is transported through bipolar and ganglion cells in the retina and then through the optic nerve to the brain.

Following cascade activation, recovery occurs through several processes, which include  $T_\alpha$  and PDE6 complex deactivation, guanylate cyclase (GC) activation for increasing cytoplasmic cGMP level,  $R^*$  deactivation, and increased channel sensitivity to cGMP.  $T_\alpha$  and PDE6 complex deactivation are not clearly related to the  $Ca^{2+}$  concentration decrease; however, the other processes are related to  $Ca^{2+}$  modulation. Because the  $Ca^{2+}$  concentration is decreased 10-fold when the cGMP-gated channel closes following light stimulation, the lower  $Ca^{2+}$  concentration in the cytoplasm feeds back to  $Ca^{2+}$  binding proteins. Guanylate cyclase activating proteins (GCAPs), recoverin, and CNGC1  $\beta$ -subunit (CNGB1) are  $Ca^{2+}$ -binding proteins that either acts to activate GC and rhodopsin kinase (RK) or to increase sensitivity of CNGC1 to cGMP. The deactivation of  $T_\alpha$  and PDE6 needs a complex including GTPase-activating proteins, composed of regulators of G-protein signaling (RGS) 9-1, the long splice variant of type 5 G-protein  $\beta$ -subunit ( $G\beta 5L$ ), and PDE6 $\gamma$ . The complex activates intrinsic GTPase  $T_\alpha$  (Arshavsky, Lamb, & Pugh, 2002; Fain, Matthews, Cornwall, & Koutalos, 2001; Stryer, 1991).

#### *Phototransduction Initiator—Rhodopsin*

Rhodopsin is an integral membrane protein with a molecular weight of 40 kilo Dalton (kDa) localized in the disc and plasma membrane of the rod outer segment (ROS) (Nathans, 1992). Rhodopsin has 7-transmembrane  $\alpha$  helices with the N-terminus exposed to the intradiskal space and the C-terminus exposed to the cytoplasm (Hargrave et al., 1983; Schertler, Villa, & Henderson, 1993). Palczewski (Palczewski, Kumasaka et al., 2000) and his colleagues revealed rhodopsin's crystal structure at 2.8 Å resolution in a

ground state, showing the detailed information of the *11-cis* retinal-binding pocket and 7-transmembrane helices.

The rhodopsin density on the disk membrane is about 25,000 molecules/ $\mu\text{m}^2$  (Liebman, Parker, & Dratz, 1987). Each vertebrate ROS contains about  $10^8$  rhodopsin molecules; each disk contains  $10^6$  rhodopsin molecules. About 99% of the rhodopsin is situated in the rod disc membrane (Lamb & Pugh, 2004); in murine retina, each mouse ROS contains  $7 \times 10^7$  rhodopsin molecules (Driessen et al., 2000).

Rhodopsin is composed of opsin and *11-cis* retinal (chromophore). In the internal hydrophobic pocket of opsin, the chromophore is covalently bound to lysine-296 in helix VII via a protonated Schiff base. The lysine has a net positive charge that forms a salt bridge with a negative charge on glutamate 113 counterion to stabilize the configuration. The state of the Schiff base protonation determines the maximum wavelength absorption of the chromophore (reviewed by Lamb & Pugh, 2004).

Upon absorbing light, rhodopsin is photoisomerized to R\* (Meta II) within 1 ms (Schoenlein, Peteanu, Mathies, & Shank, 1991). The Schiff base is deprotonated in this state; therefore, *11-cis* retinal is converted to *all-trans*-retinyl, which is finally hydrolyzed to all trans retinal (Rando, 1992). After conformational changes, rhodopsin's maximal absorbing wavelength is shifted and the rhodopsin is bleached. The other photoisomerization states, Meta I and Meta III, do not have the activating function for phototransduction. There is an equilibrium between Meta I and Meta II (Matthews, Hubbard, Brown, & Wald, 1963). The quantity of Meta III is 30% of Meta II; there is a pH-dependent equilibrium between Meta II and Meta III (Kolesnikov, Golobokova, & Govardovskii, 2003). It was found that opsin molecules were equivalent to  $10^{-5} \text{ R}^* \text{ S}^{-1}$  (Cornwall & Fain, 1994).

In addition, rhodopsin shows an extremely low rate of thermal activation to R\* ( $10^{-10} \text{ s}^{-1}$ ) at body temperature (Baylor, Nunn, & Schnapf, 1984).

Except for the covalent retinoid-binding site in the chromophore pocket, there are two additional noncovalent binding sites for retinoid, an “entrance” site and an “exit” site (Schadel et al., 2003). Generally, *11-cis* retinal binds to the entrance site before binding to the chromophore pocket, and *all-trans* retinal binds to the exit site.

#### *Photoisomerized Rhodopsin Deactivation*

It has been known that R\* deactivation needs two steps: Meta II phosphorylation and arrestin binding to phosphorylated R\* (Kuhn & Wilden, 1987). R\* phosphorylation needs a 70-kDa protein rhodopsin kinase (RK) (Shichi & Somers, 1978). Phosphorylation itself can reduce the speed of R\* catalyzing the transduction cascade (Langlois, Chen, Palczewski, Hurley, & Vuong, 1996; Xu et al., 1997). Arrestin binds to phosphorylated R\* to compete with  $\text{T}\alpha$ -GTP binding, since  $\text{T}\alpha$ -GTP associates with both phosphorylated R\* and unphosphorylated R\* (Kuhn, Hall, & Wilden, 1984). After arrestin binding to phosphorylated R\*, the deactivation of R\* is complete (Wilden, Hall, & Kuhn, 1986). Predominant phosphorylation sites of rhodopsin are at the C-terminus; there are an average of seven sites in mammalian opsins (Wilden & Kuhn, 1982). In vivo studies, however, indicate that very few phosphorylation sites are actually used. There are two typical sites in mice, Ser-344 and Ser-348 and two typical sites in bovine, Ser-348 and Ser-343 (McDowell, Nawrocki, & Hargrave, 1993; Ohguro, Van Hooser, Milam, & Palczewski, 1995). Both full-length arrestin p48 (48 kDa) and its splice variant p44 (44 kDa) are present in ROS (Smith et al., 1994). The truncated form, p44, seems to be more efficient in

turning off R\* than p48 (Langlois et al., 1996). This may be important in responding to higher levels of light.

Meta rhodopsin isomerization intermediates (Meta II and Meta III) decay, and recovery requires hydrolysis of the Schiff base. The rhodopsin recovery period, known as the metarhodopsin decay time (Dowling, 1960), takes about 8 min (Alpern, 1971). The life time of R\* is 0.1 s at body temperature. The life time of R\* means the time period from the activation to the binding of RK and arrestin (Lamb & Pugh, 2004).

### *Recoverin*

Recoverin belongs to the EF hand superfamily, of which calmodulin (CaM) and GCAPs are well-known members. Recoverin consists of 202 amino acid residues and has a molecular weight of 23.3 kDa. Recoverin has three EF hands (Ca<sup>2+</sup> binding sites); two of them (EF-2 and EF-3) are active loops (Dizhoor et al., 1991; Palczewski, Polans, Baehr, & Ames, 2000). Recoverin is distributed predominately in both rod and cone photoreceptors (Dizhoor et al., 1991; Milam, Dacey, & Dizhoor, 1993). Recoverin is characteristically N-terminal myristoylated (Ray et al., 1992). The binding of Ca<sup>2+</sup> induces the release of myristoyl group from the hydrophobic cavity of EF hands in the Ca<sup>2+</sup> unbinding state; this calcium-myristoyl switch is important for recoverin interaction in the disk membrane (Ames et al., 1997; Tanaka, Ames, Harvey, Stryer, & Ikura, 1995). The crystal structure of recoverin is more compact than CaM but similar to GCAP2 (Ames, Dizhoor, Ikura, Palczewski, & Stryer, 1999; Chattopadhyaya, Meador, Means, & Quioco, 1992; Flaherty, Zozulya, Stryer, & McKay, 1993). The Ca<sup>2+</sup> binding form of recoverin binds to rhodopsin kinase, prevents RK phosphorylating R\*, and prolongs the life time of R\*

(Kawamura, 1993; Klenchin, Calvert, & Bownds, 1995). It functions as an endogenous photoreceptor GC activator. Adding purified recoverin to washed ROS that contains GC can restore the  $\text{Ca}^{2+}$  sensitivity (review in Koch, 1992).

#### *Arrestin Translocation*

A large portion of arrestin tagged by green fluorescent protein (GFP) in *Xenopus* oocytes rods was translocated to the outer segment after light exposure and returned to the inner segment in dark adaptation (Peterson et al., 2003); this process is the reverse of transducin translocation. The translocation of arrestin is independent of the phosphorylation of  $\text{R}^*$  by  $\text{RK}^+$  and the presence of transducin, but depends on rhodopsin activation (Mendez, Lem, Simon, & Chen, 2003). Motor protein kinesin-II localized in the connecting cilium is required for opsin and arrestin translocation between the OS and IS compartments (Beech et al., 1996; Marszalek et al., 2000).

#### *Protein Phosphatase 2A (PP2A)*

PP2A regulates diverse cellular processes, including signal transduction. It has a catalytic subunit C (36-38 kDa), a structural subunit A (60-65 kDa), and a regulatory subunit B (54-130 kDa) (Khew-Goodall, Mayer, Maurer, Stone, & Hemmings, 1991). Early evidence showed that dephosphorylation of rhodopsin is catalyzed by PP2A, at least in part (King, Andjelkovic, Hemmings, & Akhtar, 1994; Ohguro et al., 1995; Palczewski, Hargrave, McDowell, & Ingebritsen, 1989). The dimer of the PP2A complex (A and C subunits), localized predominately in the disk membrane, in darkness favors the phosphorylation of opsin. The trimer of PP2A (A, B, and C) phosphorylates transducin in the

cytosol under light conditions (Brown, Carlson, Zhu, Lolley, & Craft, 2002). Dephosphorylation of opsin is accompanied by the process of *11-cis* retinal replacing *all-trans* retinal to finally restore the inactive state rhodopsin (Ridge, Abdulaev, Sousa, & Palczewski, 2003).

#### *Photoexcitation Steps in Transducin and PDE6*

Membrane-bound transducin is a member of the G-protein family, which includes signal mediators in a variety of transduction cascades. These cascades determine the specificity and temporal characteristics of a cell's response to an external signal (Hamm, 1998; Stryer, 1986). Transducin is a heterotrimer composed of  $1\alpha$ ,  $1\beta$ , and  $1\gamma$  subunits, with predicted molecular weights of 39, 36, and 10 kDa, respectively (Fung, Hurley, & Stryer, 1981). In mammalian rods transducin is present at a molar ratio to rhodopsin of 1:12 (Tsang et al., 1998).  $R^*$  activates transducin by catalyzing the exchange of GTP for bound GDP on  $T_\alpha$ .  $T_\alpha$  contains guanyl nucleotide binding and GTP hydrolysis sites, the latter representing an intrinsic GTPase function of  $T_\alpha$  (Fung, 1983).

$T_\alpha$ -GTP dissociates from  $T_{\beta\gamma}$  subunits and activates membrane-bound PDE6 by binding its inhibitory subunit  $\gamma$  and exposing catalytic subunits  $\alpha$  and  $\beta$ . Since PDE6 is a heterotetrameric complex with a stoichiometry of  $\alpha\beta\gamma_2$ , full activation requires two  $T_\alpha$ -GTP (Fung, Young, Yamane, & Griswold-Prenner, 1990). When  $T_\alpha$  binds to GTP,  $R^*$  disassociates  $T_\alpha$ -GTP and remains active to bind another transducin molecule. One  $R^*$  can activate hundreds ( $220\text{ S}^{-1}$ ) of transducins in mammalian rod disk membranes (Heck & Hofmann, 2001). The active PDE6 lowers the cytosolic concentration of cGMP in its vicinity, which in turn decreases the occupancy of cGMP on the binding sites of the

cGMP-gated channel in the plasma membrane. The maximum catalytic rate of cGMP hydrolysis is  $6 \times 10^7 \text{ M}^{-1}\text{S}^{-1}$  ( $K_{\text{cat}} / K_{\text{M}}$ ), which is close to the theoretical maximum rate. In addition to catalyzing binding sites for cGMP, PDE6 also has noncatalytic binding sites on  $\alpha$  and  $\beta$  (Yamazaki, Bartucca, Ting, & Bitensky, 1982). These sites are thought to play a role in slowing down or accelerating GTPase activity when cGMP concentrations are high or low. At lower cGMP levels,  $T_{\alpha}$ -GTP-PDE6 $_{\gamma}$  dissociates from the  $T_{\alpha}$ -GTP-PDE6 $_{\alpha\beta\gamma 2}$  complex where it helped to accelerate GTPase activity (Cote, Bownds, & Arshavsky, 1994).

#### *Phosducin Modifying G protein Function*

Phosducin is a 33-kDa soluble phosphoprotein that is phosphorylated in the dark and dephosphorylated in the light.  $T_{\beta\gamma}$  complexes tightly with unphosphorylated phosducin, indicating that phosducin down-regulates transducin activity (Gaudet, Bohm, & Sigler, 1996; Lee, Lieberman, & Lolley, 1987; Wilkins, Bitensky, & Willardson, 1996). Phosducin binding to  $T_{\beta\gamma}$  prevents  $T_{\alpha}$  and  $T_{\beta\gamma}$  reassociation and activation by  $R^*$  again (Wilkins et al., 1996; Yoshida et al., 1994). The known phosphorylation site of phosducin in the dark is situated at Ser-73, and the process is catalyzed by protein kinase A (Lee, Brown, & Lolley, 1990). In the light, it is dephosphorylated by PP2A trimer (Brown et al., 2002). Independent of illumination levels, more than 90% of phosducin is distributed in the IS; less than 10% is in the OS (Chen, Yoshida, Nakano, & Bitensky, 2005). These results imply that the regulatory activity of phosducin occurs in the IS; phosducin needs to bind or disassociate protein 14-3-3 in phosphorylated (dark) and unphosphorylated (light) condition in order to finish its cycle of function (Nakano et al., 2001).

*Complex of T $\alpha$ -GTP-PDE6 $\gamma$  and RGS9-1-G $\beta$ 5L-R9AP*

T $\alpha$ -GTP has an intrinsic GTPase function found in purified T $\alpha$ , but it is too slow to account for observed physiological conditions (Fung et al., 1981; Wagner, Ryba, & Uhl, 1988). This paradox led to the hypothesis of GTPase-activating proteins (GAPs) for heterotrimeric G-proteins existing in photoreceptors (Arshavsky & Bownds, 1992; Dratz, Lewis, Schaechter, Parker, & Kliger, 1987). The family of regulators of G protein signaling (RGS) is a family of novel GAPs (Ross & Wilkie, 2000). RGS9-1, the short splice variant of the ninth member of the RGS family, is rod and cone photoreceptor-specific GAP. RGS9-1 is responsible for accelerating the intrinsic GTPase activity of T $\alpha$ -GTP (Cowan, Fariss, Sokal, Palczewski, & Wensel, 1998; He, Cowan, & Wensel, 1998). The long splice variant of type 5 G protein  $\beta$ -subunit (G $\beta$ 5L) and RGS9-1 form a complex in vertebrate photoreceptors (Makino, Handy, Li, & Arshavsky, 1999). The normal expression of RGS9-1 and G $\beta$ 5L is interdependent, indicated by data from the RGS9-1 knockout mouse model and heterologous cell lines expression (Chen et al., 2000; He et al., 2000). Knockout of the RGS9-1 gene leads to increased rod or cone recovery, at times up to 45-60 folds. The RGS9-1-G $\beta$ 5L complex is the primary GTPase accelerator in photoreceptors (Chen et al., 2000; Lyubarsky et al., 2001). PDE $\gamma$  is the first protein found to be involved in transducin deactivation (Arshavsky & Bownds, 1992). GTPase activity is enhanced by PDE6 $\gamma$  (Angleton & Wensel, 1994). A PDE6 $\gamma$  mutant mouse model with a point mutation at codon 70 (W70A) was found to slow recovery seven-fold (1 s to 0.15 s) (Tsang et al., 1998). In the case of RGS9-1 knockout mice, the corresponding recovery time is 2.5 s, and the existence of PDE6 $\gamma$  exerts no accelerating effect on T $\alpha$  GTPase ac-

tivity (Chen et al., 2000). These two studies indicate that, in addition to RGS9-1-G $\beta$ 5L, PDE6 $\gamma$  also is required for transducin GTPase regulation.

RGS9-1-anchor protein (R9AP) is a membrane anchor for RGS9-1. R9AP is a 25-kDa phosphoprotein predominately expressed in photoreceptor outer segments. It binds to the N-terminal domain of RGS9-1 and anchors to the disk membrane through a C-terminal transmembrane helix (Hu & Wensel, 2002). An in vitro study found that R9AP increased RGS9-1 GTPase-accelerating protein activity by a factor of four following complex formation (Hu, Zhang, & Wensel, 2003). In homozygote R9AP affected patients, the photoresponse recovery time (1 min) is 30-fold longer than normal (2 s) (Nishiguchi et al., 2004). In R9AP knockout mice, not only is the photorecovery time indistinguishable from RGS9-1 knockout mice, but the expression of RGS9-1 in photoreceptors is also absent. This result indicates that membrane anchor protein R9AP determines the stability of RGS9-1 (Keresztes et al., 2004).

### *PDE6*

Membrane-associated phosphodiesterase in the rod photoreceptor outer segment is designated PDE6 (Beavo, 1995). Rod PDE6 contains  $\alpha$  (88 kDa),  $\beta$  (85 kDa), and  $\gamma$  (9 kDa) (Baehr, Devlin, & Applebury, 1979), with a stoichiometry of  $\alpha\beta\gamma_2$  (Deterre, Bigay, Forquet, Robert, & Chabre, 1988; Fung et al., 1990). The  $\gamma$  subunit is an inhibitory subunit; removal of  $\gamma$  subunits increased PDE6 activity about 1500-fold (Hurley & Stryer, 1982). The C-terminal rather than the N-terminal is critical for inhibition (Brown & Stryer, 1989). In addition to the membrane-bound  $\alpha\beta\gamma_2$ , there is a soluble form  $\alpha\beta\gamma_2$  bound to a 15-kDa PBP (formerly called the  $\delta$  subunit) that could mediate the solubility

of PDE6 (Gillespie, Prusti, Apel, & Beavo, 1989). The isozyme in cone photoreceptors has two identical catalytic subunits  $\alpha'$  and one or two  $\gamma$  and  $\delta$  subunits (Gillespie & Beavo, 1988).

A low resolution of the molecular organizations of PDE6  $\alpha\beta\delta$  and  $\alpha\beta\gamma_2$  subunit complexes has been revealed by electron microscopy and image processing (Kajimura, Yamazaki, Morikawa, Yamazaki, & Mayanagi, 2002; Kameni Tcheudji et al., 2001)

#### *Guanylate Cyclase (GC) and GC-Activating Proteins (GCAPs)*

Free cGMP in the amphibian rod is 6  $\mu\text{M}$ , which is 1/5-1/10 of the total cGMP (Nakatani & Yau, 1988b), whereas the total cGMP is about 30-60  $\mu\text{M}$  (Woodruff & Bownds, 1979). The binding form of cGMP is on PDE6 and the cGMP-gated channel in the plasma membrane. As cGMP is hydrolyzed by PDE6 in the light, GC catalyzes the conversion of GTP to cGMP to raise the cytosolic cGMP level in the dark state. There are two forms of GCs, GC-1 and GC-2, in humans (GCE and GCF in mice) (Pugh, Duda, Sitaramayya, & Sharma, 1997). The two forms of GCs are present in both rods and cones; however, GCE is more abundant in cone (Dizhoor, Lowe, Olshevskaya, Laura, & Hurley, 1994; Kachi et al., 1999). Retinal GCs belong to a family of guanylyl cyclase receptors (R. B. Yang, Foster, Garbers, & Fulle, 1995).

GCAPs are  $\text{Ca}^{2+}$ -binding proteins with MW 23.5-kDa that mediate the function of GCs through  $\text{Ca}^{2+}$  feedback. A low concentration of free  $\text{Ca}^{2+}$  activates the GCs, increasing the synthesis of cGMP (Gorczyca, Gray-Keller, Detwiler, & Palczewski, 1994; Gorczyca et al., 1995). Clear evidence of  $\text{Ca}^{2+}$  modulation by EF hands containing GCAPs was shown in 1996 (Polans, Baehr, & Palczewski, 1996). In amphibian rod pho-

toreceptors, the concentration of  $\text{Ca}^{2+}$  decreases from 500-700 nM in darkness to 30-50 nM in light (review in Fain et al., 2001), whereas in cone photoreceptors, the change is from 410 to 5.5 nM (Sampath, Matthews, Cornwall, Bandarchi, & Fain, 1999). In mice study, the concentration in rod is 250 nM in darkness and 25 nM in saturated light (Woodruff et al., 2002). GCs are half-maximally activated at a  $\text{Ca}^{2+}$  concentration of about 200 nM (Dizhoor & Hurley, 1999). Two common GCAPs, GCAP-1 and GCAP-2, are present in both human rod and cone photoreceptors, whereas GCAP-3 presents exclusively in human cone photoreceptors but is absent in mouse retina (Imanishi et al., 2002). Guanylate cyclase-inhibitory protein (GCIP) was cloned in frog retina; it inhibits GCs at high free  $\text{Ca}^{2+}$  (Li et al., 1998). GCIP genes couldn't be retrieved from human, mouse, and other mammalian (Palczewski, Sokal, & Baehr, 2004). Complementation studies in GCAP-1 and GCAP-2 knockout mice showed that GCAP-1 is the critical GCAP in murine photoreceptors (Howes et al., 2002; Mendez et al., 2001; Pennesi, Howes, Baehr, & Wu, 2003). GCAPs are members of the  $\text{Ca}^{2+}$ -binding protein family, which includes recoverin and CaM. GCAPs have four EF-hand motifs located on both N- and C-terminals; three EF hands are  $\text{Ca}^{2+}$ -active loops (EF hand 2-4). CaM has four active loops for  $\text{Ca}^{2+}$  binding, and recoverin has two active loops (EF-2 and EF-3) (Palczewski, Polans et al., 2000). Gorczyca et al. (1995) found the complex of GCAPs and GCs at low or high  $\text{Ca}^{2+}$  concentration, suggesting that the EF-hands were responsible for GC inhibition or activation by the binding of GCs in dependent of  $\text{Ca}^{2+}$  (Dizhoor & Hurley, 1996).

## A Brief Review of Mammalian Retina

### *General Information*

The average adult human eye contains approximately 100 million rods and 5 million cones. Cones are tightly packed in the center of the fovea where rod photoreceptors are absent. Rod density is highest at a 5-mm ring centered around the macula. Both cone and rod density decrease rapidly toward the peripheral retina (Curcio, Sloan, Kalina, & Hendrickson, 1990). The cones function at bright light for color vision, whereas rods are sensitive to monochromatic light of low intensity (Dowling, 1987). Retinal pigment epithelium (RPE) is a single layer of epithelium cells posterior to the photoreceptor. It contains 5 million tight junction-associated cells which, with Bruch's membrane, form the blood-retina barrier between photoreceptor and choroid vessels. The post-mitotic RPE cells are critical to photoreceptor function and maintenance, carrying a number of vital functions (Marmor and Wolfensberger, 1998)

Mature photoreceptors are functionally and structurally polarized neurons with compartmentalized morphology. The light-sensitive organelle, the outer segment (OS) of the vertebrate rod, is composed of around 1000 tightly stacked membrane disks wrapped by plasma membrane (Roof & Heuser, 1982). Each disk has a  $1.5\text{-}\mu\text{m}^2$  surface area; the length is about  $60\text{ }\mu\text{m}$ ; the distance of apposite surface of two adjacent disks is about 15 nm (O'Brien, 1982), and intradiscal space is 2 nm (Steinberg, Fisher, & Anderson, 1980); and the vertical distance of disk to plasma membrane is 10 nm (Roof & Heuser, 1982). About 100 disks are formed per day at the base of the OS in primates (Anderson, Fisher, & Steinberg, 1978; Steinberg et al., 1980; Young, 1971). Nascent disks are formed by the evagination of plasma membrane near the cilium to form adjacent lamellar surfaces of

disks; the fusion of the adjacent evagination of lamellar membrane at periphery forms a rim. Incisures form after membrane evagination but before rim formation is complete. At the same time, plasma membrane seals the outside surface of a newly formed disk (Papermaster, Schneider, Zorn, & Kraehenbuhl, 1978; Steinberg et al., 1980). Human has 9-12 incisures in the ROS; however, mouse has only one incisure (Cohen, 1965; Eckmiller, 2000; Korschen et al., 1999; Pedler & Tilly, 1967). Disk proteins synthesized at the inner segment are incorporated into newly formed membrane at the base of the OS (Young, 1967; Young & Droz, 1968). Opsin and peripherin-2 are inserted into the nascent disk independently (Arikawa, Molday, Molday, & Williams, 1992). The distal disks at the apex of the OS are shedded and phagocytosed by the adjacent RPE when the light is on (Young & Bok, 1969); the shedded disks are encapsulated in phagosome and digested by lysosome when phagosomes merge with lysosome.

#### *Visual Pigment Renewal in RPE*

The process of visual pigment renewal is called the visual cycle, which functions to regenerate *11-cis*-retinal. In the rod photoreceptor, the chromophore *11-cis*-retinal is covalently linked to opsin to form inactivated rhodopsin. After photoisomerization, the *11-cis*-retinal isomerizes to *all-trans*-retinal and dissociates from opsin through the hydrolysis of the Schiff base. *All-trans*-retinal is reduced to *all-trans*-retinol (vitamin A) by *all-trans*-retinol dehydrogenase (RDH). Alternatively, a portion of *all-trans*-retinal can bind to phosphatidylethanolamine (PE) to form a N-retinylidene-PE complex in the disk lumen and be transported the cytoplasm by an outwardly directed flippase, adenosine triphosphate (ATP)-binding cassette transporter (ABCR). *All-trans*-retinal dissociates

from PE in the cytoplasm and is reduced to *all-trans*-retinol by *all-trans*-retinol dehydrogenase. ABCR gene knockout in mice leads to accumulation of lipofuscin fluorophore (N2E) in RPE because of the accumulation of its precursor N-retinylidene-PE (Weng et al., 1999). N2E is the condensed product of N-retinylidene-PE binding a second retinal (Ben-Shabat et al., 2002). The movement of vitamin A to the RPE cell is assisted by the carrier protein interstitial retinol-binding protein (IRBP) or other retinol-binding proteins. Upon entry into the RPE cell, retinol is bound by cellular retinol-binding protein (CRBP), followed by vitamin A esterification to a retinyl ester by lecithin retinol acyl transferase (LRAT). *All-trans* retinyl esters are isomerized and hydrolyzed to *11-cis* retinol by isomerohydrolase (IMH). *11-cis* retinol is oxidized to *11-cis* retinal by *11-cis*-retinol dehydrogenase. This final product, *11-cis* retinal, binds to the carrier protein cellular retinaldehyde-binding protein (CRALBP) and IRBP in the cytoplasm of the RPE cell and in the interphotoreceptor space. Finally, it covalently binds to opsin at lys<sup>296</sup> in ROS to form rhodopsin, completing the visual cycle (Katz & Redmond, 2001; Lamb & Pugh, 2004; Pacione, Szego, Ikeda, Nishina, & McInnes, 2003; Rando, 1992). In addition, another RPE protein RPE65 plays an important role in the visual cycle. It has two forms, the membrane associated form, mRPE65, which is palmitoylated and a chaperone for *all-trans*-retinyl esters, and a soluble form, sRPE65, that is not palmitoylated and is a chaperone of vitamin A. The two forms are interconverted by LRAT. In the dark, when there is enough vitamin A, mRPE65 is converted into sRPE65 by LRAT and vitamin A is converted to the storage form, *11-cis*-retinyl esters, and chromophore synthesis is switched off (Wolf, 2005; Xue, Gollapalli, Maiti, Jahng, & Rando, 2004).

## CNGB1

*Cyclic Nucleotide-Gated (CNG) Channel*

Both CNG channels and hyperpolarization-activated cyclic nucleotide-gated channels (HCN) are members of the cyclic nucleotide-gated channel family, which is member of the superfamily of voltage-gated cation channels. CNG channels are activated directly by the binding of cGMP or cyclic adenosine monophosphate (cAMP) to a cyclic nucleotide-binding domain; photoreceptor cGMP-gated channels show a higher specificity for cGMP over cAMP (Hofmann, Biel, & Kaupp, 2003).

The photoreceptor CNG channel activity was first discovered by Fesenko and his colleagues (Fesenko, Kolesnikov, & Lyubarsky, 1985) in an excised, inside-out patch of ROS plasma membrane. It was shown that cGMP directly activated a CNG-gated channel, indicating that cGMP, not  $\text{Ca}^{2+}$ , is the second messenger in the light-sensitive conductance of the ROS. Similar channels were also reported in cone photoreceptors (L. Haynes & Yau, 1985), olfactory sensory neurons (Nakamura & Gold, 1987) and in the pineal gland (Dryer & Henderson, 1991).

CNG channels are heterotetrameric, containing  $\alpha$  or  $\beta$  subunits. There are four known  $\alpha$  (A) subunits (A1, A2, A3 and A4) and two  $\beta$  (B) subunits (B1 and B3). A is the principal subunit, which has channel function when forming homotetramer; B is a modulatory subunit that cannot function by itself. A4 is a special case; functionally, it is a modulatory subunit, but it was classified to the A group by its sequence similarity to A. CNGB1 (A1) is the  $\alpha$  subunit of rod CNG channel and has other names, such as CNG1, CNG $\alpha$ 1, and RCNC1; CNGB2 is  $\alpha$  subunit of olfactory CNG channel and has other names, such as CNG2, CNG $\alpha$ 3, and OCNC1; CNGB3 (A3) is  $\alpha$  subunit of the cone CNG

channel and has other names such as CNG3, CNG $\alpha$ 2, and CCNC1; CNGA4 is the second/modulatory subunit of olfactory CNG channel and has other names such as CNG5, CNGB2, CNG $\alpha$ 4, and OCNC2; CNGB1 (B1) is the second/modulatory subunit of rod CNG channel and has other names like CNG4, CNG $\beta$ 1 and CNGB1a; CNGB3 (B3) is the second/modulatory subunit of cone CNG channel and has other names such as CNG6 and CNG $\alpha$ 3. In addition, CNGB1b is the second modulatory subunit of olfactory CNG channel. Both CNGA4 and CNGB1b are modulatory subunits in olfactory CNG channel (Kaupp & Seifert, 2002; Bradley, Frings, Yau, & Reed, 2001).

#### *Rod CNG Channel Has Two Homologous Subunits*

Since the first CNG channel was found in 1985 in the rod photoreceptor, the components, structure and function of CNG channel had been working on. In 1987, Cook, Hanke, and Kaupp found a bovine ROS 63-kDa channel protein ( $\alpha$ -subunit or A1) that has channel function when expressed in planar lipid bilayers; however, this  $\alpha$ -subunit only channel couldn't be blocked by L-cis-diltiazem in a concentration that could block nature rod CNG channel effectively. The single channel's electrical properties were further studied in planar lipid membrane (Hanke, Cook, & Kaupp, 1988). The bovine A1 was molecular cloned and revealed a 693-amino-acid sequence with molecular weight 63-kDa (Kaupp et al., 1989). Human and mouse A1 were cloned and predicted to have 690 and 683 residues, respectively by Pittler et al. (1992). The highly homologous human A1 showed similar properties to bovine A1 (Dhallan et al., 1992). When A1 subunits were heterologously expressed in cos-1 cell or *Xenopus* oocytes through cloned complementary deoxyribonucleic acid (cDNA), the result showed that the A1 subunit had an

apparent 80-kDa polypeptide with 92 residues in N-terminal in addition to native 63-kDa A1 subunit in rod ROS. The deletion of N-terminal amino acids is presumably due to co-translational or posttranslational proteolytic processing (Molday et al., 1991). A 240-kDa polypeptide were copurified with 63-kDa A1 from bovine ROS but not identified as another channel subunit (Cook et al., 1987; L. L. Molday, Cook, Kaupp, & Molday, 1990). Until 1995 (Korschen et al., 1995), the bovine 240-kDa polypeptide was molecular cloned and identified as the secondary  $\beta$  (B1) subunit with 1394 amino acids in full length. Human B1 subunit was cloned thereafter (Colville & Molday, 1996). Earlier work also confirmed the existence of the  $\beta$  subunit; however, it was part of the sequence of the 240-kDa human B1 (Chen et al., 1993, 1994; Korschen et al., 1995). The human B1 subunit shows 30% identity to the A1 subunit (Chen et al., 1993). Heterologous expression of B1 in HEK 293 cell (Chen et al., 1993; Korschen et al., 1995) was unfunctional. Heterologous expression of A1 in *Xenopus* oocytes (Kaupp et al., 1989) and HEK cell (Chen et al., 1993; Dhallan et al., 1992) shows most but not all nature channel activities. But when coexpressing A1 with B1 resulted in properties that the A1 homomer doesn't have, but are similar to nature rod CNG channel, such as flickery channel opening and closing, 100-fold more sensitive to channel blocker L-cis-diltiazem, increased permeability to divalent ions ( $\text{Ca}^{2+}$  blockage), and ionic selectivity and  $\text{Ca}^{2+}$ -CaM modulation (Chen et al., 1994, 1993; Korschen et al., 1995).

#### *B1 and A1 Isoforms Distribution*

*Cngb1* can be expressed in rod photoreceptors in full length and is also called *Cngb1a* to distinguish it from *Cngb1b*. *Cngb1* gene products express as shorter isoforms

in olfactory sensory neurons (i.e., isoform B1b), CnRH-secreting cell line (GT1), heart, and testis. *Cngal* can be expressed in a rod photoreceptor called A1, and also in other tissues, such as retinal ganglion cell, testis, brain (pinealocytes, cerebellum, cortex, hippocampus, anterior pituitary, and GT1), heart, kidney, testis, liver, lung, spleen, pancreas, keratinocyte, adrenal gland, muscle, vascular endothelium, and M-1 cell line. In nonneuronal tissues, except for testis, none of those tissues absolutely demonstrates the existence of channel activity. Even for testis, channel activity does not show similar function of rod CNG channel (reviewed by Kaupp & Seifert, 2002).

#### *CNGB1 Gene Location, Structure, and Expression*

Most of the genetic works of human CNGB1 were done in Dr. Pittler's lab by Ardell and his colleagues. CNGB1 is located in chromosome 16q13 for human and spans an approximately 100-kb genomic DNA sequence (Ardell et al., 1996; Ardell, Bedsole, Schoborg, & Pittler, 2000). In mouse it is located in chromosome 8 and spans 68-kb of the genomic DNA sequence. A1 is located on chromosome 4 in human (Dhallan et al., 1992; Pittler et al., 1992) and chromosome 5 in mouse (Pittler et al., 1992). The B1 gene has 33 exons, and translational start codon ATG is at the second exon (Ardell et al., 2000; Ardell et al., 1995). To distinguish this subunit from the subunit expressed in olfactory neurons in nomenclature, the B1 subunit expressed in rod photoreceptor is called B1a; the other one is called B1b (CNG4.3), which was first found in rat olfactory neurons (Sautter, Zong, Hofmann, & Biel, 1998). Isoform B1b has coding exons starting from exon 16a. Its N-terminal extends to 14a, and the C-terminal ends at exon 33. B1b doesn't have a glutamic-acid-rich protein (GARP) part (Ardell et al., 2000; Sautter et al., 1998). In bovine

and human, the full-length B1 has 1394 amino acids and 1251 amino acids, respectively. The full length B1 has a bipartite structure, the N-terminal GARP part and C-terminal channel part. B1a's N-terminal GARP part is unique in all channel subunits (Ardell et al., 1996, 2000; Korschen et al., 1995). Generally, the GARP part is comprised of the first 16 exons and the channel part contains the last 17 exons (Ardell et al., 2000). In addition to being 30% homologous to the A1 subunit, the channel part of B1 contains topography similar to that of A1 subunit (Chen et al., 1993). The corresponding exons for putative transmembrane segments 1 to 6 (S1-S6) are 21-26, for the cyclic nucleotide binding domain 29-31; the major and minor  $\text{Ca}^{2+}$ /CaM binding sites (Grunwald, Yu, Yu, & Yau, 1998; Weitz et al., 1998) are distributed in exons 19 and 32 separately (Ardell et al., 2000). In addition to full-length B1a, there are two N-terminal truncated variants, GARP-1 and GARP-2, in rod photoreceptor. Bovine GARP-1 (571 amino acids) was cloned in 1991 (Sugimoto, Yatsunami, Tsujimoto, Khorana, & Ichikawa, 1991), and human GARP-2 was cloned in Pittler's lab (Ardell et al., 1995). Both bovine and human GARP-2 peptides (299 amino acids) were sequenced in Molday's lab (Colville & Molday, 1996), and human GARP1 (i.e. hGARP2.5, 502 amino acids) was cloned in Yau's lab (Grunwald et al., 1998). All GARP proteins, such as GARP-1, GARP-2, and B1 subunit, expressed in ROS only have a common gene locus CNGB1. Those GARP transcripts share the same promoter and the first 12 exons. GARP-1 and GARP-2 have a unique exon 16a and 12a at C-terminal separately, which translated to 8 and 19 amino acids in bovine, and translated to 8 and 49 amino acids in human separately (Ardell et al., 2000; Colville & Molday, 1996; Grunwald et al., 1998). The first conserved domain of GARPs is located in exons 1 and 2 in the N-terminal part. This conserved domain shows more

than 85% identity among human, rat, and bovine. Exon 2 is also a part of a glutamate-rich domain (Ardell et al., 2000). Knocking out this part will affect the expression of all GARP proteins, including B1 subunit, and will bring new phenotypes theoretically. In addition, the channel part hRCNC2a with a low abundant transcription (Ardell et al., 1996; Chen et al., 1993), has an unique first exon of 18a (Ardell et al., 2000); whether that compensately increases after N-terminal knockout is not known for sure. Since both bovine and human B1 have a bipartite structure, the mouse should also have this kind of structure as a mammalian; however, in National Center for Biotechnology Information (NCBI) gene bank, we could only find GARP-part cDNA (BC016201) and channel-part transcription (XM\_286113). To figure out the entire *Cngb1* sequence is necessary for further study of the *Cngb1* knockout mouse model.

#### *Stoichiometry of CNGC1*

Since we know that the rod CNG channel is composed of A1 and B1 subunits, we also need to know the stoichiometry of the channel. Because the Hill coefficient is above 3, the activation of the channel needs at least four cGMPs binding; the number of subunits is likely to be at least four (Cook et al., 1987; Cook, Molday, Reid, Kaupp, & Molday, 1989). Based on the sequence homology between CNG and voltage-gated K channels, the CNG channel may be a tetramer (Jan & Jan, 1990). Coexpression of the wild-type A1 and chimeric or mutant A1 subunits confirms the heterotetrameric stoichiometry of the channel (Liu, Tibbs, & Siegelbaum, 1996; Varnum & Zagotta, 1996). The channel heterotetrameric pattern was thought to be A1-A1-B1-B1 (Shammat & Gordon, 1999) or A1-B1-A1-B1 (Y. He, Ruiz, & Karpen, 2000) surrounding the pore when using different

combinations for coexpression. Using electron microscopy and imaging processing at 35 Å resolution, the purified bovine rod CNG channel was shown to be a tetramer with a pair of dimers. This study also shows that the diameter of the channel is around 10 nm (Higgins, Weitz, Warne, Schertler, & Kaupp, 2002). Until 2002, studies showed 3A1:1B1 stoichiometry of CNGC1 in native bovine rods by chemical crosslinking (Weitz, Ficek, Kremmer, Bauer, & Kaupp, 2002) or immunoaffinity chromatography (Zhong, Molday, Molday, & Yau, 2002). The same conclusion was drawn when A1 and B1 subunits were heterologously expressed in oocytes using the fluorescence resonance energy transfer (FRET) method (Zheng, Trudeau, & Zagotta, 2002). Because Zhong's study suggested that all CNG channels adopted 3A:1B stoichiometry, so the cone CNG channel should also have a 3A3:1B3 ratio; however, through functional and biochemical methods, a new published paper suggested a B3-B3-A3-A3 stoichiometry, which contradicts the previous study (Peng, Rich, & Varnum, 2004).

#### *Transmembrane Topography*

The A1 and B1 subunits are localized exclusively in the plasma membrane by immunogold labeling and occupy 7% of total protein in the plasma membrane (Colville & Molday, 1996; Cook et al., 1989; Molday et al., 1990). Both A1 and B1 subunits contain six putative transmembrane segments S1-S6, a pore loop region P between S5 and S6, a voltage sensor motif in S4, and a cyclic nucleotide binding domain (CNBD) near the C-terminal (Chen et al., 1993; Kaupp et al., 1989; R. S. Molday & Molday, 1998). The pore loop region functions as a channel gate and ion selectivity filter (Sun, Akabas, Goulding, Karlin, & Siegelbaum, 1996). Negative charged glutamate residue is found in the pore

loop in the A1 homomer channel; this underlies the  $\text{Ca}^{2+}$  blocker function of the pore region (Eismann, Muller, Heinemann, & Kaupp, 1994; Root & MacKinnon, 1993). The corresponding B1 pore loop site is a neutral residue glycine (Korschen et al., 1995; Kaupp & Seifert, 2002). The native rod CNG channel and heterologous expression of both A1 and B1 subunits can be modulated by  $\text{Ca}^{2+}$ /Calmodulin (CaM), whereas the homologous A1 channel cannot, implying that B1 has a  $\text{Ca}^{2+}$ /CaM binding domain (Chen et al., 1994). The  $\text{Ca}^{2+}$ /CaM-binding domains were found soon in the N-terminal and C-terminal channel parts of B1, and the N-terminal site located downstream of the GARP part and upstream of S1 plays a major function (Grunwald et al., 1998; Weitz et al., 1998). Both the N-terminal and C-terminal of B1 were localized to the cytoplasmic side of ROS plasma membrane by immunogold labeling (Colville & Molday, 1996; Molday et al., 1991). Bovine and human B1 subunits have an unusual bipartite structure that the A1 subunit doesn't have. The C-terminal channel part and the N-terminal GARP region have a high content of glutamic acid and proline residues (Ardell et al., 1995; Colville & Molday, 1996; Korschen et al., 1995).

### *GARPs*

GARP is a glutamate-acids-rich protein, also a proline-rich protein. The first GARP protein (GARP-1) was cloned as a 590-amino acid peptide in bovine rod photoreceptor (Sugimoto et al., 1991). Human GARP-1 is also called hGARP2.5 and has 502 amino acids in total (Grunwald et al., 1998). The 240-kDa B1 subunit has a unique bipartite structure: The N-terminal has a glutamic-rich part which has 571 and 457 residues in bovine and human, respectively; for bovine, only 19 residues in the GARP-1 C-

terminal extension are different from the GARP part of B1; the bovine channel part has 823 amino acids containing all of the functional domain characteristic of the rod CNG channel (Colville & Molday, 1996; Korschen et al., 1995). The N-terminal GARP-part and C-terminal are located in cytoplasm, while the channel part is located in the plasma membrane (Chen et al., 1993; Molday et al., 1991). In addition, the 299-amino acid GARP-2 was also found in human and bovine ROS. N-terminal 291 amino acids were shared by N-terminal GARP1 and B1, and both of them lack C-terminal 8 amino acids extension, which is unique in GARP-2. GARP-2 is more abundant than GARP-1 (Colville & Molday, 1996), about 1/100 of rhodopsin (Korschen et al., 1999). Human GARP-2 has been cloned by Dr. Pittler's lab (Ardell et al., 1995). Polypeptides containing GARPs migrate more slowly than expectation because of negative charges (glutamate); therefore, the molecular weight appears larger than it should be (Colville & Molday, 1996). The GARP part doesn't appear to affect the function of electrophysiological properties when N-terminal truncated B1 coexpressed with the A1 subunit (Chen et al., 1993). The function of GARPs is suggested to play a role in channel targeting transport and maintaining the space between plasma and disk membrane as a structure protein. GARP-1 (140 kDa) and GARP-2 (62 kDa) are soluble proteins compared to the GARP part in ROS, all of these GARP-containing proteins were found in the ROS but not in the cone (Colville & Molday, 1996; Korschen et al., 1999; Molday & Molday, 1998). Cone B3 doesn't have the GARP part (Gerstner, Zong, Hofmann, & Biel, 2000; Korschen et al., 1999). The two soluble variants, GARP-1/GARP-2, represent alternatively spliced forms (Ardell et al., 1996, 2000). Soluble GARPs are located at disk rims and incisures. Four conserved proline-rich repeats (R1-R4) are thought to serve as targets for binding pro-

teins. GARP-2 may interact with activated PDE6; this suggests an inhibition function on activated PDE6. This inhibition might play an important role for adaptation, especially at high light intensities (Korschen et al., 1999), but the inhibition activity on PDE6 was denied by the same lab, and they attributed the property to recombinant GARP-2 (Kaupp & Seifert, 2002). Soluble GARPs (GARP-2 and GARP-1) and cytosolic domain (GARP part) of B1 interact with disk Rim protein peripherin-2 and peripherin-2/rom-1 oligomeric complex suggest a function to maintain the spatial structure of disk and plasma membrane. The function may include restricting disks rotation and maintaining alignment of the ROS. Since two dimmers channel-sodium, calcium potassium exchanger 1(NCKX1) complex bind to channel  $\alpha$ -subunits, the anchoring of NCKX1 in the vicinity of rims should be the effect of these peripherin and GARPs interaction (Poetsch, Molday, & Molday, 2001; Tam, Moritz, & Papermaster, 2004). These interactions between rims vertically and rim and plasma membrane horizontally were seen as fibrous links in a freeze fracture and deep-etching technique as early as 1982 in Roof and Heuser's report (Roof & Heuser, 1982); part of the 240-kDa B1 is involved in the component of this kind of filament (Wong & Molday, 1986).

#### *Relation to NCKX1*

The 230-kDa sodium/calcium-potassium exchanger (NCKX1) is localized exclusively in the ROS plasma membrane (Cook & Kaupp, 1988; Kim, Reid, & Molday, 1998; Reid, Friedel, Molday, & Cook, 1990). It has 1216 residues (bovine) forming 11 transmembrane segments. The N-terminal and C-terminal are in the extracellular and cytosolic sides respectively (Kim et al., 1998; Tucker, Winkfein, Cooper, & Schnetkamp, 1998).

By the immunoprecipitation method, the exchanger was proved to interact with the rod CNG channel in the plasma membrane (Bauer & Drechsler, 1992; Molday & Molday, 1998; Poetsch et al., 2001). By the way, NCKX2 is located in the cone photoreceptor, and it has 661 residues in the human cone (Prinsen, Szerencsei, & Schnetkamp, 2000). The ratio of the CNG channel and exchanger is about 2:1 ( $600/\mu\text{m}^2:300/\mu\text{m}^2$ ) (Bauer & Drechsler, 1992; Cook & Kaupp, 1988; Cook et al., 1989). NCKX1 forms homodimers in the ROS plasma membrane (Schwarzer, Kim, Hagen, Molday, & Bauer, 1997). When purified channels incubate with purified exchangers, two exchangers bind with two A1 subunits of one CNG channel in western blot (Schwarzer, Schauf, & Bauer, 2000). NCKX1 transports 4  $\text{Na}^+$  inward, and 1  $\text{K}^+$  and 1  $\text{Ca}^{2+}$  outward.  $\text{Ca}^{2+}$  efflux balances the influx movement through the CNG channel in ROS (Cervetto, Lagnado, Perry, Robinson, & McNaughton, 1989; Schnetkamp, Basu, & Szerencsei, 1989).

#### *Electrical Physiology Properties and BI's Modulation Function*

Under normal conditions only 1% of the channels in ROS are open in darkness (Nakatani & Yau, 1988b; Yau & Nakatani, 1985). The advantage of small percentage of channels opening is to decrease the concentration of free cGMP in ROS and to alleviate the affinity of cGMP binding to channels, then finally to shorten the time of activation and recovery (Yau, 1994).

The rod CNG channel's 30-pA dark current is fractioned by 80%  $\text{Na}^+$ , 15%  $\text{Ca}^{2+}$ , and 5%  $\text{Mg}^{2+}$  (Nakatani & Yau, 1988a), and it provides the only source for  $\text{Ca}^{2+}$  influx into the outer segments; about 10-18% of the dark current is carried by  $\text{Ca}^{2+}$  (Kaupp & Seifert, 2002). The unusual feature of the cGMP-gated cation channel, unlike most

ligand-activating channels, is that it does not show any desensitization to prolonged exposure of cGMP. This crucial property allows channels to stay open in darkness and to be stopped only by light (Haynes et al., 1986). The expressed A1 homomeric channel shows the channel's function; however, heterologously expressed B1 have no channel function. When coexpressing A1 and B1, the heterologously expressed channel has functions similar to the native channel. There is only one B1 in the heterotetrameric channel. All evidence introduced indicates that B1 is a modulatory subunit in the rod CNG channel. When B1 is coexpressed with A1, the heterotetrameric channel shows new properties to its A1 homomeric channel. These properties include: more rapid single channel kinetics (flickery phenomenon); 100-fold more sensitive to channel blocker L-cis-diltiazem; ligand sensitivity and selectivity, 10-fold increases in the current activated by cAMP relative to homomeric A1 channel; ionic selectivity; altered ions permeation; blocked by  $\text{Ca}^{2+}$  and modulation by  $\text{Ca}^{2+}$ /CaM. Some properties are found to be related to a special structure in B1 subunit.

*Flickery channel opening and closing.* Flickery is the specific phenomenon of the native channel that channel open-close transition is very brief (Haynes et al., 1986; Taylor & Baylor, 1995; Torre, Straforini, Sesti, & Lamb, 1992). The flicker properties of native channel have been reviewed by Yau and Baylor (Yau & Baylor, 1989). This phenomenon is related to divalent cations blockage (Furman & Tanaka, 1990). It was also found in heterologously expressed hetero-oligomeric rod CNG channels but not in A1 homomeric channels (Chen et al., 1994).

*L-Cis-diltiazem is a channel blocker.* Channel blockers include L-Cis-diltiazem, pimozide, amiloride, tetracaine, polyamines, W-7, H-8, ruthenium, and neomycin (Reviewed by Kaupp and Seifert, 2002). Among them, L-Cis-diltiazem is the most extensively studied channel blocker. It is much more effective when applied intracellularly than extracellularly (Stern, Kaupp, & MacLeish, 1986). Similar to native rod channels, heterologously expressed hetero-oligomeric channels show L-Cis-diltiazem blocking properties which are about 100-fold more sensitive than those of A1 homomeric channels (T. Y. Chen et al., 1993; Korschen et al., 1995).

*Ligand sensitivity and selectivity.* The channels open probability (the gating) depends on the species of bound ligands; the open probability reflects the ligand sensitivity to channel (Finn, Grunwald, & Yau, 1996). Both cGMP and cAMP are ligands of the rod CNG channel. The Rod CNG channel is more sensitive to cGMP than to cAMP. Maximum  $I_{cAMP}/I_{cGMP}$  is around 0.2 in native channels (Tanaka, Eccleston, & Furman, 1989). Similar to native channels, the heterologously (*Xenopus oocytes*) expressed channel that coexpresses A1 and B1 subunits leads to a 10-fold increase in the current activated by cAMP relative to the homomeric A1 channel when comparing maximum  $I_{cAMP}/I_{cGMP}$  (Shammat & Gordon, 1999; Trudeau & Zagotta, 2002a; Zheng et al., 2002).

*Ion selectivity includes alkali ions selectivity,  $Ca^{2+}$  blockage, and permeation.* In native channels, permeability sequence and ratios are as follows:  $Li^+ > Na^+ \sim K^+ > Rb^+ > Cs^+$  1.14:1.0:0.98:0.84:0.58 (Menini, 1990). Coexpression of A1 and B1 subunits heterologously yields almost identical results to native channel (Korschen et al., 1995). Recombi-

nant A1 subunits have similar results; however, the preferring sequence of  $\text{Li}^+$  and  $\text{Na}^+$  are changed (Kaupp et al., 1989). Negative charged glutamate residue is found in the pore loop in the A1 homomeric channel; replacing the residue by neutral residue will abolish the  $\text{Ca}^{2+}$  blockage function (Eismann et al., 1994; Root & MacKinnon, 1993). Coexpression of B1 with the A1 subunit also decreases the  $\text{Ca}^{2+}$  affinity, because the B1 pore loop has a neutral residue glycine instead of negative glutamate (Korschen et al., 1995). In the process of the  $\text{Ca}^{2+}$  permeation,  $\text{Ca}^{2+}$  binds to glutamate residue, blocking the current of monovalent. Comparing the permeability ratio of  $\text{Ca}^{2+}$  to monovalent ( $P_{\text{Ca}}/P_{\text{M}}$ ) between the natural rod CNG channel and the A1 homomeric channel, the ratios are 6.5 and 3.1, respectively. The fraction of  $\text{Ca}^{2+}$  in dark current in the rod CNG channel is between 10% and 18% (Kaupp & Seifert, 2002). The channel's dark current fraction is 80%  $\text{Na}^+$ , 15%  $\text{Ca}^{2+}$ , and 5%  $\text{Mg}^{2+}$  (Nakatani & Yau, 1988a).

*Ca<sup>2+</sup>-CaM modulation.*  $\text{Ca}^{2+}$ -CaM modulation was first found through the B1 subunit in the rod CNG channel in Molday's lab (Chen et al., 1994; Hsu & Molday, 1993, 1994). This modulation can decrease cGMP sensitivity two fold (another expression is two fold increase of the half-activation constant  $K_{1/2}$  in the Michaelis equation). Later on the major and minor  $\text{Ca}^{2+}$ /CaM binding sites for modulation in the N- and C-terminals of channel part of the B1 subunit were discovered (Grunwald et al., 1998; Weitz et al., 1998). The major  $\text{Ca}^{2+}$ /CaM binding site, which play a major role in  $\text{Ca}^{2+}$ /CaM modulation, is in the N-terminal of B1. The accurate position is downstream to GARP and upstream to S1 in bovine and human. The minor  $\text{Ca}^{2+}$ /CaM binding site is in the C-terminal side downstream from CNBD. In bovine, the major  $\text{Ca}^{2+}$ /CaM binding site is restricted to

676-701 amino acids of the entire 1394 amino acids of the B1 subunit (Weitz et al., 1998). The A1 subunit doesn't have a  $\text{Ca}^{2+}$ /CaM binding site, so the homomeric channel of A1 subunits are not modulated by CaM (Chen et al., 1994; Hsu & Molday, 1993; Korschen et al., 1995). The binding of  $\text{Ca}^{2+}$ /CaM in B1 is done more tightly in low cGMP concentration (Gordon, Downing-Park, & Zimmerman, 1995).

*Other modulation of the Rod CNG channel.* Rod CNG channel phosphorylation and dephosphorylation are evidently involved in cGMP sensitivity modulation. ATP inhibition, inhibitors of Ser/Thr phosphatases inhibition, and type1 phosphatase activation are known (Gordon, Brautigan, & Zimmerman, 1992). However, *Xenopus* oocytes-expressed A1 homomers showed different characteristics in inhibition: inhibitors of Ser/Thr phosphatases had no effect in inhibition, whereas inhibitors of phosphotyrosine phosphatases (PTPs), such as orthovanadate and pervanadate, played this function (Molokanova, Maddox, Luetje, & Kramer, 1999; Molokanova, Trivedi, Savchenko, & Kramer, 1997). These findings suggest that B1 is involved in the modulation by phosphorylation/dephosphorylation, but the regulatory mechanisms are not clear.

Besides  $\text{Ca}^{2+}$ /CaM modulation and phosphorylation/dephosphorylation, other modulations in the Rod CNG channel include short-chain analogs of diacylglycerol (DAG) (Gordon, Downing-Park, Tam, & Zimmerman, 1995) and phosphatidyl-inositol 4,5-bisphosphate (PIP2) (Womack et al., 2000). Both of them have inhibition functions to cGMP sensitivity in the rod CNG channel. PIP2 not only inhibits the A1/B1 channel, it also has a weaker inhibition on the A1 monomer, suggesting that the modulation may not be especially related to the B1 subunit.

*Interaction between A1 and B1 subunit*

The C-terminus leucine zipper (CLZ) domain of A1 or A3 is located downstream of CNBD domain with 47 residues. Deletion of the CLZ domain in A3 abolishes 114 C-terminal residues. The CLZ domain can interact with each other in a channel (Zhong et al., 2002). Deletion of 37 amino acids in A1 C-terminal leads to retinal degeneration, because this part interacts with N-terminal 20 amino acids (746-765, upstream from S1 but not including CaM binding site) of B1 subunit. This interaction is assumed to be required for channel targeting to the cell membrane (Trudeau & Zagotta, 2002a). In addition, deletion of 85 residues (608-693) in the C-terminal of A1 shows the same result in this study. Without B1 subunits, heterologous-expressed truncated A1 homomers can be detected in the *Xenopus* oocytes membrane with channel function. The authors suggest that, if not buried by the C-terminal of the A1 subunit, the exposed N-terminal will prevent channel membrane expression. Also A1 N-terminal regions interact with their C linker and CNBD domain. Knocking out of the channel part of B1, the A1 subunit target transportation to the ROS plasma membrane was dramatically compromised, and rod photoreceptor couldn't be detected from this model (Huttl et al., 2005). The bovine N-terminal Ca<sup>2+</sup>/CaM binding site is located in 26 amino acids (676-701) of B1 subunit (Weitz et al., 1998). Another B1 N-terminal and A1 C-terminal interaction is related to the Ca<sup>2+</sup>/CaM binding site in the B1 subunit and the A1 C-terminal. The interaction was prevented by the deletion of the Ca<sup>2+</sup>/CaM binding site or the presence of Ca<sup>2+</sup>/CaM; this result implies a relationship between Ca<sup>2+</sup>/CaM inhibition and N- and C-terminal interaction. In other words, the Ca<sup>2+</sup>/CaM-binding domain of B1 (676-701) either binds to C-terminal A1 (609-693) or binds to Ca<sup>2+</sup>/CaM; this is the reason for Ca<sup>2+</sup>/CaM modulation (Trudeau &

Zagotta, 2002b). So the interactions of the N-terminal of B1 and the C-terminal A1 subunit are not only for membrane targeting of heterotetrameric channel but also for the modulation of channel by  $\text{Ca}^{2+}$ /CaM.

### Rim Proteins and Plasma Membrane Proteins

Rim proteins contain peripherin-2 (rds) (Arikawa et al., 1992; R. S. Molday, Hicks, & Molday, 1987), Rom-1 (Bascom et al., 1992; Moritz & Molday, 1996), ATP-binding cassette transporter ABCR (ABCA4 in retina) (Illing, Molday, & Molday, 1997), and guanylate cyclase (Liu et al., 1994); Plasma membrane contains the cGMP-gated channel (Cook et al., 1989), NCKX1 (Reid et al., 1990), GLUT-1 (Hsu & Molday, 1991) and rhodopsin. Rhodopsin distributes in both disc and plasma membrane (Kamps, De Grip, & Daemen, 1982; Molday & Molday, 1987). The CNG channel is abundant in bovine retinal membranes; it can comprise as much as 6% of the total plasma membrane protein (reviewed by Molday 1999).

Peripherin-2 and Rom-1 have apparent molecular weights of 33 kDa and 37 kDa, respectively, and form disulfide-linked dimers (Bascom et al., 1992; Molday et al., 1987). These two homologous integral membrane proteins share 35% identity (Bascom et al., 1992; Molday et al., 1987). Both proteins are members of the tetraspanin or transmembrane 4 superfamily (TM4SF), because both proteins have the topology of tetraspanin (Connell et al., 1991). Peripherin and Rom-1 form a tightly associated homo or hetero tetramer core via noncovalent association at D2 loops (Goldberg & Molday, 1996; Loewen & Molday, 2000; Loewen, Moritz, & Molday, 2001). Tetramers can link to each other by intermolecular disulfide bonds to form octamers and higher order oligomers

(Loewen & Molday), and a curved disk rim is formed by tetrameric peripherin-rom-1 complex interaction on the opposing membrane side through a disulfide bond (Boesze-Battaglia & Goldberg, 2002). Noncovalent homo- and hetero- tetramerization (without disulfide bonds) of peripherin is required for peripherin targeting to newly formed disk membranes in transgenic tadpole; the checkpoint that prevents the tetramerization-defective proteins from incorporating into nascent disks is the vicinity of the connecting cilium (Loewen, Moritz, Tam, Papermaster, & Molday, 2003). Another paper also shows the formation of peripherin and Rom-1 oligomer (Moritz & Molday, 1996). Peripherin is distributed not only in rims but in incisures (Arikawa et al., 1992; Loewen et al., 2003; Papermaster et al., 1978).

Even though peripherin and Rom-1 are similar in structure and interact with each other, they don't play equivalent roles, and this situation is like the ROS CNG channel A1 and B1 subunits. The well-known rds mice caused by peripherin gene disruption exhibit ablation of ROS (Sanyal & Jansen, 1981), whereas rom-1 knockout mice demonstrate a less severe phenotype, initially forming a disorganized ROS, therefore suggesting that is recessive degeneration in humans for ROM-1 mutation (Clarke et al., 2000). Photoreceptors loss in *Rom-1<sup>-/-</sup>* mice is even slower than that of *peripherin-2<sup>+/-</sup>* mice (Clarke et al., 2000; Hawkins, Jansen, & Sanyal, 1985).

ABCR is a 220-kDa protein and has two ATP-binding cassettes in cytoplasm. It is restricted to the rim region and incisures of the ROS (Illing et al., 1997). ABCR appears to be responsible for the outward directed flippase of N-retinylidene-phosphatidylethanolamine (protonated Schiff base complex of *all-trans*-retinaldehyde and phosphatidylethanolamine) from disk lumen into photoreceptor cytoplasm, finally

accumulating lipofuscin (A2E) in RPE (Weng et al., 1999). Glucose transporter GLUT-1 is present at ROS, implying that it can provide glucose to ROS for energy supply through anaerobic glycolysis (Hsu & Molday, 1991).

#### Channel Subunit-Related Mutations and Knockout Models

Inherited gene defects leading to blindness affect about one in 5000 people, and retinitis pigmentosa (RP) makes up a large percentage. RP impacts rods first with typical symptoms of night blindness, attenuated peripheral vision, and finally impacts cones. RP has three forms, autosomal dominant RP (adRP), autosomal recessive RP (arRP), and X-linked RP (X-RP) (Farber, Heckenlively, Sparkes, & Bateman, 1991; Frederick, Bronson, & Baehr, 2000). More than 100 distinct mutations have been found in rhodopsin; about 30 to 40% of autosomal dominant RP is caused by rhodopsin mutations (Retinal Information Network, 2005). CNGB1 mutation leading to arRP has been found in channel part of the gene (Bareil et al., 2001; Kondo et al., 2004), but there is no evidence in the GARP part. Possible pathogenic sequence changes have been found in Dr. Pittler's lab, but the families were too small to establish segregation (personal contact). Five mutant sequences of CNGA1 has been found to cosegregate with arRP (Dryja et al., 1995). Defects in CNGA3 and CNGB3 causing color blindness have been found (Kohl et al., 2000, 1998). Mutations causing RP or other phenotypes have also been found in other rim, disk, and plasma proteins of ROS, such as rhodopsin (Dryja et al., 1990), peripherin (Dryja, Hahn, Kajiwara, & Berson, 1997; Kajiwara et al., 1991), peripherin and Rom-1 digenic mutations (Dryja et al., 1997; Kajiwara, Berson, & Dryja, 1994), Rom-1 (Martinez-Mir et al., 1997), PDE6 $\alpha$  (Huang et al., 1995), PDE6 $\beta$  (McLaughlin,

Sandberg, Berson, & Dryja, 1993), guanylate cyclase (Kelsell et al., 1998), T $\alpha$  (GNAT1, phenotype of congenital stationary night blindness) (Dryja, Hahn, Reboul, & Arnaud, 1996), and ABCA4 (Cremers et al., 1998). No pathogenic mutations definitely associated to retinal degeneration have been established in the NCKX1 gene (Sharon et al., 2002).

Corresponding mouse gene knockout models have been created in the laboratory as follows: CNGB1 (Huttl et al., 2005), CNGA3 (Biel et al., 1999), rhodopsin (Humphries et al., 1997), Rom1 (Clarke et al., 2000), ABCA4 (Weng et al., 1999), GC-E (GUC2D) (R. B. Yang et al., 1999), T $\alpha$  (GNAT1) (Calvert et al., 2000), and PDE $\gamma$  (Tsang et al., 1996); gene mutation of PDE $\gamma$  hasn't been associated with RP.

Naturally occurring gene knockout animal models are as follows: PDE6 $\beta$  (rd or rd1 mice) (Pittler, Keeler, Sidman, & Baehr, 1993); peripherin-2 (rds or rd2 mice) (Connell et al., 1991; Travis, Brennan, Danielson, Kozak, & Sutcliffe, 1989); and PDE6 $\alpha$  (Cardigan Welsh corgi dog) (Petersen-Jones, Entz, & Sargan, 1999).

#### Effects of Genetic Modifiers on Human Disease and Mouse Gene Knockout Model

Genetic modifiers are the gene loci that affect the phenotypic result of a given genotype by interaction in the same or a parallel biological pathway. They can either enhance or alleviate the phenotype of the disease, even restore the wild-type phenotype. They can also alter the traits of the disease (Pacione et al., 2003). A single-gene mutation or knockout should be in a permissive genetic background to demonstrate a disease genotype, otherwise a combination of modifier genes may act together to create a cumulative effect on phenotypic expression (Haider, Ikeda, Naggert, & Nishina, 2002). A typical example of modifier genes of human inherited photoreceptor degeneration is the digenic RP

caused by unlinked mutations at peripherin-2 (L185P) and Rom1 (three different mutations), whereas a single allele mutation has no or minimal abnormalities (Dryja et al., 1997; Kajiwara et al., 1994). The evidence of modifier genes in mouse inherited photoreceptor degeneration was shown in the rhodopsin knockout model (Humphries et al., 2001). When comparing the rhodopsin knockout mice in the C57BL/6J background with the 129Sv background, the C57BL6 background shows protected effects due to unknown genetic modifiers. Very few genetic modifiers loci have been chromosomally localized, although many studies are reporting the phenotypic variability.

#### Technologies to Produce Genetically Altered Animal

Transgenic technique incorporates a transgene construct, often containing a mutation linked to disease, into a mouse or other animal's genome; the mutant transgene will only be expressed in a specified tissue or cells and transmitted to the progeny. The corresponding gene can express normally in homozygote knockout genotype. Knockout is a technique of replacing part of a gene by targeting a construct in the process of homologous recombination that disrupts the expression of the gene. The normal gene is absent in a homozygote knockout genotype. Knockin is a technique similar to knockout; the difference is the targeting construct. Instead of a nonfunctional targeting construct in knockout technique, the knockin targeting construct is part of the targeting gene containing a mutation. A conditional knockout is used when a universal knockout of the gene is lethal during embryonic development. The first step is using *loxP* sites to flank the targeting construct for replacement; Cre recombinase is expressed in desired cell types in the second step by transgenic technique; finally cre recombinase excises the genomic DNA flanked

by *loxP* (Frederick et al., 2000). The *Cngb1*<sup>-/-</sup> mouse model studied here is a product of a standard knockout technique.

## ERG History and Major Components Origin

### *History of ERG*

The electroretinogram (ERG) is a complex field potential evoked by light. The field potential is generated by the electrical responses of retinal cells. Therefore ERG can provide an efficient and effective noninvasive screen of retinal function in the knockout mice. Three major waves, the a-wave, b-wave, and c-wave, construct the basic waveform of ERG. Additional minor components of ERG, the d-wave, the oscillatory potentials (OPS), the M-wave, the early receptor potential (ERP), and the scotopic threshold response (STR), can also be observed in special conditions. The order of a, b, c, and d also reflects the timing of the appearance of these waves in ERG.

ERG was first discovered by Holmgren in 1865 in an experiment on living frog eye in Sweden. Independent similar findings were reported by Dewar and M'Kendrick in 1873 in Scotland. Gotch (1903) first reported the corneal negative wave (a-wave) followed by the larger cornea positive wave (b-wave). In 1908, the corneal positive c-wave was found, and all major components of a, b, and c waves were shown in one graph by Einthoven and Jolly. The corneal positive d-wave was an off effect found by Piper in 1911. Ragnar Granit (1933) discovered P-I, P-II, and P-III processes that disappeared sequentially when the anesthesia was deepened in cat. The fundamental findings of P-I, P-II, and P-III provided a basis for the study of ERG components origin (Armington, 1974). Based on the experiment of Granit in 1933, the negative a-wave is the leading edge of the

negative P-III component; the b-wave (above baseline) is the summation of P-II and P-III; and the c-wave reflects the summation of P-I and P-III.

#### *The a-wave Originates in Photoreceptors*

Intraretinal ERG proved that the a-wave (fast P-III or leading edge of P-III) originates in the photoreceptor layer (Brown, 1968). It reflects the reduction of dark current in photoreceptors due to the closure of cGMP-gated cation channels under light condition, because the “light” current exiting OS and reentering the IS corresponds to the a-waveform and sign (Penn & Hagins, 1969). L-aspartate and 2-aminoethoxydiphenyl borate (APB) are competitors of the photoreceptor neurotransmitter, glutamate. Using either L-aspartate, APB, or glutamate, synaptic transmission from the photoreceptors to the postsynaptic neurons can be blocked. An example using L-aspartate for isolating photoreceptors from neuroretina is the Peperberg experiment (Peperberg, Brown, Lurie, & Dowling, 1978). The a-waveform is affected by P-II (or b-wave).

#### *The b-wave's Origin*

The corneal positive b-wave measured from base line to peak is the summation of P-II and P-III. If measured from trough to peak, it reflects the postsynaptic response P-II but less estimated because actual P-III is larger than the leading edge of P-III (Hood & Birch, 1990a, 1992). The first evidence that the b-wave is mainly contributed by depolarized ON-bipolar cells is from the pharmacological blocking transmission between photoreceptors and ON-bipolar cells. When metabotropic glutamate receptors are blocked in ON-center bipolar cell, b-wave is eliminated. The agonists used for blocking me-

metabotropic glutamate receptors include L-aspartate (Pepperberg et al., 1978), APB, and glutamate (Gurevich & Slaughter, 1993). The APB-sensitive metabotropic glutamate receptors are only found in ON-bipolar cells (Slaughter & Miller, 1981). The second evidence is from mGluR6 knockout mouse. Neurotransmitter receptor mGluR6 is located in ON-bipolar cells and receives the signal from the photoreceptor. Targeted disruption of mGluR6 also eliminates the b-wave (Masu et al., 1995). The third evidence is that the blockage of  $K^+$  permeability on the Müller cell by barium ions didn't decrease the b-wave (Lei & Perlman, 1999). Barium ions can block the  $K^+$  permeability (the inward and outward currents) of Müller cells (Linn, Solessio, Perlman, & Lasater, 1998; Newman, 1989). The  $Ba^{2+}$  blockage experiment excludes the possibility that  $K^+$  currents carried by Müller cells are responsible for the characteristic corneal positive b-wave, but the  $K^+$  current carried by Müller cells is responsible for slow P-III, which actually decreases the positive b-wave (Lei & Perlman).

The b-wave also contains minor contributions from other cell sources. The Müller cell can contribute a negative component to the b-wave. Using glutamate receptors blocker L-aspartate and APB, slow P-III can be studied in the neuroretina in isolated P-III process. The decreased  $K^+$  concentration in the extracellular space of hyperpolarized photoreceptors, and the increased  $K^+$  concentration of the inner and outer plexiform layers, lead to Müller cell transmembrane potential changes, which are expressed as slow P-III (Witkovsky, Dudek, & Ripps, 1975).  $Ba^{2+}$  blocks  $K^+$  channels in the Müller cell, therefore eliminating slow P-III and increasing b-wave (Green & Kapousta-Bruneau, 1999; Lei & Perlman, 1999). OFF-bipolar cells can contribute with a minor signal that is opposite to ON-bipolar cells; this is a "push-pull model" of the bipolar cell (Sieving, Mu-

rayama, & Naarendorp, 1994). Other postsynaptic signals from inner retina also affect the final b-waveform. Antagonists of third-order neuron receptors can have different effects. When the gamma aminobutyric acid (GABA) a-type receptors or glycine receptors are blocked by bicuculline or strychnine, the amplitudes of the b-wave are increased (Dong & Hare, 2000; Kapousta-Bruneau, 2000). On the other hand, when the GABA<sub>c</sub>-type receptors are blocked by 3-aminopropylphosphono acid (3-APMPA), the b-wave signal is reduced (Kapousta-Bruneau, 2000). If the third-order neurons are disrupted mechanically, the b-wave will be enhanced (Awatramani, Wang, & Slaughter, 2001). In general, postsynaptic third-order neurons only make minor contribution to the b-wave; most likely, the summarized contribution is corneal negative.

#### *The c-wave Originates in Retinal Pigment Epithelium (RPE) Cells*

The c-wave is normally elicited by a 40-s stimulus under direct current (DC). The c-wave comes from the P-I component but is also affected by slow P-III. The direct evidence comes from an intraretinal recording in RPE cell where the waveform is identical in shape and temporal properties to c-wave (Steinberg, Schmidt, & Brown, 1970). When the retina is separated from the RPE cell, the c-wave disappears, only a- and b-wave are present (Pepperberg et al., 1978). The RPE cell's apical membrane is more permeable to K<sup>+</sup> than basal side that cause positive potential in apical membrane (retinal side) and negative potential in basal side (choroidal side). The reduction of extracellular K<sup>+</sup> due to photoreceptor hyperpolarization leads to increased transmembrane potential, and the apical membrane is more positive relative to the choroidal side. Therefore, K<sup>+</sup> ERG (KRG) shows similar shape and temporal characteristics to c-wave. The c-wave can also be used

to assess the function of photoreceptors, since c-wave depends on  $K^+$ , which is caused by photoreceptor hyperpolarization (Oakley, 1977; Oakley & Green, 1976). In addition to b-wave, c-wave is also contributed by corneal negative slow P-III generated by Müller cells.

#### *Other Minor ERG Components' Origin*

The d-wave is the corneal positive signal seen in the light offset when the light duration is longer than 100 ms. It originates in OFF-bipolar cells because current source-density analysis locates its source to be the OFF-bipolar cell (X. Xu & Karwoski, 1995). Furthermore, the d-wave can be eliminated by receptor blocker in OFF-bipolar cells (Gurevich & Slaughter, 1993; Sieving et al., 1994).

The oscillatory potentials (OPS) are the high-frequency oscillating waves on the rising phase of the b-wave under bright light. Those 4-6 wavelets with 100-150 Hz frequencies can be seen under a band-pass filter (Asi & Perlman, 1992). Evidence shows that OPS are generated in inhibitory postsynaptic neurons, most likely amacrine cells and bipolar cells (Heynen, Wachtmeister, & van Norren, 1985; Wachtmeister & Dowling, 1978).

The early receptor potential (ERP) occurs in very bright light and ends within 1.5 ms before a-wave. ERP is believed to originate in photoreceptors (Murakami & Pak, 1970).

The scotopic threshold response (STR) is the corneal negative wave, which is recorded with dim light close or lower than rod threshold. STR originates in Müller cells (Frishman & Steinberg, 1989). STR has been found in human and rat, but there are no reports on mice so far.

In light-adapted conditions, M-wave with characteristic ON and OFF negative waves can be seen. M-wave also originates in Müller cells (Karwoski, Lu, & Newman, 1989).

#### Dark Current and Channels on Photoreceptors

In rod photoreceptors, the channels of cGMP-gated cation channels (CNGC1) and NCKX1 on the ROS plasma membrane have been reviewed in CNGB1 section. NCKX1 is an  $\text{Na}^+$ -gated channel not affected by voltage; the ratio of ions is 4  $\text{Na}^+$  in and 1  $\text{Ca}^{2+}$  and 1  $\text{K}^+$  out. About 1% CNGC1 opens in darkness on the outer segment of the plasma membrane. In darkness, the inward current of CNGC1 consists of 80%  $\text{Na}^+$ , 15%  $\text{Ca}^{2+}$ , and 5%  $\text{Mg}^{2+}$ , and it is also permeable to  $\text{K}^+$ . This inward current to ROS leads to depolarization of the photoreceptor, with the interior more negatively charged than the exterior of the plasma membrane. The rest potential is -40 mV. The CNGC1 makes a major contribution to inward current versus NCKX1. The rod inner segment (RIS) has two voltage-gated  $\text{K}^+$  channels: Kx channel effluxes  $\text{K}^+$  in the depolarized state; h channel influxes  $\text{K}^+$  in the hyperpolarized state. These two  $\text{K}^+$  channels play a role for light adaptation. In darkness, inner segment Kx and outer segment CNGC1 form a circulating loop called dark current (Barnes, 1994). Normal dark current is 30 pA. The energy source comes from ATP consumed by the inner segment Na/K exchange pump, which pumps 3  $\text{Na}^+$  out and 2  $\text{K}^+$  in; in this process, ions are transported against their electrochemical gradient. Dim or very bright light causes CNGC1 to partially or completely close; therefore dark currents decrease or stop. This results in an “outward” current opposite to inward dark current, and the photoreceptors hyperpolarizing. The maximum hyperpolar-

izing potential is -70 mV. The rod photoreceptor can detect only one photon; this was proved in the suction electrode recording of a monkey rods experiment. The pulse of light contained a few photons, and the response signals were shown as none, smaller, or larger amplitude. The small signal came from single photon stimulation (Tucker, Chang, Prince, Gillespie, & Mapstone, 1998). Even one photon can elicit photocurrent about 1 pA with 50% possibility; it is 3-5% of saturated photocurrent or dark current (30 pA). Single CNGC1 channel current is 3 fA; this ensures the smooth effect of a single photon. The advantages of having only a 1% CNGC1 channel open in darkness are that it prevents ATP depletion and aids in light adaptation (Baylor, 1987). The photocurrent is reverse to dark current. Fast P-III reflects the photocurrent after light, and the a-wave is the initial phase of fast P-III, so the ERG a-wave reflects the photocurrent in light (Hagins, Penn, & Yoshikami, 1970; Penn & Hagins, 1969). Single-rod ERG can detect one photon-elicited photocurrent (Baylor et al., 1979). The inner segment has other channels, such as voltage-gated  $\text{Ca}^{2+}$  channel and  $\text{Cl}^-$  channel. The voltage-gated  $\text{Ca}^{2+}$  channel activates the  $\text{Cl}^-$  channel and controls glutamate release in IRS when photoreceptors are hyperpolarized (Barnes, 1994).

#### Isolating Rod- and Cone-Mediated Responses from Mouse

Mouse retina has  $6.4 \times 10^6$  rod cells (Jeon, Strettoi, & Masland, 1998; Lyubarsky, Daniele, & Pugh, 2004) and occupies 96.5% to 97% of total photoreceptors. The remaining 3 to 3.5% of the total photoreceptors are cones (Carter-Dawson & LaVail, 1979). The cone proportion in mouse is slightly lower than in human (4.8%, 4.6 million cones over 92 million rods) (Curcio et al., 1990) but higher than rat (1.5%) (Carter-Dawson &

LaVail, 1979). The mouse retina doesn't have fovea centralis or a visual streak. Most mammalian rhodopsin has a maximum absorbance at around 500 nm, such as human, macaque, bovine, dog, rat, mouse and rabbit; mouse, has a peak absorbance at 498 nm (Yokoyama, 2000). By in situ measurement of absorbance difference spectra, mouse rhodopsin's maximum sensitivity is at 510 nm (Goto, Peachey, Ripps, & Naash, 1995). The mouse rhodopsin has a known maximum spectrum of 498 nm and an ERG peak sensitivity of 498 (Lyubarsky, Falsini, Pennesi, Valentini, & Pugh, 1999) to 503 nm (Calvert et al., 2000), which is very close to M/L cone pigment with a maximum spectrum at 508 nm (Sun, Macke, & Nathans, 1997) and ERG peak sensitivity at 511 nm (Jacobs, Neitz, & Deegan, 1991). Another cone pigment (UV cone pigment) has a peak sensitivity of 360 nm (Jacobs et al., 1991; Lyubarsky et al., 1999). Compared with human photopigments, rhodopsin and L-, M-, and S-cone pigments have maximum spectra at 498, 534, 563, and 420 nm, respectively (Bowmaker & Dartnall, 1980).

A common method used to separate rod and cone response is based on spectral sensitivity in human. A short-wavelength flash ( $\lambda_{\max} = 470$  nm, half-bandwidth = 55 nm) -elicited response is assumed mainly from rod photoreceptors but still contains a minor portion of cone response. When short-wavelength stimuli are above 0.75 log scot td-sec the cone component is countable. However, the long-wavelength flash ( $\lambda_{50\% \text{ cut-on}} = 605$  nm) -elicited response is assumed mainly from cone photoreceptors but still contain a minor portion of rod response. The rod-isolated response is obtained by subtracting the photometrically matched long wavelength stimulus from the mixed rod and cone response in short wavelength; cone-isolated response is obtained by subtracting the scotopically matched short wavelength response from mixed rod and cone responses in

long wavelength (Birch & Fish, 1987; Hood & Birch, 1990a, 1990b). Since mouse rod and cone has similar spectrum sensitivity in ERG (498 and 511 nm), the spectral method is not suitable to distinguish rod and cone systems.

Another common method to separate cone response from rods is by desensitizing the rod photoreceptor (or saturating the rod photoreceptors). Since rod pigment is about 3 log units more sensitive than M-cone pigment, two methods are applicable, the double flashes method and the background method. The background method is to elicit response by a stimulus against a steady rod-desensitizing adapting field; the response is supposed to be a cone-isolating response. The background method had been compared to the spectral method; cone response separation had similar results using these two methods (Birch & Fish, 1987; Hood & Birch, 1990a). The adapting field usually is 3.2 log photopic td or 3.4 log scot td. A similar background method to desensitize rods and isolate cones has also been confirmed by a spectral method in a different lab (Peachey, Alexander, & Fishman, 1989). They used 1.34 log  $\text{cd}/\text{m}^2$  ( $21.7 \text{ cd}/\text{m}^2$ ) achromatic background light during a 10-min period of light adaptation. The background method under a certain luminance ( $20\text{-}40 \text{ cd}/\text{m}^2$ ) by white light lasting 7-10 min before stimuli can be used in mouse, just because it is a good method in human (Peachey et al., 1989; Peachey, Goto, al-Ubaidi, & Naash, 1993). The background light can be  $200\text{-}800 \text{ cd}/\text{m}^2$  white light; increasing the background light decreases the amplitude of b-wave response (Ekesten, Gouras, & Moschos, 1998). Increasing either the time and intensity of background light can decrease the implicit time of b-wave in mouse, because cone ERG is suppressed under dark-adapted conditions in human (Peachey, Alexander, Derlacki, & Fishman, 1992b). Lyubarsky et al. simplified the background method by decreasing the background (520

nm) duration to 2 s before probe flash. Also 3000-6000 R\*/rod per s is sufficient to saturate rod photocurrent (Lyubarsky et al., 1999). A single flash producing  $2.8 \times 10^5$  R\*/rod is sufficient to elicit maximum photoresponse in ERG (Lyubarsky & Pugh, 1996).

The double flash approach is a popular method used in isolating cone-driven ERG. A probe flash is preceded by a condition flash, which is intense enough to saturate rod response (Lyubarsky et al., 1999, 2001).

Critical fusion frequency (CFF) is another experimental approach to separate rod-mediated vision from cone-mediated vision based on the relatively slower temporal properties of rod compared to cone. The rod or cone component will cancel each other in a certain frequency. The typical b-wave peak is 60 ms for rod and 30 ms for cone. Under lighting conditions, signals from rods may arrive as much as 1/10 of a s later than those from cones, so both can be simultaneously activated (MacLeod, 1972). The relatively slow rod response will make rod CFF smaller than cone CFF. Rod's maximal flickering frequency is about 15 Hz; with more careful recording it can reach 28 Hz (Conner & MacLeod, 1977; Stockman, Sharpe, Ruther, & Nordby, 1995). However, cone vision can perceive 30-50 Hz bright stimuli (Conner & MacLeod, 1977). Therefore a 30-Hz frequency is a classic frequency to isolate the cone system in flickering ERG (Peachey et al., 1992b).

#### Sensitivity of Rod Photoreceptor

The Naka-Rushton function expressed as  $R/R_{\max} = I^n/(I^n + k^n)$  is a hyperbolic equation to study the relationship between light intensity and ERG response. In this equation, R is the response under stimulus intensity I;  $R_{\max}$  is response under super-saturating

stimulus;  $K$  is a semisaturation constant, which is the stimulus intensity required to elicit half-maximal response; and  $n$  is an exponent describing the slope of the function. This equation was used in human ERG as early as 1978;  $n$  is 1 in that study (Fulton & Rushton, 1978). When  $n = 1$ , the Naka-Rushton function is also called the Michaelis-Menten function. Naka-Rushton is the general form of Michaelis-Menten with the third parameter exponent  $n$  (Hood, 1998). Later on, this equation was used in other studies (Birch & Fish, 1987; Hood & Birch, 1990a, 1992; Peachey et al., 1989). The a-wave amplitude is measured from baseline to the trough of the a-wave; the b-wave is measured from the trough of the a-wave to the peak of the b-wave. The function has been widely applied to fit stimulus intensity and the b-wave amplitude. Since the light stimulus intensity and b-wave response curve are not monotonic, in the moderate intensity the curve is flat, but when the light intensity is very high, the b-wave amplitude increases and finally is saturated. The typical intensity-response curve shows two limbs. The two-limb curve is an artifact of the interference destruction of b-wave in a certain range of light intensity when P-III and P-II increase at same amplitude. Fitting the lower limb can be used for rod photoreceptor study in some papers (Toda, Bush, Humphries, & Sieving, 1999), but some authors think that is not enough, because the higher limb most likely reflects the rod function (Peachey et al., 1989). An isolated rod b-wave fitting will be much more reasonable in human (Hood & Birch, 1990a); however, the isolation method in human is not permitted in mouse, because mouse rod and M/L-cone have similar spectral sensitivity (498 and 511 nm, respectively). Since rod is about 3 log units more sensitive than cone, the cone component can be counted only three log units after the rod threshold (Birch & Fish, 1987). Fitting all lower light intensity b wave responses and calculated rod maximum re-

response (see methods) to Naka-Rushton function will closely reflect real rod intensity-response. The b-wave is supposed to be a postsynaptic signal, but because we measured from the a-wave trough to the b-wave peak, this measurement is larger than P-III + P-II and less than P-II in moderate light intensity. The b-wave reflects both photoreceptor and postsynaptic response (Hood & Birch, 1992). Also, if the photoreceptor completely degenerates, the ERG is extinguished. That means that the b-wave mostly reflects post-photoreceptor retinal response, but it also indirectly reflects the driving force of the photoreceptor. This is the reason we study retinal degeneration by calculating b-wave K-value, which can be used as an index of rod sensitivity.

#### Photoreceptor Degeneration, Equivalent-Light Hypothesis, and Recovery Kinetics

Photoreceptor death may be caused by different mechanisms, such as elevated  $Ca^{2+}$  and cGMP in ROS, disruption of the structure of photoreceptors, and constitutive real- or equivalent-light activation of transduction cascade are three major candidates (Fain & Lisman, 1999; Frasson et al., 1999). Increased  $Ca^{2+}$  or cGMP may lead to retinal degeneration, as has been shown in PDE6 $\beta$  and GCAP1 Y99C mutations (Farber, 1995; Sokal et al., 1998). An example of the disruption of the outer segment structure can be seen in peripherin-2 mutation mice, due to peripherin-2 is a disk rim protein (Sanyal & Jansen, 1981). A possible reason for photoreceptor death may be oxygen toxicity (Travis, 1998). There is no doubt real light leading to retinal degeneration, since exposing an animal to continuous light for long time leads to photoreceptor degeneration that results in blindness (Noell, Walker, Kang, & Berman, 1966). The equivalent-light hypothesis was proposed by Lisman and Fain (Fain & Lisman, 1993; Lisman & Fain, 1995). This hypothesis

states that the photoreceptor death caused by the constitutive activation of the phototransduction cascade may be equivalent to continuous real light exposure. The deep reason for photoreceptor death in the hypothesis may be lower  $\text{Ca}^{2+}$  concentration, raised  $\text{O}_2$  tension, and toxicity because of low  $\text{O}_2$  consumption and disrupted vital circadian process (Fain & Lisman, 1993, 1999; Travis, 1998). In some animal models of retinal degeneration, phototransduction cascade are activated constitutively, which support the equivalent-light hypothesis: RK and arrestin knockouts compromise the deactivation of  $\text{R}^*$  and the recovery kinetics of rhodopsin (C. K. Chen et al., 1999; J. Chen, Simon, Matthes, Yasumura, & LaVail, 1999); mutations of the CNGA1 subunit and GC1 also result in similar effect of continuously presenting of light (Dryja et al., 1995; Semple-Rowland, Lee, Van Hooser, Palczewski, & Baehr, 1998); vitamin A deprivation and RPE65 knockout lead to a decreased concentration of rhodopsin and an increased concentration of opsin, which has an activation function about  $10^{-(6-7)}$   $\text{R}^*$  (Fain & Lisman, 1993; Fan, Woodruff, Cilluffo, Crouch, & Fain, 2005). In arrestin, RK, RPE, or other gene knockout that abnormally extend the life of  $\text{R}^*$  or increase opsin concentration definitely delayed the recovery kinetics of ERG (Birch et al., 2001; Chen, Burns et al., 1999; Lyubarsky, Chen, Simon, & Pugh, 2000; Nusinowitz et al., 2003). A study of recovery kinetics will further clarify the mechanism of retinal degeneration in our *Cngb1*<sup>-/-</sup> mouse model and find the potential protein interaction between *Cngb1* products and proteins that affects recovery. We have known that GARP proteins (including *Cngb1*) interact with peripherin-2/rom-1 oligomer, NCKX1, CNGA1, and PDE6 (Korschen et al., 1999; Poetsch et al., 2001); so recovery kinetics study may reveal direct or indirect interactions of GARP proteins with other proteins that affect recovery, such as deactivating proteins of  $\text{R}^*$  and  $\text{T}\alpha$ -GTP-PDE6 complex,

proteins involved in *11-cis* retinal cycle. A double-flash method for recovery is an easier method used in some studies (Fulton & Hansen, 2003; Hansen & Fulton, 2005; Lyubarsky et al., 2001).

#### Hypothesis (Research Plan)

A summary of introductory material gives us the reasonability to make a 5'-end *Cngb1* gene knockout mouse model. The cyclic GMP-gated cation channel (CNGC1) is located in the plasma membrane in rod photoreceptors and plays an important role in the phototransduction cascade. Liganded by cyclic GMP, CNGC1 opens or closes in dark or light. This channel has a  $3\alpha:1\beta$  stoichiometry. The  $\alpha$ -subunit is a functional subunit when expressed heterologously, whereas the  $\beta$ -subunit plays a modulatory role. So far there is no complete cDNA sequence in the NCBI gene bank. The mutations in the  $\alpha$ -subunit and the channel part of the  $\beta$ -subunit can lead to retinal degenerations, but not in the GARP part. Although some pathogenic sequence changes were found in the GARP part in RP cases, the family was too small for segregation. The *Cngb1* channel part knockout mouse model has been set up recently (Huttl et al., 2005). In this model the exon 26 (expressed as pore loop region) was knockout; the degeneration was slight in one month; the electrical physiology of rod photoreceptor was impaired severely. In order to clarify free GARPs and the  $\beta$ -subunit's functions in rod photoreceptor, we made the 5'-end *Cngb1* knockout mouse in inGenious Targeting Laboratory, Inc., Stony Brook, NY. We set out to answer the following questions:

1. Does this gene knockout design affect other genes in the vicinity?
2. Is this "knockout mouse" a true *Cngb1* gene knockout mouse for further study?

3. What is the entire *Cngbl* gene cDNA sequence? What is the structure map of *Cngbl* and alternative splicing products in mouse?
4. Are other genes' expressions in the rim region or the plasma membrane affected after *Cngbl* gene knockout?
5. What is the general phenotype outside of the eye of our *Cngbl*<sup>-/-</sup> mouse?
6. What are the morphological changes in the photoreceptor in the *Cngbl*<sup>-/-</sup> model?
7. What are the ERG changes of a- and b-wave in a 4-month period?
8. Does rod degenerate faster than cone?
9. What is the sensitivity difference between knockout (KO) mice and wild-type (WT) mice?
10. Are the rod recovery kinetics of rod affected after *Cngbl* knockout?

Through comparing our 5'-end *Cngbl* knockout mouse with the 3'-end knockout mouse in general phenotypes, retinal morphology, and electrophysiology, we can further understand the function of GARP proteins (including the GARP part of *Cngbl*) in some fields, such as disk morphogenesis, a structural role for stability of disks, and the activation and deactivation of the phototransduction cascade. This new model also helps us to identify the degeneration classification, in which equivalent light is a common reason (Fain & Lisman, 1993).

## METHODOLOGY

### Generation of *Cngbl* Knockout Mice

Genomic fragments spanning the promoter region and exons 3-10 were amplified by polymerase chain reaction (PCR) as short and long arm from the 129/sv mouse genomic DNA library. These fragments, 1.4 kb and 7 kb in length, respectively, were cloned into vector p*Cngbl*-KO flanking the 1.8-kb neomycin resistance (Neo) cassette to generate targeting vector. Ten micrograms of targeting vector was linearized by restricted enzyme Not I and transfected by the electroporation of the 129 SvEv embryonic stem cells for homologous recombination (Figure 1). After selection in G418, neomycin-resistant colonies were expanded. PCR was done using primer pairs CNGSA6 and NEO1 to verify the successful homologous recombination. Primer CNGSA6 is located 80 base pairs (bp) upstream to short arm with a sequence 5'-GAAGAGCCTACCTTGGAAGCAGAG-3', and primer Neo1 is located in the phosphoglycerate kinase (PGK) promoter region of the Neo gene cassette with the sequence 5'-TGCGAGGCCAGAGGCCACTTGTGTAGC-3'. Targeted cloned ES cells were injected into C57BL/6 blastocysts, which were implanted to a foster mother (C57BL/6) to generate chimeras. After crossing with wild-typed C57BL/6 mice, the stable heterozygotes were derived. The genotypes of mice were determined by PCR. All manipulations of ES cells and the establishment of mouse chimeras were done at inGenious Targeting Laboratory, Inc., Stony Brook, NY. The knockout mice were produced on hybrid backgrounds of C57BL6 and 129SvEv. Crossing of heterozygote mice produced

## Strategy for Targeted Deletion of *Cngb1*

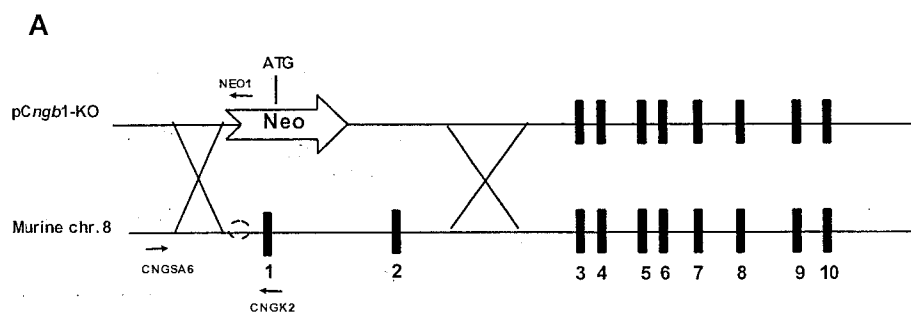


*Figure 1.* Schematic of genome deletion strategy. The targeting plasmid p*Cngb1*-KO contains a Neo cassette flanked by a 1.4-kb short arm and a 7-kb long arm of *Cngb1* excluding 3.5 kb of genomic sequence, including a presumed promoter (dotted circle) and exons 1 and 2. The Neo cassette is a 1.8-kb construct consisting of phosphoglycerate kinase (PGK) promoter, neomycin phosphotransferase (neomycin resistance), and PGK polyA signal. The first ATG of the protein coding region for all three protein products (GARP-1, GARP-2, and  $\beta$ -subunit) is located within exon 2. CNGSA6, CNGK2, and NEO1 (indicated by the direction of arrows) are three primers used in multiple PCR.

wild-type, heterozygote, and homozygote knockout mice. All experimental procedures were done in compliance with National Institutes of Health guidelines, as approved by the Institutional Animal Care and Use Committees of the University of Alabama at Birmingham.

### Genomic PCR for Genotyping

Mice tails were cut and genomic DNA was extracted following the DNA purification kit instruction manual (Promega, Madison, WI). Tag polymerase was used in amplification following the instruction manual (Promega). The PCR profile was as follows: denaturation at 94 °C for 5 min, 32 cycles with 94 °C for 45 s, 61 °C for 45 s, 72 °C for 1 min 45 s, and 72 °C for 7 min. Products were visualized by ethidium bromide staining and separated in 1% agarose gel. Primers were designed under Generunner software (Hastings, Inc. Hackensack, NJ). The multiplex PCR contains a forward primer CNGSA6 and two reverse primers, CNGK2 (on exon 1 of wild-type allele with a sequence 5'-TGTCAGCGGCTAGCCAGGAA-3') and NEO1 (on Neo cassette of knockout allele). PCR products 1.8 kb and 1.6 kb will be found in wild-type and knockout mice, respectively. The sequences of primers are shown in Table 1.

### RT-PCR Analysis of Transcription Level of *Cngbl*, Neo, and Other Genes

Extraction and reverse transcription (RT) of messenger ribonucleic acid (mRNA) were done following the protocols of Ambion's RT-PCR kit (Ambion, Austin, TX). One mouse eye was used in mRNA extraction from each genotype of mouse. DNase was used after mRNA extraction to digest genomic DNA. Around 1.5 µg template mRNA was

Table 1

*PCR and Sequencing Primers Designed and Used*

Name	Sequence (5'-3')	Forward (F)/ Reverse (R)	Gene or vector	Position and accession number
CNGSA6	GAAGAGCCTACCTTGGAAGCAGAG	F	<i>Cngbl</i>	Promotor
NEO1	TGCGAGGCCAGAGGCCACTTGTGTAGC	R	Neo cassette	PGK promotor
CNGK2	TGTCAGCGGCTAGCCAGGAA	R	<i>Cngbl</i>	Exon1 BC016201
ME4F	GGTTGCTGTTGCCAAGGTGA	F	<i>Cngbl</i>	Exon4 BC016201
ME4R	TGTTACCTTGGCAACAGCA	R	<i>Cngbl</i>	Exon4 BC016201
ME8F	TGGCTTGAGCAGAATCTGGA	F	<i>Cngbl</i>	Exon8 BC016201
ME9R	AGACAGCAGCCTCAGGTTCA	R	<i>Cngbl</i>	Exon9 BC016201
ME12F	CCTGGGATGTGTGACGTACA	F	<i>Cngbl</i>	Exon12 BC016201
ME12aR	AGGTCCCCTCTCCCTTGTTT	R	<i>Cngbl</i>	Exon12aBC016201
ME13R	TGTTCCACGGGGAGGATGCT	R	<i>Cngbl</i>	Exon13 XM-286113
ME15R	CTAGCTCTGACGGTGTCTT	R	<i>Cngbl</i>	Exon15 XM-286113
ME15F	TTGGTGGTGCAGGCTGATGT	F	<i>Cngbl</i>	Exon15 XM-286113
ME18F	CGAAGAGCTCAAGGCCCTGT	F	<i>Cngbl</i>	Exon18 XM-286113
ME18R	TGGTGACAGGGCCTTGAGCT	R	<i>Cngbl</i>	Exon18 XM-286113
ME21R	GCCACAAGATGTACATGAGG	R	<i>Cngbl</i>	Exon21 XM-286113
ME26R	CAGCCCAGTAGTAGCATCGA	R	<i>Cngbl</i>	Exon26 XM-286113
ME27F	GGACAGCACAGTGAAGTACA	F	<i>Cngbl</i>	Exon27 XM-286113
ME30R	CCGCCTGGATAATGTACATC	R	<i>Cngbl</i>	Exon30 XM-286113
ME33R	TCTCCCCCAGCTTCTTGCGA	R	<i>Cngbl</i>	Exon33 XM-286113
RCC54	TCAGGATGTTGGGCTGGGTCCA	F	<i>Cngbl</i>	Exon2 BC016201
RCC259	CTCA(t)GGTGG(c)AGCCTCTTCAGG*	R	<i>Cngbl</i>	Exon2 BC016201
RCC2526	GATGCGTAATAAT(c)TACCTGAA*	F	<i>Cngbl</i>	Exon22 XM-286113
RCC3387	ATGGA(g)AAGGCTGTC(a)CTGGTGAC*	F	<i>Cngbl</i>	Exon30 XM-286113
NEOR1	ACTCGTCAAGAAGGCGATAG	R	Neo cassette	Neomycin resistance
NEOF1	CCCGTGATATTGCTGAAGAG	F	Neo cassette	Neomycin resistance
NEOR2	TGCCTCGTCCTGCAGTTCAT	R	Neo cassette	Neomycin resistance

Table 1 (Continued)

Name	Sequence (5'-3')	Forward (F)/ Reverse (R)	Gene or vector	Position and accession number
NEOF2	CTATGACTGGGCACAACAGA	F	Neo cassette	Neomycin resistance
NEOR3	CGTAGCTCCAATCCTTCCAT	R	Neo cassette	Neomycin resistance
NEOR3	CGTAGCTCCAATCCTTCCAT	R	Neo cassette	PGK Poly A tail
NEOR4	CCTTCAGTAAAGAGCAGGCA	R	Neo cassette	PGK Poly A tail
CNGA-1	GAGGAGAAGAAAGAAGTCGTGG	F	<i>Cngal</i>	Exon6 NM_007723
CNGA-2	ACTAGCAGCCCTTGTTCCAG	R	<i>Cngal</i>	Exon8 NM_007723
NCK1	AGACCTCAGCAAGCCCAGTG	F	<i>NCKX1</i>	Exon2/3 NM_144813
NCK2	GGCTGCTTTCTGCTTTGGTC	R	<i>NCKX1</i>	Exon5 NM_144813
PER1	ACGGACTCAAGAATGGGATG	F	<i>Per2</i>	Exon1 NM_008938
PER2	TGTTGGTGAGCTGGTACTGG	R	<i>Per2</i>	Exon1 NM_008938
ROM1-1	TTGGTGTTTCAGTGGGTCAGC	F	<i>Rom1</i>	Exon1 NM_009073
ROM1-2	AATACCGCAAACCAAGGAGC	R	<i>Rom1</i>	Exon3 NM_009073
MP6G1	GAGCCACCCAAGGGTGAGAT	F	<i>Pde6g</i>	Exon2 NM_012065
MP6G2	ACTAGCAGCCCTTGTTCCAG	R	<i>Pde6g</i>	Exon4 NM_012065
MGCE1	ACACAATGCTGGGCAGAGCA	F	<i>Gucy2d</i>	Exon11 L41933
MGCE2	GTGGTAAAGCCCACGATGTC	R	<i>Gucy2d</i>	Exon13 L41933

Note: PCR primers were designed based on DNA sequences through a search of the Genbank database (<http://www.ncbi.nlm.nih.gov>). Software used to design primers was GeneRunner; \* Rcc primers are from homologous rat sequences; lower case letters in parenthesis are mouse nucleotides that are different than left upper case rat nucleotides. There are only one or two different nucleotides in these primers, and the different nucleotides are at least 8 bp to the last nucleotide in primers, so the reactions were not affected in our mouse RT-PCR. The Neo cassette is a 1.8-kb sequence, which contains PGK promoter, neomycin gene, and poly A tail. This cassette replaced the deleted sequence of *Cngb1* in the knockout allele.

used in a 20- $\mu$ l RT reaction. One  $\mu$ l RT product was used in each PCR reaction. PCR conditions includes: 94 °C for 2 min (denaturation), 33-35 cycles with 94 °C for 30s (denaturation), 55 °C for 30s (annealing), 72 °C for 45 s (extension), and 72 °C for 7 min. Bands were visualized in 1% agarose gel after ethidium bromide staining. In order to exclude the possible amplification of contaminated genomic DNA, forward and reverse primers are located in different exons for each cDNA amplifying product except for primer pairs in Neo cassette and exon 2. Targeted cDNAs for RT-PCR include: *Cngbl*, neomycin resistance gene, PDE6 $\gamma$ , NCKX1, peripherin-2, Rom1, and Gucy2d. Primers were designed under the Generunner program. All primer sequence and locations are shown in Table 1. In addition, a few primers from rat cDNA sequence were used in the analysis of *Cngbl* cDNA, such as RCC54 (E2F), RCC259 (E2R), RCC2526 (E22F), and RCC3387 (E30F). These cDNA sequences are highly conserved in mouse; nucleotides in the parentheses correlate to mouse nucleotides.

#### Sequencing of RT-PCR Products

To find the gap cDNA sequence between the GARP and channel portions of mouse *Cngbl* gene and to confirm neomycin transcription and Neo-*Cngbl* hybrid transcription, we sequenced two RT-PCR products. RT-PCR product of primer pair E12F and E15R in heterozygote was cut from agarose gel and purified by the PCR purification kit (Qiagen). About 10 ng/ $\mu$ l product was sequenced directly in both forward and reverse directions. Together with available cDNA sequences (BC016201 and XM\_286113) in NCBI, the entire mouse *Cngbl* sequence was figured out and confirmed by multiple alignment with human and rat CNGB1 sequences. Another RT-PCR product of primer

pair NEOF1 and ME4R was also purified by same method. TOPO TA cloning® kit (Invitrogen) was used for PCR product cloning reaction and transformation. After propagation and extraction of plasmid DNA by Miniprep kit (Sigma), plasmid DNA containing PCR product (200 ng/μl) was sequenced. All sequencing was done in the genomics core facility of the Heflin Center for Human Genetics at UAB.

#### Northern Blot of *Cngb1* Transcripts by Probing N-terminal GARP Region

Total RNA was isolated from mice retina by the squeezing and slipping method. RNA was isolated from 6-8 retinas from the same genotyped mice by RNeasy kit (Qiagen). Five μg RNA of each genotype was size-fractionated to 0.8% denaturing agarose gel, transferred to a 0.2-μm nylon membrane (Schleicher & Schuell, Keene, NH) overnight and crosslinked by 120J/cm<sup>2</sup> UV light. RNA marker and 18-s and 28-s rRNA bands were stained by methylene blue, and wild-type and knockout lanes were detected in roughly equal amounts of 18 s and 28 s rRNA. The blue color was destained by DEPC water. A 323-bp DNA fragment spanning exon 4 to 9 was amplified by RT-PCR with primers ME4F and ME9R. This fragment was labeled with [ $\alpha$ <sup>32</sup>P]-dCTP using random priming, following the manufacturer's instructions (DECAprime II, Ambion). Hybridization of the probe to the mRNA was allowed to proceed overnight, and membranes were washed and exposed to Dupont Reflection Autoradiography film (Gold Biotechnology INC., St. louis, MO) at -80 °C for a week then developed. Detailed method see Tucker's paper (Tucker et al., 1998).

### ROS Isolation and Western Analysis of ROS Proteins

Mouse retinas dissected from wild-type (+/+), heterozygous (+/-) and homozygous (-/-) knockout mice were vortexed lightly in Tris buffer (20 mM Tris, pH 7.3; 65 mM NaCl, 2 mM MgCl<sub>2</sub>), and complete protease inhibitor (Roche) and spun for 10 s in a table top centrifuge. The supernatant containing the ROS was layered on top of 500  $\mu$ l of 50% (W/V) sucrose in Tris buffer and overlaid with 200  $\mu$ l of 10% sucrose in Tris. After centrifugation at 25,000 rpm for 30 min in an Optima TLS 55 rotor, the ROS membranes were collected from the top of the 50% sucrose layer and washed once with Tris buffer. To analyze the expression of the *Cngb1* products, Western analysis using well established protocols was performed with the GARP 4B1 monoclonal antibody against the common N-terminal of  $\beta$  and GARP (Poetsch et al., 2001). After blocking with 1% milk in PBS, the membranes were reacted with the GARP 4B1 antibody for 1 hr and subsequently labeled with a secondary antibody tagged with CW800 for analysis by infrared imaging using a Li-Cor Odyssey Imager. Western analysis was also done, with well-characterized monoclonal antibodies against several known photoreceptor proteins: the cGMP-gated  $\alpha$ -subunit (PMc 2G11), ABCA4 (Rim 3F4), rhodopsin (rho 1D4), peripherin-2 (Per 5H2), Rom-1 (Rom 1C6), GC1 (GC 2H6), and a polyclonal antibody against PDE6 $\alpha$  (Affinity BioReagents).

### Immunocytochemistry Analysis of ROS Proteins

The retinal cryosections were blocked with 0.1 M phosphate buffer (PB), PH 7.3, containing 0.2% Triton X-100 and 10% goat serum for 20 min and labeled overnight with the primary antibody. The sections were washed in PB and labeled for 1 hr with Alexa

488 conjugated secondary antibody (Green). Images were merged with DAPI nuclear staining (blue). The sections were viewed on a Zeiss LSM510 confocal microscope.

### Light and Electron Microscopy

Morphologic analysis was done using a procedure of analyzing the effect of drugs on the morphology of rat retina (Pittler, Fliesler, Fisher, Keller, & Rapp, 1995). Briefly, for light microscopy (LM), the eyes were oriented with marker dyes following sacrifice and fixed with a mixture of 1.2% paraformaldehyde and 0.8% glutaraldehyde in 0.1 M PBS, PH 7.4. The anterior segment including the lens was removed, followed by osmium tetroxide fixation. The eye cup was embedded in Epon/Araldite, and thin and semithin sections were cut with an ultramicrotome. Semithin sections were stained with 2% toluidine blue. Light micrographic images were obtained on a Zeiss Axioplan 2 imaging and axiophot 2 universal microscope equipped with a 4-megapixel digital camera. Ultrathin sections for transmission electron microscopy (TEM) were prepared as previously described (Pittler et al., 1995) and visualized with a Hitachi H-7000 electron microscope.

### Basic ERG Response Recording

Animals were dark-adapted overnight and anesthetized with Avertin 300  $\mu\text{g/g}$  body weight. Tested eyes received topical anesthesia by 0.5% proparacaine (Bausch Lomb, Tampa, FL), and eyes were dilated with 2.5% phenylephrine (OCuSOFT, Inc., Richmond, TX) and 1% tropicamide (Alcon Laboratories, Inc., Fort Worth, TX). During recordings the mouse rested on a 39°C heating pad (Model 39 DP, Braintree Scientific, Inc., Braintree, MA) in a Faraday cage. The head was fixed by a bite-bar, and 2.5% hy-

droxypropyl methylcellulose (Goniosol, CIBA Vision Corp, Duluth, GA) was applied to the platinum wire electrodes. The reference and recording electrodes were placed on the right and left corneas, respectively. A dedicated optical bench focused light from a 100-watt tungsten halogen source onto a fiber optic cable that delivered the light to a 2.2-mm diameter translucent adaptor into which a platinum wire electrode was embedded (Lyubarsky & Pugh, 1996). The stimulus was 505-nm light attenuated in discrete steps by a set of six inconel neutral density (ND) filters. A second optical channel delivered light from a camera flash unit that was calculated to deliver approximately  $5.63 \times 10^4$  R\*/rod equivalent 505-nm photons. Data was digitized and recorded with National Instrument (Austin, TX) hardware and software under dim red light. Corneal electrodes were placed using dim red light, which was extinguished for approximately 5 min prior to recording. Total recording time was about 30 min. At each measured intensity, 3-20 repeated responses were averaged with 2.2 to 15.2 s interstimulus intervals (ISI). Light intensities were measured as photons/ $\mu\text{m}^2$  and calculated as log R\* (Lyubarsky et al., 2004). T-test were used in all comparison analysis; variability in the results is presented as standard deviation (STDEV) or standard error of mean (SEM).

#### Isolation Cone Photoreceptor Response Under Dark-Adapted Conditions

Mice were dark adapted over night before ERG recording. Rod photoreceptors are sensitive in dim light and saturated in bright light. We used ND filter 2.4, stable 505-nm green light (band width 35 nm) lasting for 30 s before white camera flash and lasting for 15 s after bright flash. The background light was able to photoisomerize 7300 R/ rod per s. This intensity is a little stronger than 3000-6000 R\*/ rod per s for 2 s, which was suffi-

cient to saturate rod photocurrent in a previous report (Lyubarsky et al., 1999). In respect to rod photoreceptors, the luminance of the 505-nm background light was  $3 \text{ cd/m}^2$  in our measurement, which is close to 20-40  $\text{cd/m}^2$  white light for light adaptation (Peachey et al., 1989, 1993). We also tested ND 3.0 and ND 1.8 in addition to ND 2.4: the ERG of ND 2.4 was the same as ND 1.8 but a littler smaller than ND 3.0. The stable b-wave suggested that the rods were fully bleached; therefore ND 2.4 was the optimum choice for light adaptation, because ND 3.0 may not be enough to saturate the rods, and ND 1.8 may compromise cone's response. The bright white light we used to elicit the maximal cone ERG under a stable background was  $5.63 \times 10^4 \text{ R}^*/\text{rod}$  in our experiment and was the brightest light we could acquire. That is less than  $2.8 \times 10^5 \text{ R}^*/\text{rod}$ , which is known to be sufficient to elicit maximum ERG response (Lyubarsky & Pugh, 1996).

#### Sensitivity of ERG Rod b-wave

There are two methods to calculate the sensitivity of the b-waves: one is calculating the threshold intensity, another method is calculating the K-value after fitting the Naka-Rushton function,  $R/R_{\max} = I^n/(I^n+k^n)$  (Birch & Fish, 1987; Hood & Birch, 1990a).

Here ERG threshold intensity is defined as the light intensity which elicits  $15 \mu\text{V}$  for each genotype. Because the initial responses recorded from each individual were different, the threshold intensity is calculated by the formula  $[15 (\mu\text{V})/\text{lowest response } (\mu\text{V})] \times \text{light intensity } (\text{photons}/\mu\text{m}^2)$ . The lowest response is the response close to  $15 \mu\text{V}$ ; the light intensity is the intensity that elicited the lowest response. We picked up five mice from each genotype at 1-month-old; they are littermates from three litters, and experiment date is close for each litter (within 2 months).

The b-wave amplitudes were measured from the trough of the a-wave to the peak of the b-wave. The b-wave amplitudes were plotted in a light intensity-response graph; by fitting those points to a Naka-Rushton function we calculated the K-value in the function using the IGOR data analysis software program. The b-wave sensitivity was quantified by measuring the K-value defined as the light intensity required to evoke a half-maximal response of rod b-wave. This sensitivity method can provide a whole view of all points. The maximal rod b-wave was acquired by subtracting the light-adapted b-wave (cone b-wave) from the maximal response (rod and cone mixed) for each mouse. The mixed maximal response came from a white camera flash setup. We recorded the ERG of wild type (WT, n = 12), heterozygote (HT, n = 12) and knockout (KO, n = 11) in 1- and 2-month-old; the K-values were calculated in a 2-month period.

#### Recovery of ERG b-wave by Multiple Flashes

Three 505-nm flashes (bandwidth 35 nm, without neutral density filter) were given to each mouse in a specified interstimulus interval (ISI) at dark-adapted conditions. This flash intensity could photoisomerize  $1.7 \times 10^4$  R\*/rod. A series of specified ISI were given in a decreased sequence, 32, 16, 8, 4, 2 sec. The interval between every three flashes is 3 min, so the total recording period was 15 min. The first flash recorded was about 25 min after anesthesia. Since the amplitudes of the second and the third flashes were very close, we averaged the second and third flashes and normalized that as a percentage of the first flash for a specified ISI. Mice were divided into three groups, wild type (WT, n = 16), heterozygote (HT, n = 17) and knockout (KO, n = 15) for 1-month-old ERG recovery. Since we wanted to observe the change of recovery in a 4-month period,

we subdivided each genotype into three small groups. Generally each small group contains three mice. Group A shows the recovery from 1- to 2-month old; group B shows the recovery from 1- to 3-month-old; and group C shows the recovery from 1- to 4-month-old.

## RESULTS

### Genotyping Mice by Genomic DNA Multiple PCR

PCR is a simpler and more efficient method than the Southern Blot method for genotyping in a mouse model. The multiple PCR method was used in our experiment. In the *Cngb1* gene knockout allele, a 3.5-kb genomic sequence including exon 1, exon 2, intron 1, part of intron 2 (237 bp), and the predicted proximal promoter region (256 bp) is absent and replaced by a 1.8-kb Neo cassette including the PGK promoter, neomycin resistance gene, and poly A tail in the process of homologous recombination (Figure 1). Therefore, we made a common forward primer CNGSA6 upstream of knockout sequence in the mouse genome, reverse primers in exon 1 called CNGK2, and another reverse primer in Neo cassette PGK promoter region called NEO1. Sequences of these primers are shown in Table 1. Primer pair CNGSA6 and CNGK2 has a 1.8-kb product; primer pair CNGSA6 and NEO1 has a 1.6-kb product. In order to test the multiplex PCR method, we tested the two primer pairs separately in each genotype (+/+, +/-, -/-) and also put the three primers together to test the heterozygous mouse. All reactions including the negative control had expected results, which are shown in Figure 2. The DNA ladder is in the left column and arrows show the size of each band. All of the following genotyping experiments were tested by the multiple PCR method with three primers in each mouse genomic DNA sample.

### General Phenotype of Our *Cngbl* Knockout Mouse

Figure 3 shows the *Cngbl* gene's position in murine chromosome 8. This figure was drawn according to the results of a search on the National Center for Biotechnology Information (NCBI) Map Viewer website in 2005. Upstream gene matched a Riken cDNA sequence that is homologous to human testis/prostate/placenta-expressed protein (TEPP). This TEPP gene is 5 kb to *Cngbl* in the reverse direction. TEPP might have a role in reproductive biology (Bera, Hahn, Lee, & Pastan, 2003). Downstream gene kinesin family member c3 (*kifc3*) is 127 kb to *Cngbl* in the forward direction. A pseudo-gene *Map11c3-ps6* (microtubule-associated protein 1 light chain 3 pseudo-gene copy 6) is very close to the N-terminal *Cngbl* gene that is 260 kb to the knockout region and 516 bp to exon 1 of *Cngbl*. Since the pseudo-gene is unable to translate protein, and the other two closer genes are far away from the knockout area, our design of *Cngbl* gene knockout is unlikely to affect other gene expression. We didn't find an abnormal mortality rate in our 5'-end *Cngbl* knockout mice. In addition, we compared the body weight of all three genotypes at postnatal 1- and 2-month, and found no significant difference ( $p < 0.01$ ) in the two genotypes (Table 2). Heterozygous crossings produced all three genotypes of mice (+/+, +/-, -/-) that corresponds to the expected Mendelian ratio.

### Structure of the Complete Murine *Cngbl* Gene

Two mouse cDNA clones related to *GARP* and *Cngbl*, BC016201 and XM-286113, are found in the NCBI nucleotide data base. By multiple alignment analysis of these two clones with human and rat CNGB1 cDNA sequences available from NCBI, we found that BC016201 spans exons 1-12a and XM-286113 spans exons 15-33 correspond

Table 2

*Body Weight of WT and KO Mice*

	WT	Number	KO	Number	P-value (T-test)
PN1M					
Male	17.6 ± 0.8	15	16.2 ± 0.9	19	0.24
Female	13.9 ± 0.4	18	13.8 ± 0.5	15	0.91
Total	15.6 ± 0.5	33	15.2 ± 0.6	34	0.58
PN2M					
Male	24.0 ± 0.9	7	22.8 ± 0.8	12	0.33
Female	17.9 ± 0.5	12	19.2 ± 0.4	6	0.07
Total	21.2 ± 0.8	19	21.0 ± 0.7	18	0.85

Note: The body weight of wild-type and knockout mice are compared in the postnatal first (PN1M) and second (PN2M) months. No significant difference is found between WT and KO mice in any time points (T-test,  $p > 0.05$ ).

ingly; the two unoverlaped sequences leave an unfilled gap between exons 12 and exon 15. The gap was filled by RT-PCR amplification using primers in exons 12 (E12F) and 15 (E15R), generating a 538-bp product that was sequenced on both strands at the Heflin Center for Human Genetics in UAB. Freely available genome sequence manipulation programs were used to determine the gene structure: Genome Blat, 2005; Nucleotide entry in NCBI, 2005; and GeneBee Molecular Biology Server, 2005.

The cDNA sequence of *cngb1* and all 33 exons are shown in Figure 4A. The translated protein sequence is shown in Figure 4B. The protein sequence is translated using Genrunner software and is also comparable to human and rat CNGB1 sequence.

To identify the *Cngb1* gene and exons in mouse genomic DNA, we used a blast search to find similar sequences, and multiple alignment to compare the similarity of different species. A sequence of exon 16a in human was found by a computer search of Dr. King-Wai Yao's hGARP 2.5 (hGARP1) (Grunwald et al., 1998). Exon 16a does not exist in the entire cDNA sequence of *Cngb1*, but exists in the hGARP1 transcript. GARP-1

protein translation stops at exon 16a. A RT-PCR reaction between the primer pair of E15 and E18 [Figure 6, A(g), top band] shows an additional top band (not sequenced) that is presumed to be exon 16a. Also, hGARP1 contains an extended exon 18 (18L) that is predicted to exist in mouse. Both corresponding 16a and 18L sequences were found in the mouse genome and were similar to human's and rat's corresponding cDNA. However, we didn't do sequencing of the two exons in mouse. Exon 4 in rat olfactory CNG4.3 (Ardell et al., 2000; Sautter et al., 1998) (AJ000515 in NCBI gene bank) was also found to be homologous to exon 16a of hGARP1 and *mGARP1*. The first exon of rat CNG4.3 is predicted between exons 14 and 15 of B1; we name it 14a. Rat CNG4.3 is homologous to murine *Cngblb* (Kaupp & Seifert, 2002). The results are summarized in Figure 5. The murine *Cngbl* locus consists of at least three exons and undergoes multiple modes of alternative splicing, generating transcripts and encoded proteins diversity in the retina and olfactory. Based on coding potential, the gene can be subdivided into exons encoding the GARP portion, which includes four proline-rich repeats, and exons encoding the channel portion including N- and C-terminal  $\text{Ca}^{2+}$ /CaM binding domains, six transmembrane segments, a pore-like region, and a cyclic nucleotide-binding domain.

#### Incomplete *Cngbl* Gene Transcription in mRNA Level

In the RT-PCR reaction, the amplification product of exon 2 didn't exist, indicating a successful homologous recombination. However, the remaining exons (exons 4 to 33) without homologous recombination were transcribed in *Cngbl*<sup>-/-</sup> mice; obviously the transcription level was lower than *Cngbl*<sup>+/+</sup> and *Cngbl*<sup>+/-</sup> mice in RT-PCR (Figure 6A). It is critical to find how truncated mRNA transcript is produced in our study.

Because the lower mRNA transcription level of remaining exons of *Cngbl* presented in knockout mice, we suspected that the transcription was driven by the PGK promoter. Figure 6A(b) and Figure 7A showed the 261-bp RT-PCR amplification of primer pair NEOF1 and ME4R. NEOF1 is a forward primer in the neomycin resistance gene of the Neo cassette, and ME4R is a reverse primer in exon 4. Sequencing analysis of this PCR product (Figure 7B) revealed that the sequence included part of the Neo gene, 8 bp of the PGK 3' untranslated region, *Cngbl*'s exon 3 and part of exon 4. Amplifications at the 5' and 3' ends of the Neo gene and amplification from the 5' end of the Neo gene to exon 4 also have the expected length of PCR products (primer pairs NEOF2/NEOR2, NEOF1/NEOR1, and NEOF2/ME4R) (Figure 7A). We underlined the stop codon for the Neo gene (Figure 7B). In addition, RT-PCR amplification between NEOF1 and NEO3R in the PGK polyA tail also has a product (Figure 7A). These results indicate at least two alternative splicing products present because of the PGK promoter; at least one Neo/truncated *Cngbl* hybrid mRNA is produced in the *Cngbl* knockout mouse; and a neomycin resistance gene could also be expressed in the knockout mice.

In order to know the transcription level of the Neo/*Cngbl* hybrid mRNA and evaluate the function of the PGK promoter, we did northern blot to compare the hybrid mRNA of knockout mice with the wild-type *Cngbl* mRNA (Figure 8). Retinal mRNA was extracted from littermates of each genotype, total 5- $\mu$ g mRNA of each genotype was loaded to gel, P<sup>32</sup> labeled 323-bp probe, which was a RT-PCR product of exon 4 to 9 [Figure 6(c)], was used to detect *Cngbl*, GARP-1, GARP-2, and their hybrid products. In wild-type mice, we found a 6.2-kb full-size *Cngbl* mRNA, and a more intense 1.6-kb GARP-2 mRNA, but could only find a blurred band in the supposed GARP-1 position

between those two bands. However, in *Cngbl*<sup>-/-</sup> mice, we did not see any bands of *Cngbl* transcripts and hybrid products. The positive control by G3PDH probing showed equal bands in KO and WT mice (not shown here). This result demonstrates that the *Cngbl* transcripts disappear and hybrid mRNA of *Cngbl* or GARPs is very low in KO mice. The *Cngbl* gene has at least three products in ROS; they are expressed as  $\beta$ -subunits in the plasma membrane and as two free forms, GARP-1 and GARP-2, in the cytoplasm. Before we study the potential interaction between the proteins translated by *Cngbl* transcripts and other proteins in ROS, it is necessary to study the mRNA levels of other ROS proteins (Figure 6B). The following proteins, such as *Cnga1*, *NCKX1*, *peripherin-2*, *rom1*, *pde6 $\gamma$* , and *Gucy2d*, are in close vicinity to *Cngbl* and the other two free GARPs. We used the RT-PCR method to amplify a part of each gene transcript (including at least two exons) in all three genotypes. The mice were 1-month-old and from the same litter. There were no obvious differences in transcription levels among all three genotypes. This suggests that the knockout of *Cngbl* does not affect other genes' transcription in ROS.

#### *Cngbl* Gene Products Are not Detectable in the KO Mouse Retina

To demonstrate that the knockout mouse is a true *Cngbl* null at the level of the photoreceptor, Western analysis was performed on isolated ROS with an antibody GARP 4B1 recognizing an N-terminal epitope shared by mouse GARPs and  $\beta$ -subunit. As shown in Figure 9A, mouse GARPs and the  $\beta$ -subunits (*Cngbl* or *cngbla*) are apparent in wild-type and heterozygous mouse retinal extracts, but are not detectable in knockout mice samples, consistent with the KO mouse being a true null allele. A Rom-1 antibody

was used to reprobe the membrane in Figure 9A; we found equal density of different lanes (not shown).

#### The cGMP-gated Cation Channel $\alpha$ -subunit Is Diminished or Absent in the KO Mouse ROS

To our surprise, the  $\alpha$ -subunit (*Cnga1*) also could not be detected in KO mouse ROS on Western blots (Figure 9B). In order to differentiate a global effect on ROS protein expression and distribution from a specific effect on channel subunits, we performed Western analysis of ROS with antibodies that recognize disk membrane proteins (*Per/rds*, *Rom-1*, *GC1*, rhodopsin, and *ABCA4*) and a membrane-associated protein (*PDE6 $\alpha$* ) in ROS. While not quantitative, all of these proteins were found at levels near wild type (Figure 9C). These results are consistent with a specific effect on  $\alpha$ -subunit expression and localization due to the absence of *Cngb1* locus encoded proteins in the retina.

#### Channel Subunits Are not Mislocalized in the Retina

We next examined the spatial distribution of protein expression in 1-month-old retinas to evaluate possible ectopic localization of outer segment proteins using an immunocytochemistry technique. In agreement with Western analysis (Figure 9), the GARP/ $\beta$ -subunit antibody (GARP) detects proteins only in ROS of WT and heterozygous mice; no GARP-containing proteins were detected anywhere in the KO retina (Figure 10, upper panel). Labeling with an  $\alpha$ -subunit antibody (CNGA1) also shows a strong signal confined to the OS of wild-type and heterozygous mice retinas. In the KO mouse retina CNGA1 labeling is greatly reduced but still specially localized to ROS. In contrast, an antibody against *Per/rds* shows comparable labeling in all three genotypes. These results

are consistent with a specific effect on the  $\alpha$ -subunit due to the absence of *Cngb1* gene products in the retina.

### Morphology of the KO Mouse Retina

The KO retina (-/-) is normal in appearance prior to outer segment maturation beginning 8-10 days postnatally but is later structurally compromised as outer segments reach maturation. Retinal stratification of all layers in the KO retina was apparent at one month; however, ROS are shorter and nonuniform in appearance (Figure 11A). Retinas of heterozygous mice (+/-) appear structurally normal even at 2 years old (Figure 11B). In contrast, homozygous knockout mice retinas exhibit a complete loss of the photoreceptor layer within one year. Ultrastructurally, in the KO mouse, relatively normal-appearing disk stacks are punctuated by disoriented and sometimes abnormally elongated disks (Figure 11D). In contrast to wild-type ROS (Figure 11C), where tight, uniform cylindrical stacks of disks are surrounded by a thin plasma membrane, KO mouse ROS appear nonuniform, and often shows misalignment of disks. KO mouse ROS display extracellular membranous material (arrows), the space between photoreceptors is greater, and remnants of ROS are observed (double arrow), both phenomena are indicative of an ongoing degeneration.

### Dark-Adapted ERG a- and b-wave Show Significant Differences Between WT and KO Mice in 1-Month-Old Results

The dark-adapted ERG was evoked by bright white flashes in continuous darkness. KO mice have lower amplitudes and longer implicit times of a- and b-waves than WT mice. One-month ERG results of all three genotypes, WT, heterozygote (HT), and

KO, are shown in Table 3, Figure 12A and B, and Figure 13A and B. As shown in Table 3 and Figure 12A and B, the total b-wave amplitude of KO mice under dark-adapted

Table 3

*1-Month-Old Mice ERG Under Dark-Adapted and Light-Adapted Conditions*

	Implicit Time (ms)			Amplitude ( $\mu$ V)		
	WT (n = 12)	HT (n = 12)	KO (n = 11)	WT (n = 12)	HT (n = 12)	KO (n = 11)
Dark-adapted						
b-wave	35.2 $\pm$ 1.8	34.9 $\pm$ 1.7 ns	58.0 $\pm$ 5.3 P < 0.001	964 $\pm$ 295	955 $\pm$ 402 ns	485 $\pm$ 194 P < 0.001
a-wave	13.4 $\pm$ 1.3	13.1 $\pm$ 0.8 ns	14.9 $\pm$ 1.7 P < 0.05	341 $\pm$ 141	338 $\pm$ 141 ns	40 $\pm$ 19 P < 0.001
Light-adapted						
b-wave	38.6 $\pm$ 7.2	38.3 $\pm$ 6.0 ns	46.5 $\pm$ 5.7 P < 0.01	247 $\pm$ 80	238 $\pm$ 91 ns	229 $\pm$ 97 ns
a-wave	13.2 $\pm$ 1.1	13.3 $\pm$ 1.5 ns	13.2 $\pm$ 2.3 ns	97 $\pm$ 42	84 $\pm$ 38 ns	15 $\pm$ 9 P < 0.001

Note: ERG elicited by bright white flash was done under dark- and light-adapted conditions. Amplitudes ( $\mu$ V) and implicit time (ms) of a- and b-waves are shown in the table by average  $\pm$  STDEV. KO and HT mice results were compared to WT mice by T-test: there is no significant difference between HT and WT mice; in dark-adapted conditions, all parameters of the KO mouse are significantly different from those of WT mouse; in light adapted-conditions, only the b-wave implicit time and a-wave amplitude show significant differences.

conditions (485  $\pm$  194  $\mu$ V) is about one-half that of WT mice (964  $\pm$  295  $\mu$ V) (P < 0.001); and the b-wave implicit time of KO mice (58.0  $\pm$  5.3 ms) is 60% longer than that of WT mice (35.2  $\pm$  1.8 ms) (P < 0.001). The a-wave amplitude and implicit time of WT and KO mice under dark-adapted conditions were shown in Table 3 and Figure 13A and B. The a-wave amplitude of KO mice (40  $\pm$  19  $\mu$ V) is about 1/9 that of WT mice (341  $\pm$

141  $\mu\text{V}$ ) ( $P < 0.001$ ); The a-wave implicit time of KO mice ( $14.9 \pm 1.7$  ms) is longer than that of WT mice ( $13.4 \pm 1.3$  ms) ( $P < 0.05$ ). The parameters of HT mice didn't show any differences from WT mice ( $P > 0.05$ ). Values are shown by average  $\pm$  STDEV.

#### Light-Adapted ERG b-wave Amplitudes Do not Show Significant Differences Between WT and KO Mice in 1-Month-Old Results

The light-adapted ERG was elicited by bright white flashes in the presence of background light (505 nm, 7300  $\text{R}^*/\text{sec}$  rod). The light-adapted ERG results of 1-month-old mice are shown in Table 3, Figure 12C and D, and Figure 13C and D. As shown in Table 3 and Figure 12C and D, the KO mice b-wave amplitude ( $229 \pm 97$   $\mu\text{V}$ ) under light-adapted conditions is similar to that of WT mice ( $247 \pm 80$   $\mu\text{V}$ ) ( $P > 0.05$ ); however, the b-wave implicit time ( $46.5 \pm 5.7$  ms) is 20% delayed if compared to WT mice ( $38.6 \pm 7.2$  ms) ( $P < 0.01$ ). The a-wave amplitude and implicit time of WT and KO mice under light-adapted conditions were shown in Table 3 and Figure 13C and D. There is a significant reduction (85%) of a-wave amplitude in KO mice ( $15 \pm 9$   $\mu\text{V}$ ) compared to WT mice ( $97 \pm 42$   $\mu\text{V}$ ) ( $P < 0.001$ ); however, there is no significant difference in the a-wave implicit times of KO and WT mice. The above a- and b-waves parameters of heterozygous mice (+/-) were not different from WT mice ( $P > 0.05$ ). Values are shown by average  $\pm$  STDEV.

#### ERG Threshold Intensity of 1-month-old KO mice Is 2.8 Log Units Higher Than That of WT Mice

For our study, ERG threshold intensity was defined as the light intensity (505 nm, band width 35 nm) that elicits a 15- $\mu\text{V}$  response for each genotype. For WT mice, the

threshold is  $0.51 \pm 0.18$  photons/ $\mu\text{m}^2$ ,  $0.06 \pm 0.02$  R\*/rod ( $n = 5$ ). The KO mice are  $322 \pm 211$  photons/ $\mu\text{m}^2$ ,  $35.4 \pm 23.2$  R\*/rod ( $n = 5$ ), which is 600-fold (2.80 log units) stronger than that of wild-type mice. The difference is significant between WT and KO mice ( $P < 0.01$ ); on the other hand, there is no difference between WT and HT ( $n = 5$ ) mice ( $P = 0.18$ ) (Table 4, Figure 14).

Table 4

<i>ERG Thresholds of Three Genotypes</i>			
	WT ( $n = 5$ )	HT ( $n = 5$ )	KO ( $n = 5$ )
Threshold (photon/ $\mu\text{m}^2$ )	$0.51 \pm 0.18$	$0.34 \pm 0.19$	$322 \pm 211$
T-Test (P value)		0.18	$< 0.01$
Log threshold(log photon/ $\mu\text{m}^2$ )	-0.29	-0.47	2.51
Log (ratio)	0	-0.18	2.80
Threshold (R*/rod)	$0.06 \pm 0.02$	$0.04 \pm 0.02$	$35.4 \pm 23.2$

Note: ERG threshold intensity is defined as the light intensity that elicits a 15- $\mu\text{V}$  response for each mouse. The threshold intensity is calculated by the formula  $[15(\mu\text{V})/\text{lowest response } (\mu\text{V})] \times \text{light intensity (photons}/\mu\text{m}^2)$ . The lowest response is the response close to 15  $\mu\text{V}$ . The KO mice threshold intensity is 2.80 log units stronger than that of wild-type mice. The threshold intensity can also be expressed as R\*/rod. The difference is significant between WT and KO mice ( $P < 0.01$ ); on the other hand, there is no significant difference between WT and HT mice ( $P = 0.18$ ).

#### Rod b-wave Sensitivity ( $I_{1/2}$ ) of KO Mice Is 1.41 Log Units Higher Than That of WT Mice at 1-Month-Old

The intensity response function is drawn by plotting amplitude of the b-wave vs. the stimulus intensity that generated the response. The 1-month intensity-response curve of *Cngb1* mice shows an obvious right shift in the KO mouse (-/-, solid triangle) compared to the WT (+/+, solid circle) mouse (Figure 14). The rod b-wave sensitivity ( $I_{1/2}$ ) was defined as the light intensity required to evoke a half-maximal response of rod b wave (Figure 15). The log unit of sensitivity (K-value) for each genotype in Table 5 is

Table 5

*1-Month-Old Rod b-wave Sensitivities ( $I_{1/2}$ ) of Three Genotypes*

	WT (n = 12)	HT (n = 12)	KO (n = 11)
$I_{1/2}$ (log photons/ $\mu\text{m}^2$ )	185 $\pm$ 54	250 $\pm$ 141	4980 $\pm$ 2577
Log $I_{1/2}$ (log photons/ $\mu\text{m}^2$ )	2.25 $\pm$ 0.13	2.34 $\pm$ 0.22	3.66 $\pm$ 0.18
$I_{1/2}$ (R*/rod)	20.3 $\pm$ 5.9	27.5 $\pm$ 15.5	548 $\pm$ 283
P (T-test)		P = 0.228	P < 0.001

Note: Sensitivity ( $I_{1/2}$ ) of the rod b-wave is measured by the light intensity which elicits one-half maximal rod b-wave response. The sensitivity is shown by log units of light intensity, which can be photons/ $\mu\text{m}^2$  or R\*/rod. The difference between WT and KO mice is 1.41 log units (26 folds) (P < 0.001). There is no difference in sensitivity between WT and HT mice (P > 0.05).

shown as average  $\pm$  STDEV. The k-value of the KO mouse (3.66  $\pm$  0.18) (n = 11) is 1.41 log units higher than that of WT (2.25  $\pm$  0.13) (n = 12) (P < 0.001). Therefore, KO mice rod photoreceptors are 26-fold less sensitive than that of WT mice based on the  $I_{1/2}$  measure of sensitivity. For HT mice, the intensity-response curve and K-values (not shown) are similar to that of WT mice (P = 0.228).

#### The b-wave Recovery of 1-Month-Old KO Mice Under Multiple Flashes Is Faster Than That of WT Mice

Three multiple flashes were given under 0.0 ND of 505-nm light (band width 35 nm) in dark-adapted conditions with one of five interstimulus intervals (ISI). The sequence of ISIs was as follows, 32, 16, 8, 4, and 2 s. The interval between each three flashes set was 3 min, so the total recording period was about 15 min. Figure 16 is an example of ERG recovery recording using 8- and 32-s ISI. Because the b-wave amplitudes of the second and the third flashes are very close, we averaged them and normalized the average amplitude as a percentage of the first flash for different ISI recordings. As shown in Table 6 and Figure 17, generally, the longer ISI displays a better recovery for all three

Table 6

*1-Month-Old b-wave Recovery Under Multiple Flashes*

	Interstimulus Interval (ISI)				
	32 (s)	16 (s)	8 (s)	4 (s)	2 (s)
WT (%) (n = 16)	95.3 ± 2.2	86.5 ± 1.9	78.9 ± 2.1	79.1 ± 2.5	78.0 ± 4.8
HT (%) (n = 17)	95.3 ± 1.5 P = 0.96	87.4 ± 3.4 P = 0.35	80.8 ± 3.3 P = 0.06	79.7 ± 2.4 P = 0.53	77.1 ± 3.3 P = 0.56
KO (%) (n = 15)	96.7 ± 4.9 P = 0.29	91.0 ± 5.7 P < 0.01	86.2 ± 5.6 P < 0.001	84.3 ± 5.6 P < 0.01	83.5 ± 5.5 P < 0.01

Note: The ERG b-wave responses were elicited by 505 nm flashes (bandwidth 35 nm,  $1.7 \times 10^4$  R\*/rod) under a specified interstimulus interval (ISI) at dark-adapted conditions. A series of specified ISI were given in a decreased sequence, 32, 16, 8, 4, 2 s. The interval between every three flashes is 3 min. The averaged second and third flashes are normalized as a percentage of the first flash for a specified ISI. Mice were divided into three groups, wild type (WT, n = 16), heterozygote (HT, n = 17), and knockout (KO, n = 15), for 1-month-old b-wave recovery. T-test is used in comparison. There is no significant difference when  $P > 0.05$ .

genotypes; the recovery declines from about 95% at 32 s ISI to around 78% at 2 s ISI for all three genotypes. Surprisingly, the recovery of KO mice (n = 15) is more complete than that of WT mice (n = 16) ( $P < 0.001$  for ISI of 16, 8, 4, and 2 s). For a 32-s ISI, there is no significant difference between KO and WT mice ( $P = 0.29$ ). ERG recovery of HT mice (n = 17) is similar to that of WT mice in all recording points (no significant difference). Results are shown for each group and each recording point as average ± SEM.

#### Dark-adapted b-wave Amplitude Declines Faster Than Light-Adapted b-wave Amplitude for KO Mice During a 4-Month Period

The b-wave amplitude changes over a 4-month period under dark-adapted and light-adapted conditions were shown in Tables 7 and 8. The KO mice b-wave shows a dramatically decreasing trends in both dark-adapted (Table 7, Figure 18) and light-adapted (Table 8, Figure 19) conditions. The WT and HT mice show a slightly increasing

Table 7

*1- to 4-Month-Old b-wave Amplitudes Under Dark-Adapted Conditions*

		1 Mon	2 Mon	3 Mon	4 Mon
WT (n = 12)	$\mu\text{V}$	964.0 $\pm$ 85.0	910.1 $\pm$ 92.3	1093.7 $\pm$ 101.6	1190.6 $\pm$ 103.5
	Norm	1	0.966 $\pm$ 0.085	1.196 $\pm$ 0.139	1.328 $\pm$ 0.151
HT(n = 12)	$\mu\text{V}$	954.5 $\pm$ 116.0	1118.6 $\pm$ 113.3	1169.4 $\pm$ 135.7	1168.8 $\pm$ 98.2
	Norm	1	1.264 $\pm$ 0.114	1.293 $\pm$ 0.143	1.350 $\pm$ 0.134
KO (n = 11)	$\mu\text{V}$	485 $\pm$ 58.5	339.7 $\pm$ 32.3	234.0 $\pm$ 34.0	139.0 $\pm$ 26.3*
	Norm	1	0.763 $\pm$ 0.09	0.542 $\pm$ 0.107	0.328 $\pm$ 0.078*

Note: WT, HT, and KO mice b-wave responses elicited by bright white flash under dark-adapted conditions are shown here. For each type of mice, 2-, 3-, and 4-month responses are normalized to 1-month data. Norm, Normalized; \*, n = 9. The value of each cell in the table is average  $\pm$  SEM.

Table 8

*1- to 4-Month-Old b-wave Amplitudes Under Light-Adapted Conditions*

		1 Mon	2 Mon	3 Mon	4 Mon
WT (n = 12)	$\mu\text{V}$	246.8 $\pm$ 23.2	259.9 $\pm$ 22.8	288.0 $\pm$ 26.4	314.4 $\pm$ 36.2
	Norm	1	1.243 $\pm$ 0.166	1.279 $\pm$ 0.174	1.388 $\pm$ 0.192
HT(n = 12)	$\mu\text{V}$	238.4 $\pm$ 26.4	284.9 $\pm$ 28.2	317.4 $\pm$ 35.7	310.7 $\pm$ 30.5
	Norm	1	1.272 $\pm$ 0.126	1.357 $\pm$ 0.157	1.374 $\pm$ 0.142
KO (n = 11)	$\mu\text{V}$	229.2 $\pm$ 29.2	176.9 $\pm$ 18.8	132.8 $\pm$ 20.5	80.7 $\pm$ 13.5*
	Norm	1	0.827 $\pm$ 0.092	0.643 $\pm$ 0.121	0.422 $\pm$ 0.092*

Note: WT, HT, and KO mice b-wave responses elicited by bright white flash under light-adapted conditions are shown here. For each type of mice, 2-, 3-, and 4-month responses are normalized to 1-month data. Norm, Normalized; \*, n = 9. The value of each cell in the table is average  $\pm$  SEM.

trend during the 4-month period. In order to document the degeneration of retinal functions, we normalized the data collected at 2-, 3- and 4-months-old to the starting value at 1-month-old; both real and normalized amplitudes are shown as average  $\pm$  SEM of each month. The KO b-wave shows a dramatic decrease trend in dark- and light-adapted conditions in 4-month normalized data (Figures 18 and 19). We know that the average KO mice b-wave amplitude at 1 month under dark-adapted conditions is only one-half of WT mice, but under light-adapted conditions, the average b-wave amplitude is not statistically

different from that of WT mice. In order to reflect the relative changes of light- and dark-adapted b-wave amplitudes, we calculated the ratios of the two b-wave amplitudes during a 4-month period of each genotype (Table 9 and Figure 20). The b-wave ratios of KO

Table 9

*1- to 4-Month-Old b-wave Amplitude Ratios of Light- Over Dark-Adapted Conditions*

	B-wave Amplitude Ratio (Light-Adapted / Dark-Adapted)			
	1 Mon	2 Mon	3 Mon	4 Mon
WT (n = 12)	0.255 ± 0.008	0.291 ± 0.011	0.266 ± 0.009	0.257 ± 0.011
HT (n = 12)	0.258 ± 0.013	0.257 ± 0.009	0.274 ± 0.004	0.263 ± 0.010
	ns	p = 0.023	ns	ns
KO (n = 11)	0.479 ± 0.025	0.526 ± 0.035	0.564 ± 0.032	0.606 ± 0.051*
	P < 0.00001	P < 0.00001	P < 0.00001	P < 0.00001

Note: Ratios of light-adapted to dark-adapted b-wave amplitude elicited by bright white flash are shown in this table by average ± SEM in each month data (amplitude values see Tables 7 and 8). \*, n = 9. There is a significant difference between WT and KO mice at all time points (T-test, p < 0.00001); There is no significant difference between WT and HT mice except for the 2-month results (P = 0.023).

mice are significant different from that of WT mice in all time points; however there are no significant differences between WT and HT mice, except at the 2-month point (P = 0.023). There is not only an initial higher ratio in KO mice (0.48) than that of WT mice (0.26), but also a slight increasing trend of the ratios in KO mice; in HT and WT mice, the lines for the ratios are flat (Figure 20). These results demonstrate that although both light and dark-adapted b-wave amplitude decrease over a 4-month period in KO mice, the light-adapted b-wave amplitude decrease slower than dark-adapted b-wave.

The b-wave Implicit Time of KO Mice Under Dark-Adapted Conditions  
Is Delayed at all Ages Tested

The b-wave implicit times elicited by bright white flash under dark-adapted conditions are shown in Table 10 and Figure 21 by average and SEM during a 4-month period. There is no difference between WT and HT mice for b-wave implicit times during a 4-month period, but between KO and WT mice, the difference is significant during the 4-month period ( $P < 0.0001$ ). There is at least a 23-ms delay in KO mice if compared with WT mice at all time points (Table 10). There is also an increasing trend for each genotype; for KO mice, this trend is more obvious. Significant differences can be found between 1- and 3- or 4-month in KO mice ( $P = 0.044$  or  $P = 0.039$ ); in WT mice, the difference is significant between 1- and 4-month ( $P = 0.0048$ ).

Table 10

*1- to 4-Month-Old b-wave Implicit Times Under Dark-Adapted Conditions*

		1 Mon	2 Mon	3 Mon	4 Mon
WT (12)	ms	$34.9 \pm 0.5$	$35.3 \pm 1.2$	$36.3 \pm 0.8$	$37.7 \pm 0.7$
	Norm 1		$1.001 \pm 0.028$	$1.032 \pm 0.024$	$1.072 \pm 0.21$
HT (12)	ms	$34.9 \pm 0.5$	$36.2 \pm 0.5$	$36.5 \pm 1.0$	$37.6 \pm 1.1$
	Norm 1		$1.041 \pm 0.015$	$1.049 \pm 0.033$	$1.080 \pm 0.031$
KO (11)	ms	$58.0 \pm 1.6$	$60.4 \pm 2.2$	$63.2 \pm 2.0$	$66.7 \pm 3.9^*$
	Norm 1		$1.043 \pm 0.030$	$1.097 \pm 0.041$	$1.163 \pm 0.064^*$
			$P < 0.0001$	$P < 0.0001$	$P < 0.0001$

Note: WT, HT and KO mice b-wave response elicited by bright white flash under dark-adapted conditions are shown here. For each type of mice, 2-, 3- and 4-month responses are normalized to 1-month data. Norm, Normalized; \*,  $n = 9$ . The variability is represented by SEM.

Over 1- to 4-Month-Old a-wave Amplitudes Under Light-Adapted  
Conditions Continuously Decrease

WT, HT, and KO mice a-wave amplitudes elicited by bright white flash under light-adapted conditions are shown in Table 11 and Figure 22. The amplitudes are not different statistically between WT and HT mice over a 4-month period, but the differences between WT and KO are significant ( $P < 0.0001$ ). WT a-wave amplitudes did not decrease during a 4-month period ( $P > 0.05$ ), but in KO mice, the decrease existed (1- and 2-month to 3- and 4-month,  $P < 0.05$ ). The averaged a-wave amplitudes of KO mice were decreased from 40  $\mu\text{V}$  (1 month) to 20  $\mu\text{V}$  (3 month). In the 4-month results of KO mice,  $n = 9$ .

Table 11

<i>1- to 4-Month-Old a-wave Amplitudes Under Light-Adapted Conditions</i>					
		1 Mon	2 Mon	3 Mon	4 Mon
WT (n = 12)	$\mu\text{V}$	$341.3 \pm 40.6$	$350.6 \pm 39.1$	$380.5 \pm 37.4$	$423.9 \pm 31.2$
HT (n = 12)	$\mu\text{V}$	$337.5 \pm 40.6$	$404.4 \pm 44.4$	$420.2 \pm 47.2$	$407.0 \pm 31.2$
		ns	ns	ns	ns
KO (n = 11)	$\mu\text{V}$	$39.5 \pm 6.0$	$38.8 \pm 5.4$	$20.3 \pm 6.6$	$18.3 \pm 3.6^*$
		$P < 0.0001$	$P < 0.0001$	$P < 0.0001$	$P < 0.0001$

Note: There is no significant difference between WT and HT mice in 4-month period, but the difference between WT and KO is significant ( $P < 0.0001$ ). There is no decrease for WT a-wave amplitudes (1- to 4-month,  $P > 0.05$ ), but in KO mice, the decrease exists (1- and 2-month to 3- and 4-month,  $P < 0.05$ ). \*,  $n = 9$ . The variability is represented by SEM.

Rod b-wave Sensitivities Did not Change in 2-Month-Old Mice

The KO mice  $\log I_{1/2}$  is  $3.52 \pm 0.31$ , which is similar to 1-month data  $3.66 \pm 0.18$ ; there is no change statistically ( $P > 0.05$ ); the WT mice didn't show change in  $\log I_{1/2}$  at 2-month-old, either. The sensitivity difference between KO and WT at 2-months-old is

1.37 log units which is similar to the 1.41 log unit of the 1-month comparison (Table 12, Figure 23). Log  $I_{1/2}$  values are shown by average  $\pm$  STDEV. There is no significant difference ( $P2 > 0.05$ ) between WT and HT mice at all corresponding time points; however, there is a significant difference between WT and KO mice ( $P2 < 0.001$ ).

Table 12

*1- and 2- Month-Old Rod b-wave Sensitivities*

	Sensitivity (Log $I_{1/2}$ )(log photons/ $\mu\text{m}^2$ )	
	1 Month	2 Month
WT (n = 12)	2.25 $\pm$ 0.13	2.15 $\pm$ 0.24 ( $P1 > 0.05$ )
HT (n = 12)	2.34 $\pm$ 0.22 ( $P2 > 0.05$ )	2.24 $\pm$ 0.24 ( $P1 > 0.05$ ) ( $P2 > 0.05$ )
KT (n = 11)	3.66 $\pm$ 0.18 ( $P2 < 0.001$ )	3.52 $\pm$ 0.31 ( $P1 > 0.05$ ) ( $P2 < 0.001$ )

Note: The sensitivity (log  $I_{1/2}$ ) is shown by log units of light intensity (photons/ $\mu\text{m}^2$ ). 1- and 2-month log  $I_{1/2}$  values are shown by average  $\pm$  STDEV. There is no significant difference ( $P2 > 0.05$ ) between WT and HT mice over the 2-month period; however, there is a significant difference between WT and KO mice during the 2-month period ( $P2 < 0.001$ ). There is no significant difference between 1- and 2-month-old data for all three genotypes ( $P1 > 0.05$ )

## Multiple Flash Responses Recorded Over Different Ages

We measured b-wave recovery using multiple flashes presented at various intervals from 32-s ISI to 2-s ISI. Generally, like 1-month-old recovery data, KO recoveries at 2-, 3- and 4-months-old are faster than the WT standard (Table 13, Figures 24, 25, and 17), but we can find that the 2- and 3- month KO mice recoveries are slower than the WT standard at 2-s and 4-s ISI (Figure 25, panels D and E). For HT mice, results are similar to standard WT (Figure 25, panels A, B and C), but in Figure 25, panel B, 1-month-old HT recovery shows larger variability at 8- and 16-s ISI. For KO mice, 2- and 3-month

Table 13

*The b-waves Recoveries During a 4-Month Period*

			Interstimulus Interval (s)				
	GM	N	32	16	8	4	2
WT	A1	3	96.7±4.2%	86.1±2.7%	79.0±2.8%	81.4±2.4%	81.4±3.1%
	A2	3	93.3±2.0%	85.6±0.5%	81.3±2.1%	85.5±0.7%	81.7±2.4%
	B1	3	94.7±2.4%	86.5±1.7%	78.3±1.4%	79.3±1.8%	78.1±4.9%
	B3	3	95.4±2.4%	85.6±1.1%	79.7±3.5%	79.7±2.5%	77.4±6.0%
	C1	5	94.2±1.2%	85.4±1.5%	78.0±1.8%	77.6±0.8%	75.4±3.4%
	C4	5	91.5±3.3%	83.4±1.9%	79.6±1.3%	82.0±2.7%	80.6±2.0%
	All	22	94.1±2.9%	85.2±1.8%	79.2±2.1%	80.7±3.1%	78.9±4.0%
HT	A1	3	95.2±1.3%	85.2±0.9%	78.8±0.9%	78.4±2.1%	77.6±3.3%
	A2	3	95.0±1.5%	84.0±2.1%	79.9±0.6%	82.3±3.6%	78.7±5.8%
	B1	4	96.0±2.3%	90.0±4.8%	86.0±1.1%	82.4±2.6%	80.8±3.1%
	B3	4	93.8±3.9%	83.7±3.2%	78.1±2.0%	83.2±1.6%	82.0±3.7%
	C1	6	95.1±1.5%	86.4±3.4%	79.2±1.7%	79.0±2.0%	74.5±2.1%
	C4	6	92.0±2.8%	87.0±5.4%	81.6±3.2%	84.5±2.7%	81.9±5.1%
	All	22	94.1±2.9%	85.2±1.8%	79.2±2.1%	80.7±3.1%	78.9±4.0%
KO	A1	3	95.9±2.1%	91.9±7.5%	88.4±6.7%	88.6±9.8%	87.2±9.1%
	A2	3	94.6±2.4%	87.3±2.3%	81.6±3.3%	77.6±4.9%	73.3±6.6%
	B1	3	95.7±6.2%	89.2±8.1%	84.1±6.4%	78.8±5.9%	79.1±6.9%
	B3	3	96.2±4.7%	87.5±3.6%	79.9±3.5%	74.8±7.8%	76.1±8.3%
	C1	3	95.3±5.8%	87.8±5.0%	83.1±3.6%	86.4±2.0%	85.3±1.5%
	C4	3	96.5±2.5%	95.7±5.3%	91.9±10.4%	86.1±10.5%	83.6±5.5%
	All	21	95.1±2.5%	88.5±4.5%	84.1±5.5%	80.1±6.5%	78.8±5.5%

Note: WE subdivided each genotype of mice into small groups A, B, and C. A is the 1- to 2-month group; B is the 1- to 3-month group; C is the 1- to 4-month group; the number represents the month. GM represents group and month. The table lists all the recordings of recovery ERG, which has two time points recording. The WT recordings are used to make Figure 23. We found WT recovery is not changed during a 4-month period, so we averaged all WT recoveries and used it as a standard curve (average ± STDEV) for HT and KO study in Figure 24.

recoveries are slower than the 1-month recovery, but at 4-months the variability is larger at 8- and 16-s ISI. The confused results may be caused by small sample sizes for the 2-, 3- and 4-month recovery study, because the number is three for most of the small groups, six at most.

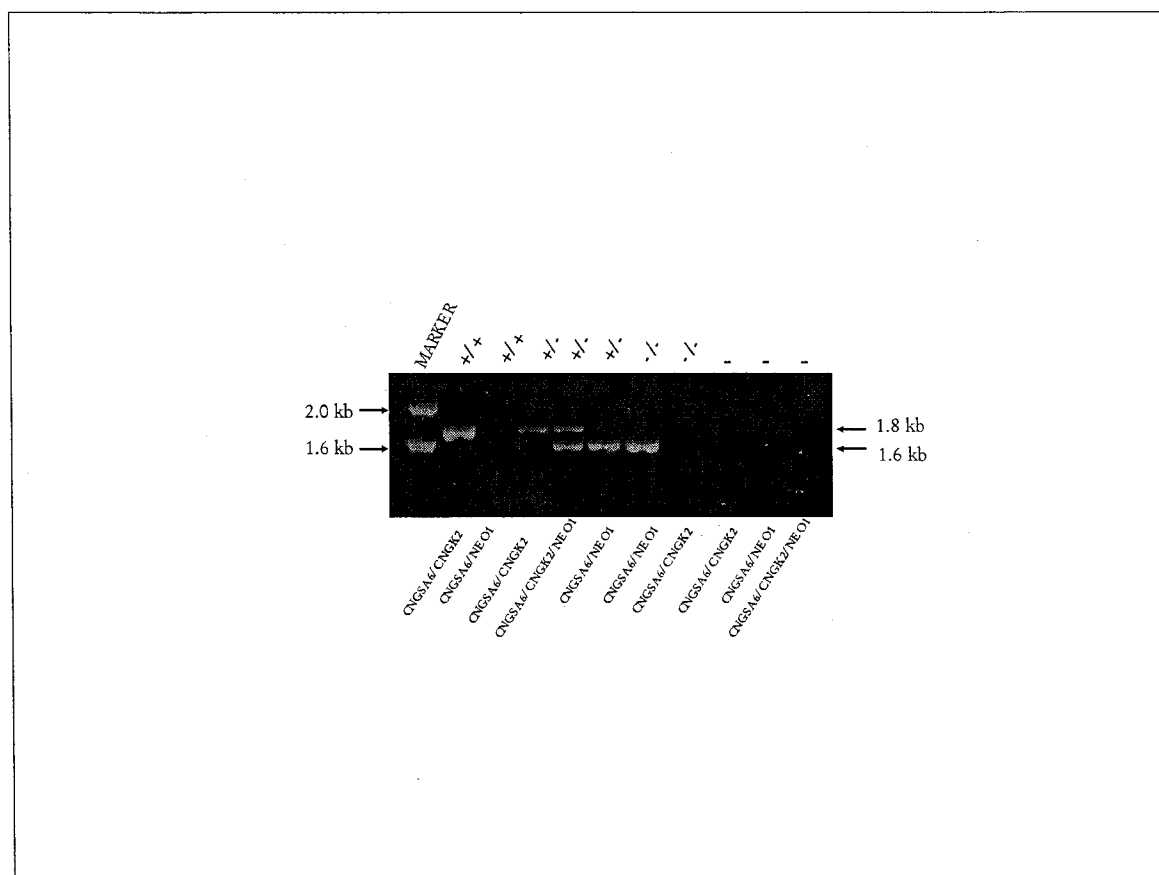


*Figure 2.* PCR amplification of mouse genomic DNA. Genotyping for the targeted alleles was done using primers (Figure. 2) specific for the endogenous gene in exon 1 (primer CNGK2) or for the Neo cassette (primer NEO1) and a primer common to both alleles (CNGSA6)., A 1.8-kb PCR product was generated with a primer pair (CNGSA6/CNGK2) specific to the wild-type allele, and a 1.6-kb PCR product was produced with a primer pair (CNGSA6/NEO1) specific to the deleted allele. Multiple PCR with all three primers CNGSA6/CNGK2/NEO1 yielded both products using heterozygous mouse genomic DNA as a template. In the absence of template DNA no PCR products were observed (lanes designated “-”).

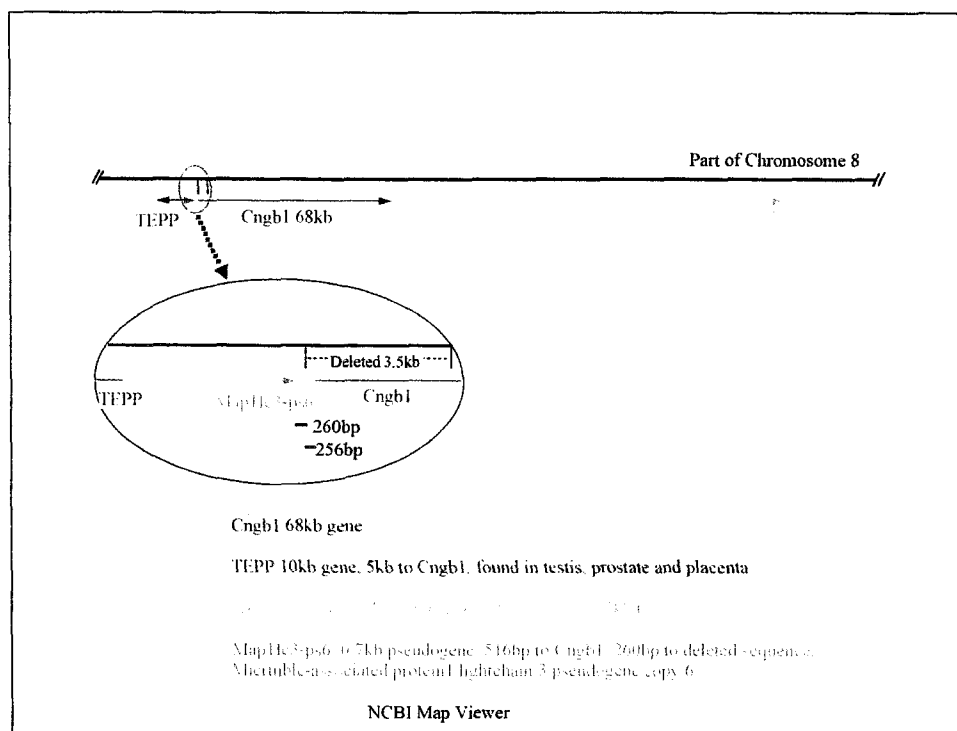


*Figure 3.* *Cngb1* gene in murine chromosome 8. The upstream and downstream genes to *Cngb1* are shown. Riken cDNA or Testis/prostate/placenta-expressed protein (TEPP) is a 10-kb gene that is situated 5 kb upstream and in a reverse direction to *Cngb1*; kinesin family member C3 (*kif3*) is a 11-kb gene that is situated 127 kb downstream and in a forward direction to *Cngb1*; a pseudogene *Map1k3-ps6* is situated 260 bp to the N-terminal deleted sequence. Because pseudogene does not express protein, N-terminal knockout of *Cngb1* is at least 5 kb to *TEPP* and *Kifc3* genes, this gene knockout model is unlikely to affect other genes. The map is summarized from available data of NCBI Map Viewer (<http://www.ncbi.nih.gov/mapview>).



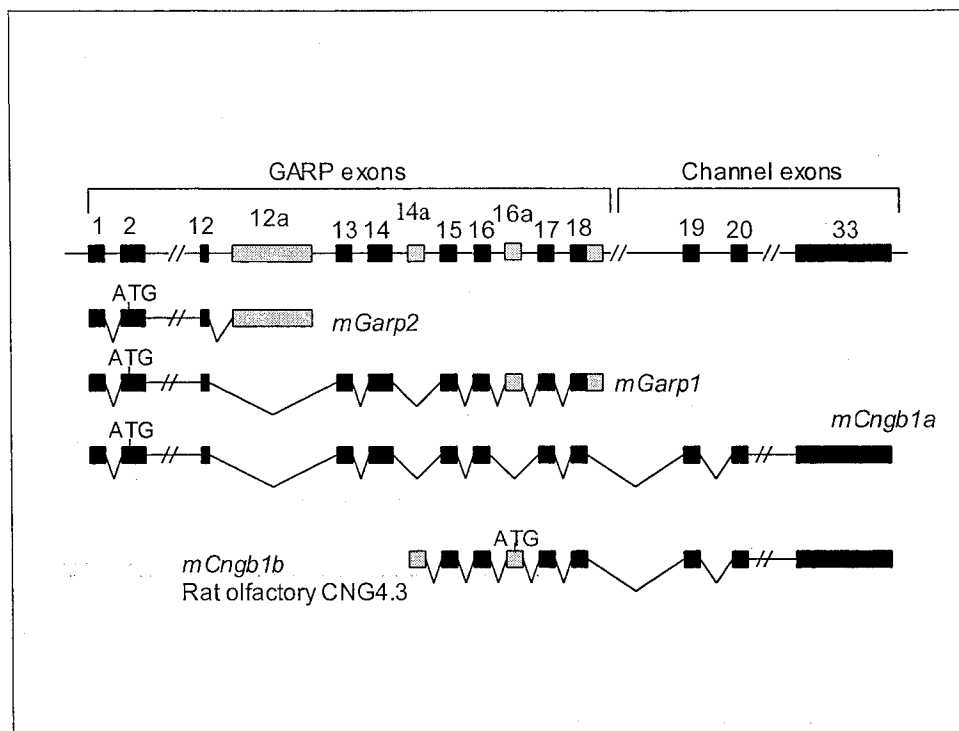


*Figure 5.* Map of *Cngb1* gene exons and alternative transcripts. Like the human gene (Ardell et al., 2000), the murine *Cngb1* locus consists of at least 36 exons and undergoes multiple modes of alternative splicing, generating transcript and encoded protein diversity. The *mGarp2* transcript is composed of exons 1-12 and a unique exon designated 12a. Transcript *mGarp-1* consists of exons 1-18 and alternate exon 16a [Figure 6A(g)]. The 3' exon of *mGarp1* contains all of exon 18 found in the  $\beta$ -subunit transcript and an additional predicted 364-bp sequence (hGARP1, Grunwald et al., 1998) downstream of the end of exon 18 (designated 18L). Exon 16a of *mGarp1* is also present in the olfactory cyclic nucleotide-gated channel subunit CNG4.3 (Sautter et al., 1998), also designated as *Cngb1b* (Kaupp and Seifert, 2002). The rod  $\beta$ -subunit transcript (*Cngb1a*) consists of exons 1-33, excluding all of the alternate exons shown (12a, 14a, 16a, 18L). Based on coding potential, the gene can be subdivided into exons encoding the GARP-portion, which includes proline-rich repeats and the channel-like domain that includes two  $\text{Ca}^{2+}$ /CaM binding domains, six transmembrane domains, a pore-like region, and a cyclic nucleotide-binding domain. Only the rod photoreceptor expresses GARP proteins that comprise protein sequences encoded by exons 2-12. Transcript *mCngb1b* is distributed in olfactory. Exons 1 and 2 and the predicted promoter region are within the region targeted for deletion.

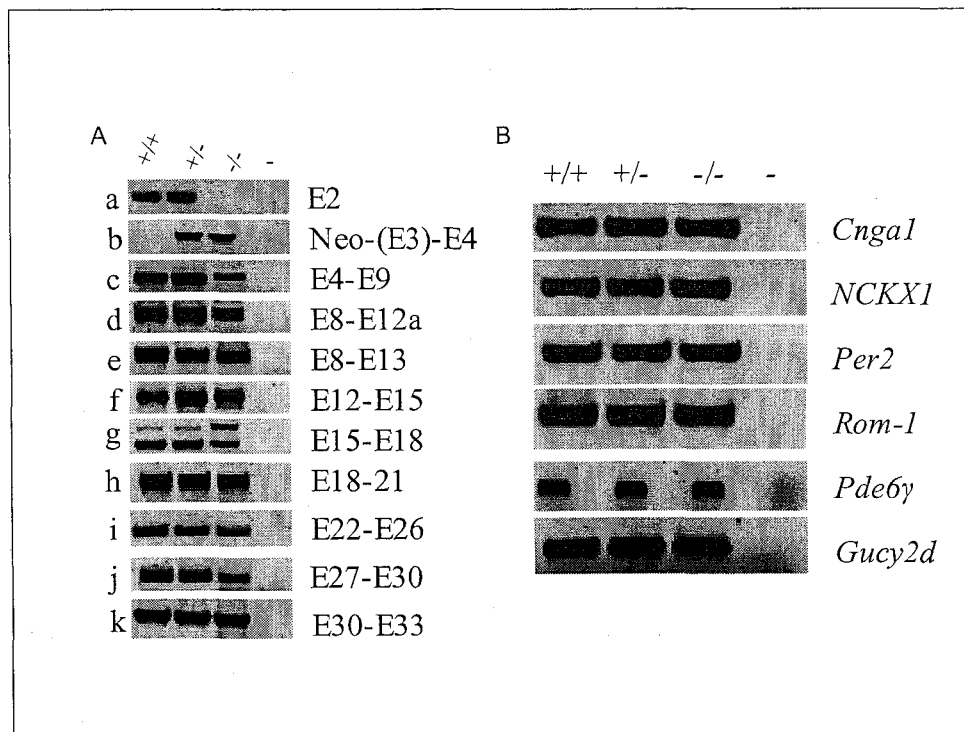


**Figure 6.** RT-PCR analysis of *Cngb1* and other photoreceptor loci. RT-PCR analysis of *Cngb1* and other photoreceptor loci. A. RT-PCR of *Cngb1* encoded transcripts. Amplification reactions covered all 32 protein-coding exons of the *Cngb1* gene and Neo cassette cDNA. Exons covered by each primer pair are shown to the right of each panel. Panel a shows that exon 2 is deleted in the homozygous KO mouse genome. Panel b demonstrates that the Neo-*Cngb1* hybrid mRNA forms and the PGK promoter is functional in the Neo cassette in KO mice. Panels c-k show that PCR products are generated for all three genotypes; however, the signal does appear weaker in knockout mice for several primer pairs (e.g., panels c, d, i, and j). Panel d shows that an alternatively spliced exonic region, designated 12a of GARP2 cDNA, is also present in the -/- RNA pool. The difference in size of the PCR products of E15-E18 (panel g) is consistent with the presence of exon 16a specific for *mGarp1*. B. Amplification of several photoreceptor-specific transcripts. Primer pairs were generated to specifically amplify genomic DNA, encoding several photoreceptor-specific gene products: cGMP-gated cation channel  $\alpha$ -subunit (*Cngal*), Na/Ca-K exchanger (*Nckx1*), peripherin 2 (*Per2*), *Rom-1*, cGMP phosphodiesterase type 6-subunit (*Pde6 $\gamma$* ), and guanylate cyclase 1 (*Gucy2d*). For each primer pair, comparable levels of product were obtained. *Pde6 $\gamma$*  amplification products were loaded into smaller wells and separated by an empty lane to increase spacing. No products were observed in the absence of template (lanes designated "-"). Although the results are not quantitative, it is strongly suggested that none of the transcripts analyzed are of greatly reduced abundance in the homozygous KO mice.

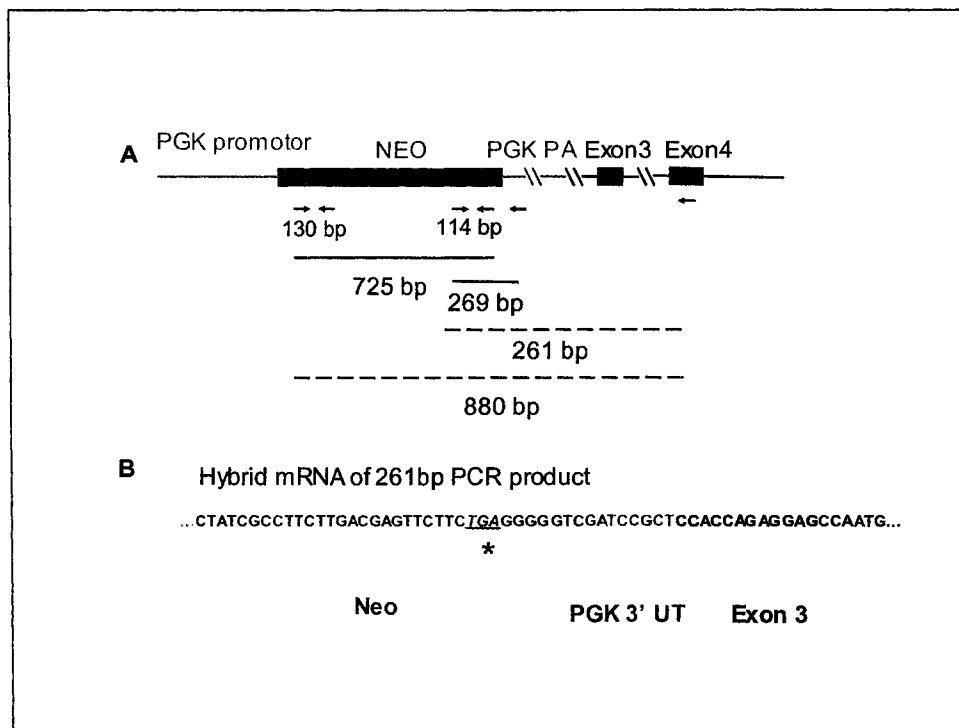


*Figure 7.* A Neo/*Cngb1* hybrid mRNA is produced in *Cngb1*-KO mice. **A.** Scheme for amplification of hybrid and Neo transcripts. Sense and antisense primers were synthesized within the neomycin resistance (Neo) gene near the 5' and 3' ends, which amplify 130 (NEOF2/NEOR2) and 114 (NEOF1/NEOR1) bp products, respectively. A 725-bp product (NEOF3/NEOR2) is observed using the 5'-sense Neo and 3'-antisense Neo primers. Amplification with the 3'-sense Neo and a poly A (pA) antisense primer pair (NEOF1/NEOR3) yields a 269-bp product. To test for the presence of Neo/*Cngb1* hybrid transcripts, amplifications were done with either the 5' or 3' sense Neo primers (NEOF2 or NEOF1) and a reverse primer specific for exon 4 (ME4R) of the *Cngb1* locus, producing 880-bp or 261-bp products, thereby establishing the presence of at least one hybrid transcript. **B.** Sequence analysis of hybrid cDNA. A partial sequence derived from the complete sequencing of the 261-bp RT-PCR product in **A** is shown. This 261-bp band is also shown in Figure 6A(b). The sequence is consistent with an intact Neo coding region, including the Neo stop codon, and 8 bp 3'-UTR followed by the entire exon 3 sequence of *Cngb1*. The presence of the premature stop codon should preclude expression of any *Cngb1* encoded sequences.

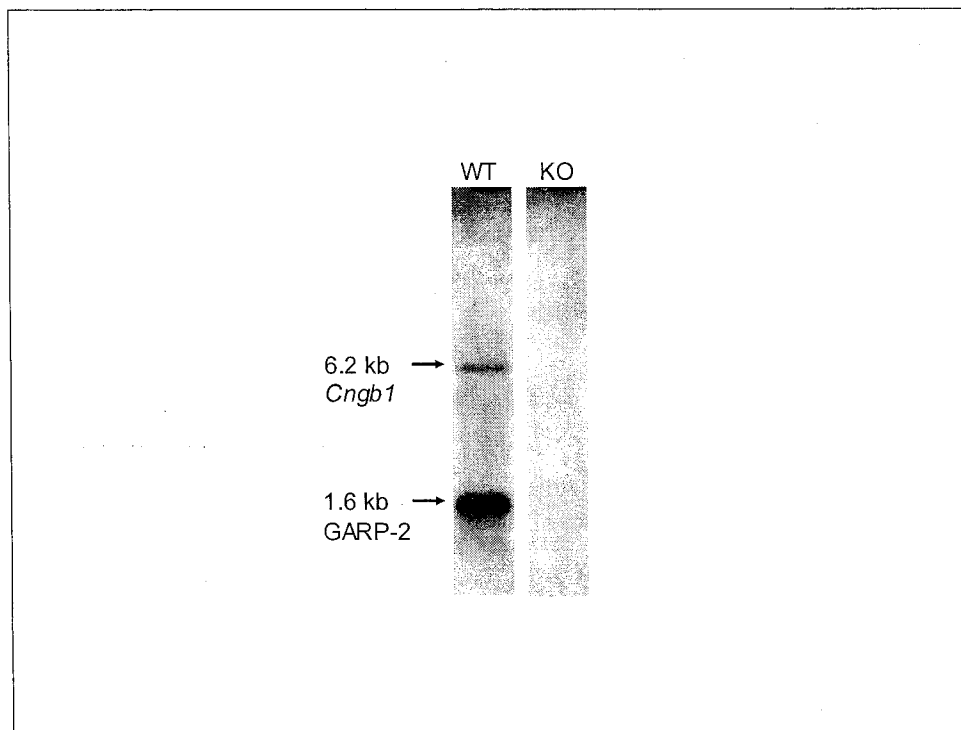


*Figure 8.* Northern blot analysis of *Cngb1*-KO and wild-type littermate total RNA. Approximately 5  $\mu$ g of total RNA was electrophoresed through a 0.8% formaldehyde containing agarose gel, transferred to a nylon membrane, and probed with a  $P^{32}$  labeled 323-bp fragment within the 5'-region [Exon 4-9, PCR product in Figure 6A(c)] common to both GARPs and the channel  $\beta$ -subunit. A strong band of 1.6 kb and a weaker band 6.2 kb are observed, consistent with transcripts encoding GARP-2 and the  $\beta$ -subunit, respectively. GARP-1 transcript presumed to be 2.6 kb is not apparent; however, there are a couple of regions where faint somewhat diffuse bands appear that may represent the low abundance GARP-1 transcripts. There is no signal apparent in homozygous KO mice, indicating that *Cngb1*-related transcripts are either absent or of very low abundance. The membrane was reprobbed by G3PDH (glyceraldehyde-3-phosphate dehydrogenase) and comparable bands were found in both lanes (not shown).

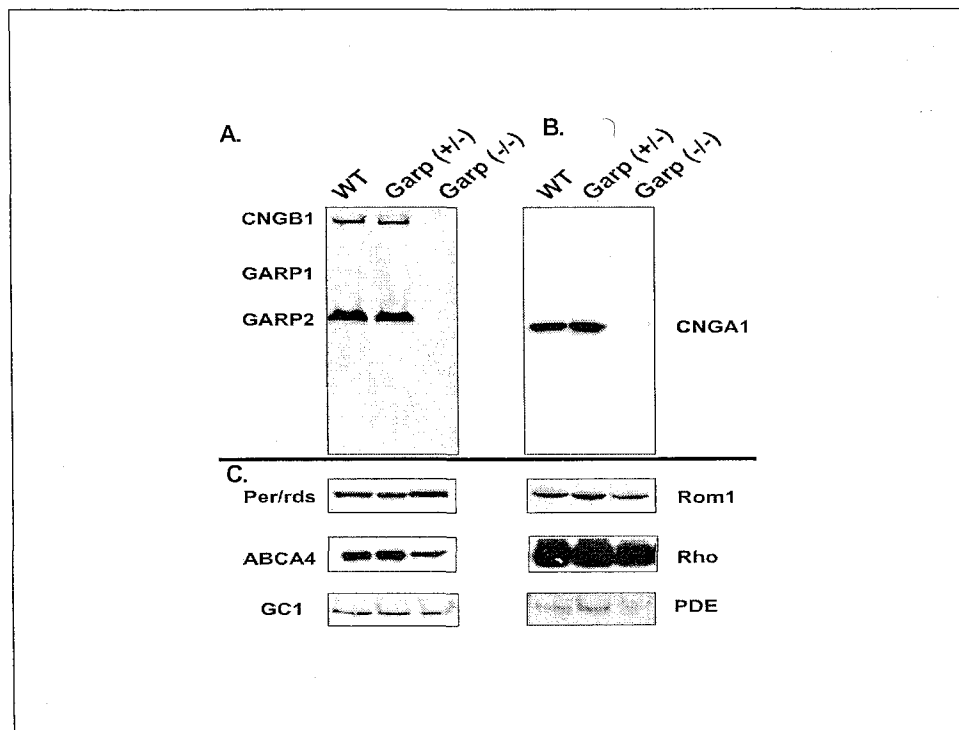


**Figure 9.** Expression of photoreceptor proteins in the *Cngbl* knockout mouse. **A.** *Cngbl*-related gene products are undetectable in mouse ROS. In wild-type (WT) and heterozygous (*Garp* +/-) mice,  $\beta$ -subunits and GARP-2 proteins are easily detected, and a weaker GARP-1 band is observed when common N-terminal monoclonal antibody GARP 4B1 was used. In homozygous KO (*Garp* -/-) mice, no  $\beta$ -subunit or GARP proteins are detected, consistent with the *Cngbl*-KO being a true null. **B.** The cGMP-gated cation channel  $\alpha$ -subunit is not detected in knockout ROS homogenates. Monoclonal antibody PMc 2G11 against the channel  $\alpha$ -subunit (CNGA1) readily detected the 63-KD channel subunit in wild-type and heterozygous mice, but no signal was seen in homozygous *Cngbl*-KO mice. **C.** Western analysis of other ROS Proteins. To verify the presence of other ROS proteins in the ROS, monoclonal antibodies to Per/rds (Per 5H2), ABCA4 (rim 3F4), GC1 (GC 2H6), Rom1 (Rom 1C6), Rhodopsin (rho 1D4), and polyclonal antibody to PDE( $\alpha$ ) were used for Western analysis. All of the proteins were observed in comparable amounts in the mouse ROS homogenates.

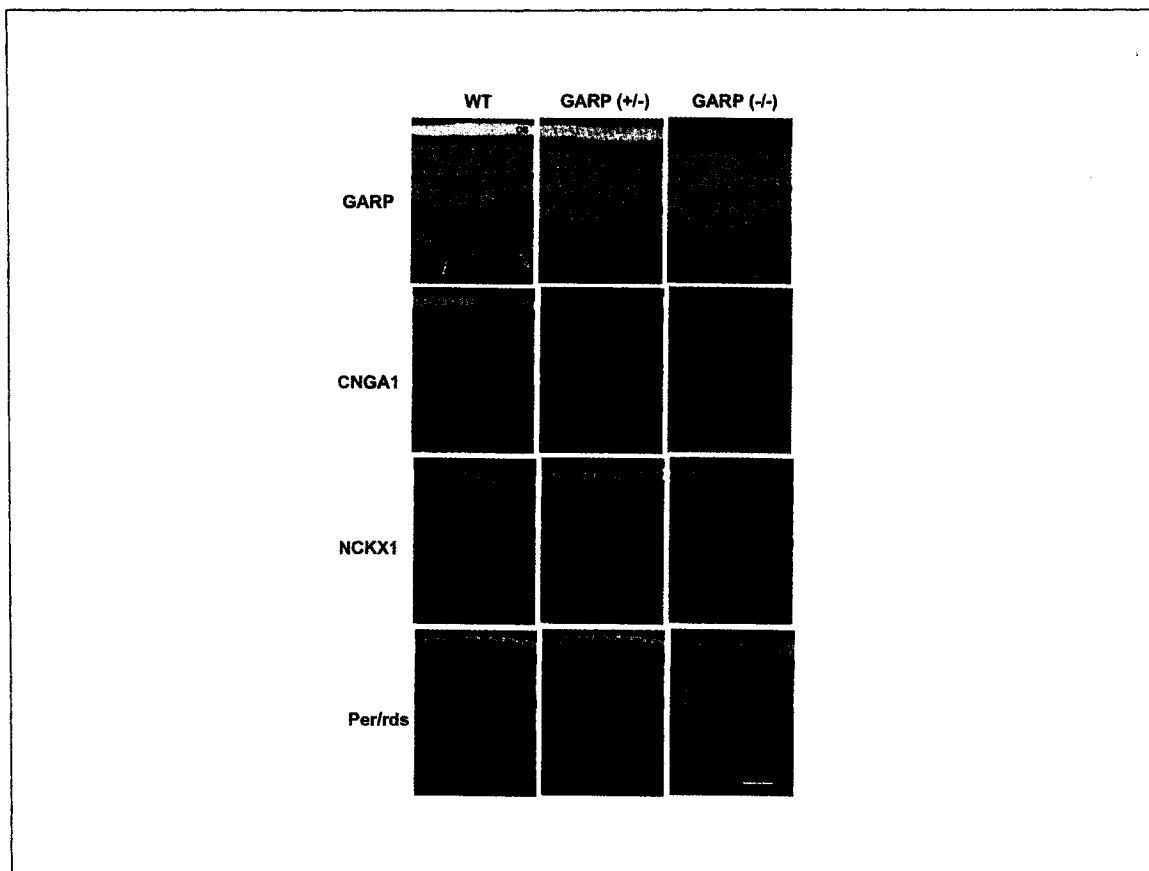


*Figure 10.* Immunolocalization of ROS proteins. Frozen retina sections from littermates of wild type (WT), heterozygote [GARP (+/-)], and homozygous *Cngb1* knockout [GARP (-/-)] were labeled (green) with antibodies against the channel  $\beta$ -subunit and GARP (GARP 4B1, upper row panels), the channel  $\alpha$ -subunit (CNGA1, second row panels), Na/Ca-K exchanger (NCKX1, third row panels), and peripherin-2 (Per/rds, lower panels). All of the antibodies show comparable and appropriately distributed labeling in the ROS of WT and heterozygous retinas. In the knockout retina, labeling is absent with the  $\beta$ -subunit /GARP antibody, and only a very weak signal is observed in the ROS with the channel  $\alpha$ -subunit antibody (CNGA1). In contrast, antibodies against Na/Ca-K exchanger (NCKX1) and peripherin-2/rds (Per/rds) appear to be of relatively normal abundance and distribution in the knockout retina. Nuclei are counterstained with DAPI (blue); scale bar = 50  $\mu$ m.

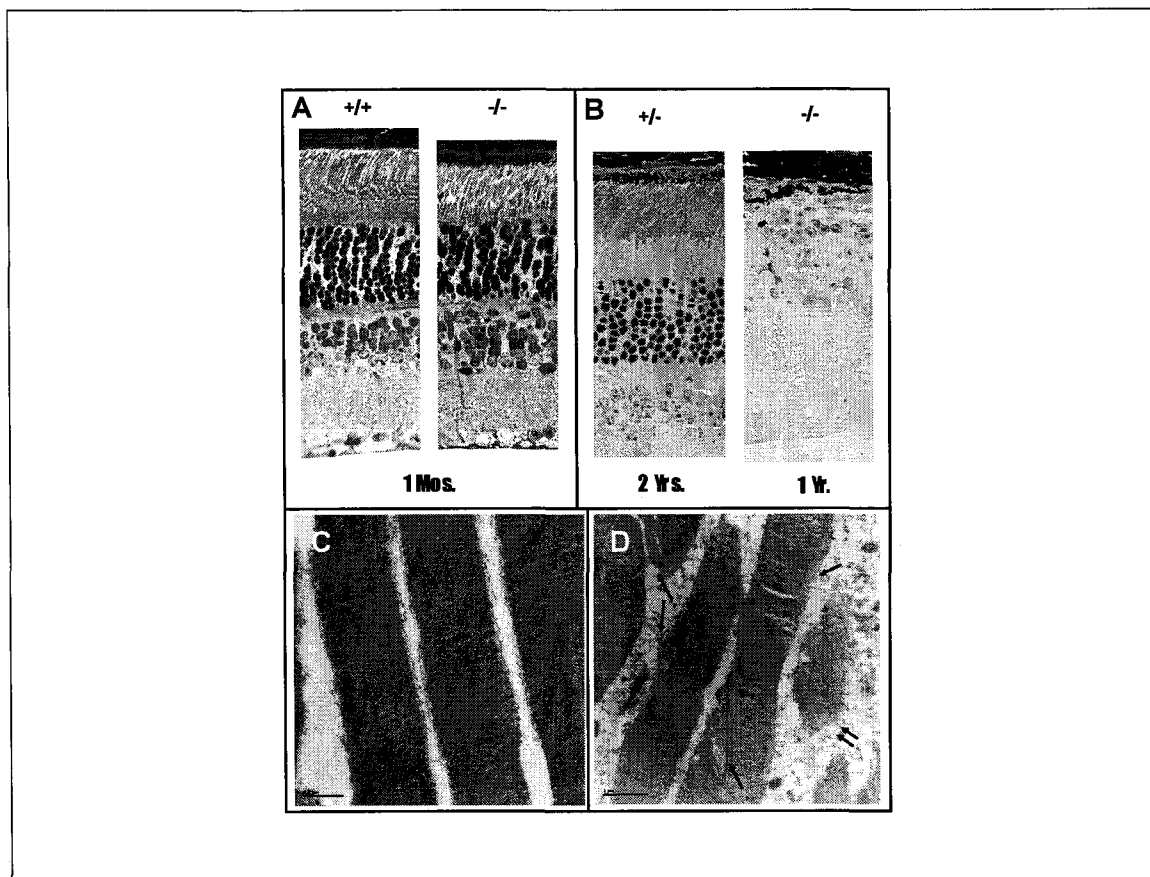


*Figure 11.* Morphology of *Cngb1*-KO mouse retina. A. Light microscopic analysis of the *Cngb1*-KO retina. In the normal mouse retina (+/+), the normal stratification into layers of appropriate thickness is observed (original magnification x 400). In contrast to the knockout retina (-/-), rods appear uniformly cylindrical and have thicker RIS and ROS layers. In the knockout retina both ROS and RIS are shorter and nonuniform in appearance, and somewhat disoriented (original magnification. x 400). Other layers appear normal, but pyknotic nuclei are apparent in the ONL and INL. B. Effects of age on heterozygous and KO retinas. Even at advanced age, heterozygous KO mice (+/-) are normal in appearance throughout all retinal layers. Within one year in homozygous KO mice the entire photoreceptor layer is absent; the INL is disrupted and is directly apposed to the RPE. C, D. Ultrastructure of wild-type and KO mouse photoreceptors. Tightly spaced, uniformly shaped photoreceptors are apparent in wild-type mice retinas in panel C (scale bar = 0.5  $\mu\text{m}$ ). In KO mice (panel D) the density of ROS is reduced and abnormal structural features are apparent (arrows). Every rod photoreceptor examined had some abnormal extracellular material running along portions of the plasma membranes (single arrows). Several disks in each field were in the process of disintegration (double arrow), consistent with a progressive reduction in the total number of photoreceptors.

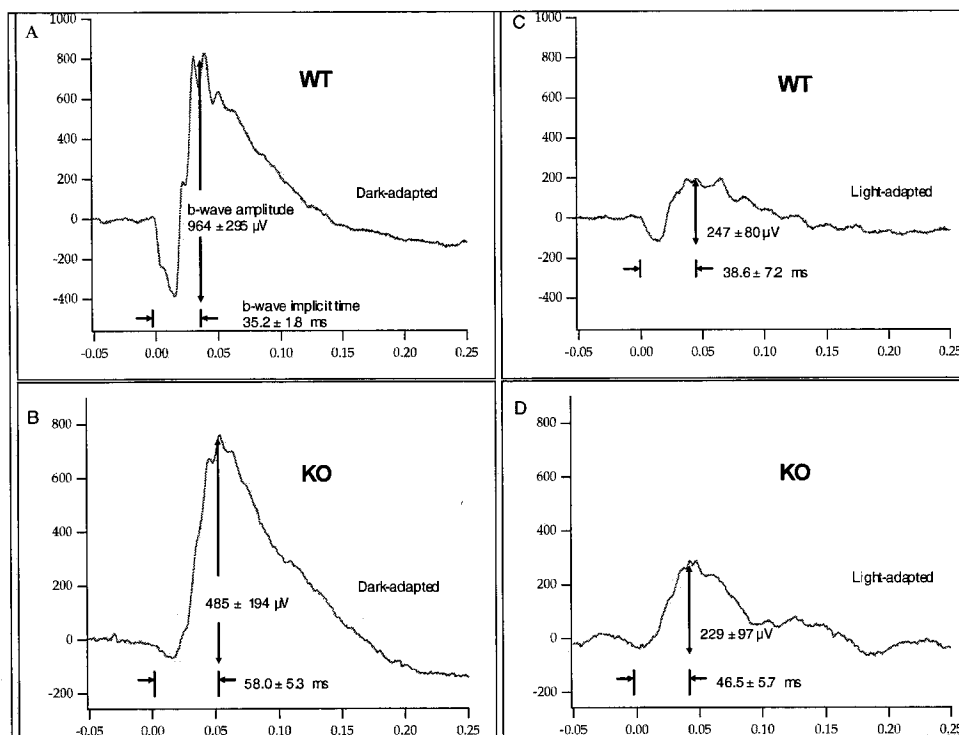


*Figure 12.* The b-wave amplitude and implicit time in 1-month-old mice. Results shown are WT and KO mice b-waves elicited by bright white flash under dark-adapted and light-adapted conditions. The bright white flash was calculated to isomerize  $5.63 \times 10^4$   $R^*$ . A and B show the b-wave results under dark-adapted conditions; C and D show the b-wave results under light-adapted conditions. The intensity of the 30-s background light (505 nm, green) is at neutral density filter (ND) 2.4, which was calculated to photoisomerized 7300  $R^*/\text{Rod}$  per s. The b-wave amplitude is measured from the trough of the a-wave to the peak of the b-wave. The b-wave implicit time is the time period between the flash and the peak of the b-wave. Values are shown on each panel by average  $\pm$  STDEV; also see Table 3 for details.

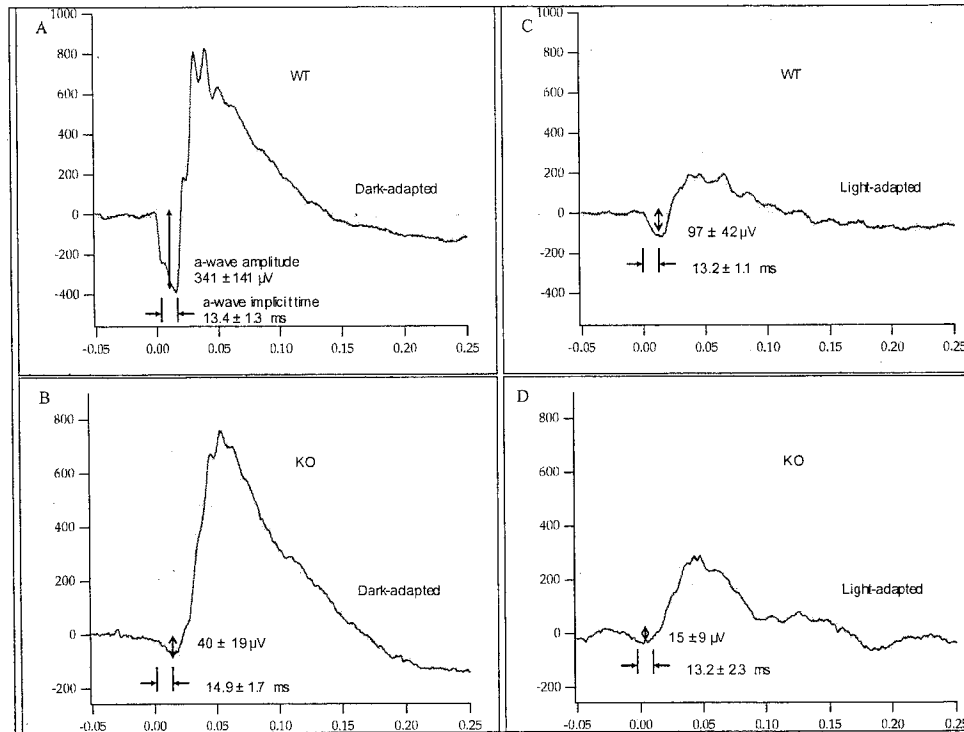


*Figure 13.* The a-wave amplitude and implicit time in 1-month-old mice. Results shown are WT and KO mice a-waves elicited by bright white light under dark-adapted and light adapted conditions. The bright white flash was calculated to isomerize  $5.63 \times 10^4 R^*$ . A and B show the a-wave results under dark-adapted conditions; C and D show the a-wave results under light-adapted conditions. The intensity of the background light (505 nm, green) is in neutral density (ND) 2.4, which was calculated to produce 7300  $R^*/\text{sec}$ . The a-wave amplitude is measured from the baseline to the trough of the a-wave. The a-wave implicit time is the time period between the flash and the trough of the a-wave. Values are shown on each panel by average  $\pm$  STDEV; also see Table 3 for details.

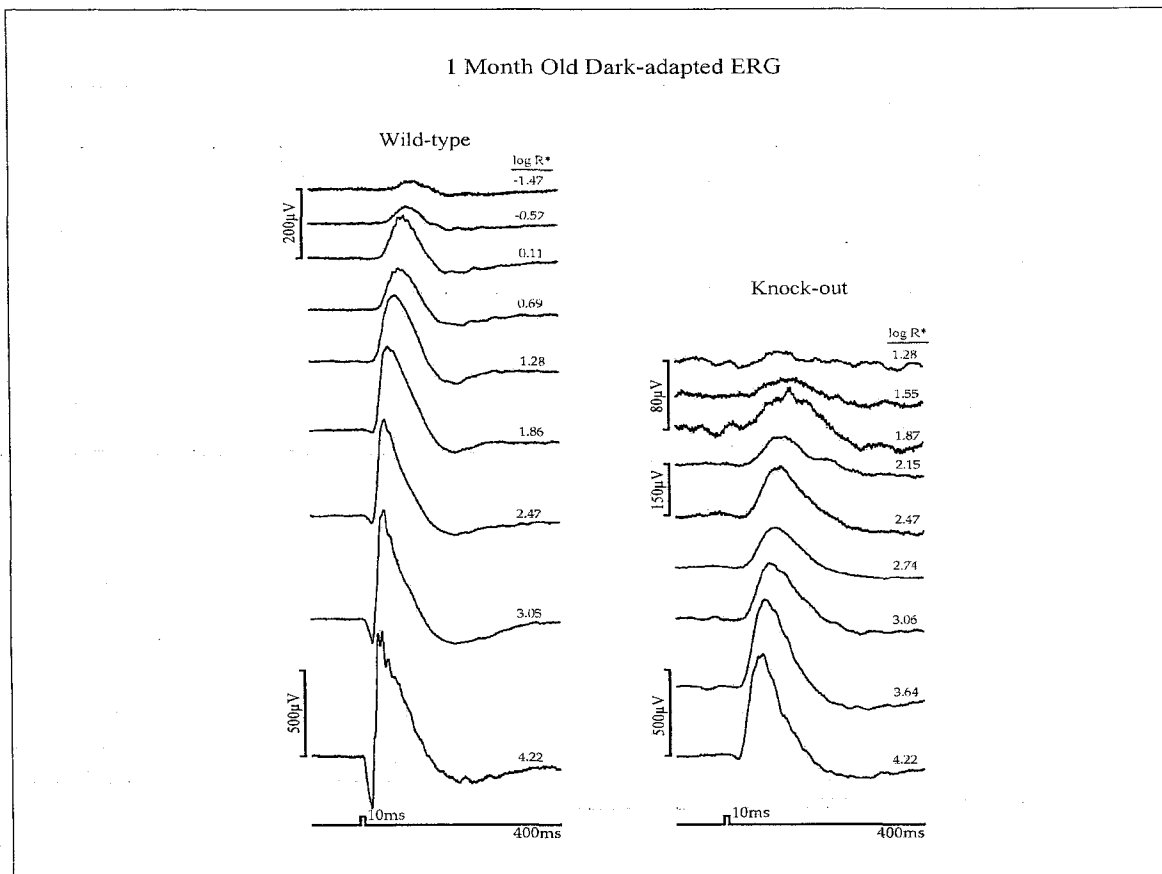


*Figure 14.* 1-month-old dark-adapted ERG. The ERG recordings of mice with WT and KO were elicited by 505-nm (bandwidth 35 nm) test flashes. Stimulus intensities from dimmer to brighter (upper to lower traces) are indicated by the number near each trace ( $\log R^*/\text{rod}$ ). Each trace is the average of 3-20 responses. The heterozygote (not shown) and wild-type mouse have similar responses to flashes. The knockout mouse, however, has a threshold 2.75 log units greater than the wild-type mouse here. Responses to 505-nm flashes (ND 0.0) are similar to the results of white flashes (not shown) for each genotype. KO mice shows following abnormalities: a smaller a-wave (1/7 of WT); a reduced b-wave (1/2 of WT); obvious delayed implicit time of b-wave.

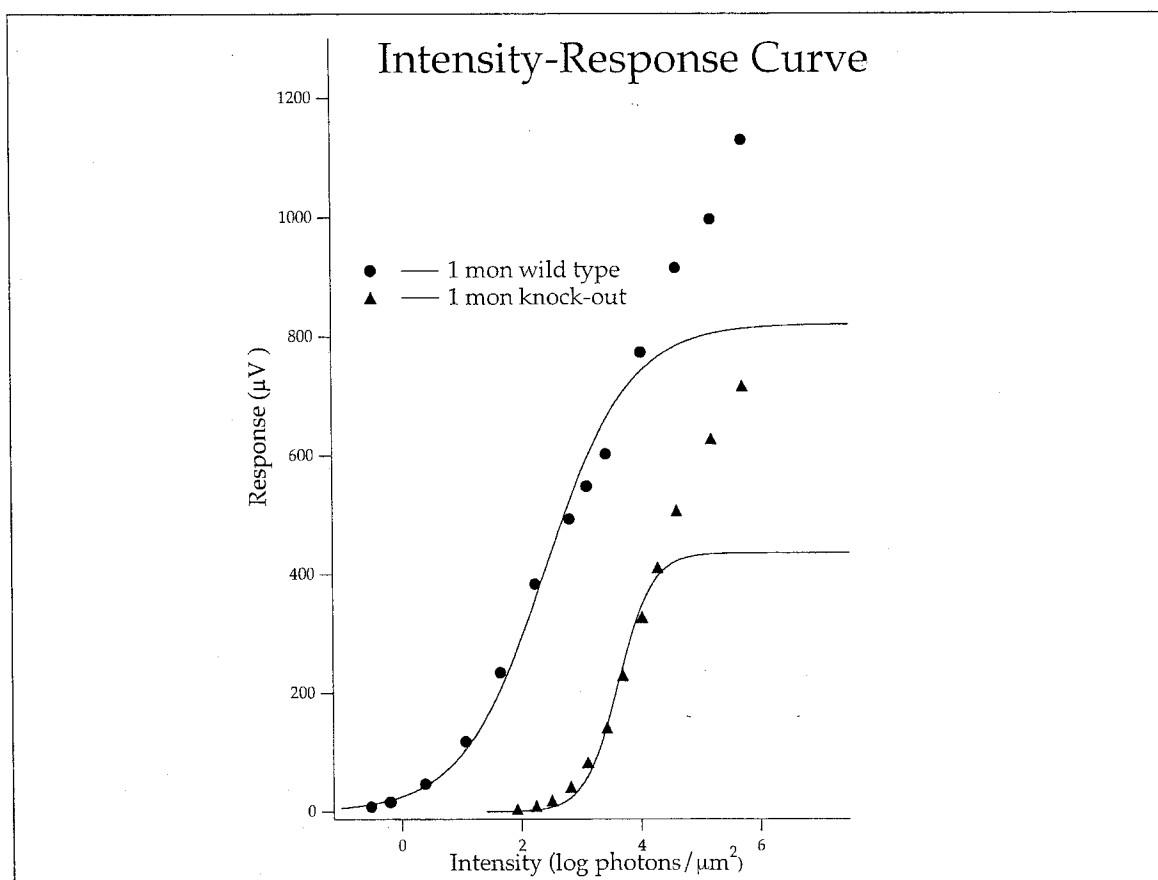


*Figure 15.* Intensity-Response curve fitting in 1-month-old mice. The amplitude of the averaged flash response (b-wave) is plotted against the log units of the stimulus intensity used to evoke each response. The intensity-response points in the lower limb were fitted to a modified Michaelis-Menten (Naka-Rushton) function using the IGOR data analysis software program. There is an obvious right shift of the knockout mouse curve (-/-, solid triangle) compared to the WT (+/+, solid circle) mouse curve. The b-wave sensitivity ( $I_{1/2}$ ) was quantified by measuring the light intensity required to evoke a half-maximal response of the rod b-wave. The maximum rod b-wave is the maximum response (rod and cone mixed) subtracted by light adapted b-wave (cone b-wave). The maximum response (rod and cone mixed) for each data set at the right of the graph came from a white camera flash setup ( $5.63 \times 10^4$  R\*/rod equivalent to 505-nm green light). The log unit of sensitivity or  $I_{1/2}$  (K-value) for KO mice is 1.4 log units right shift.

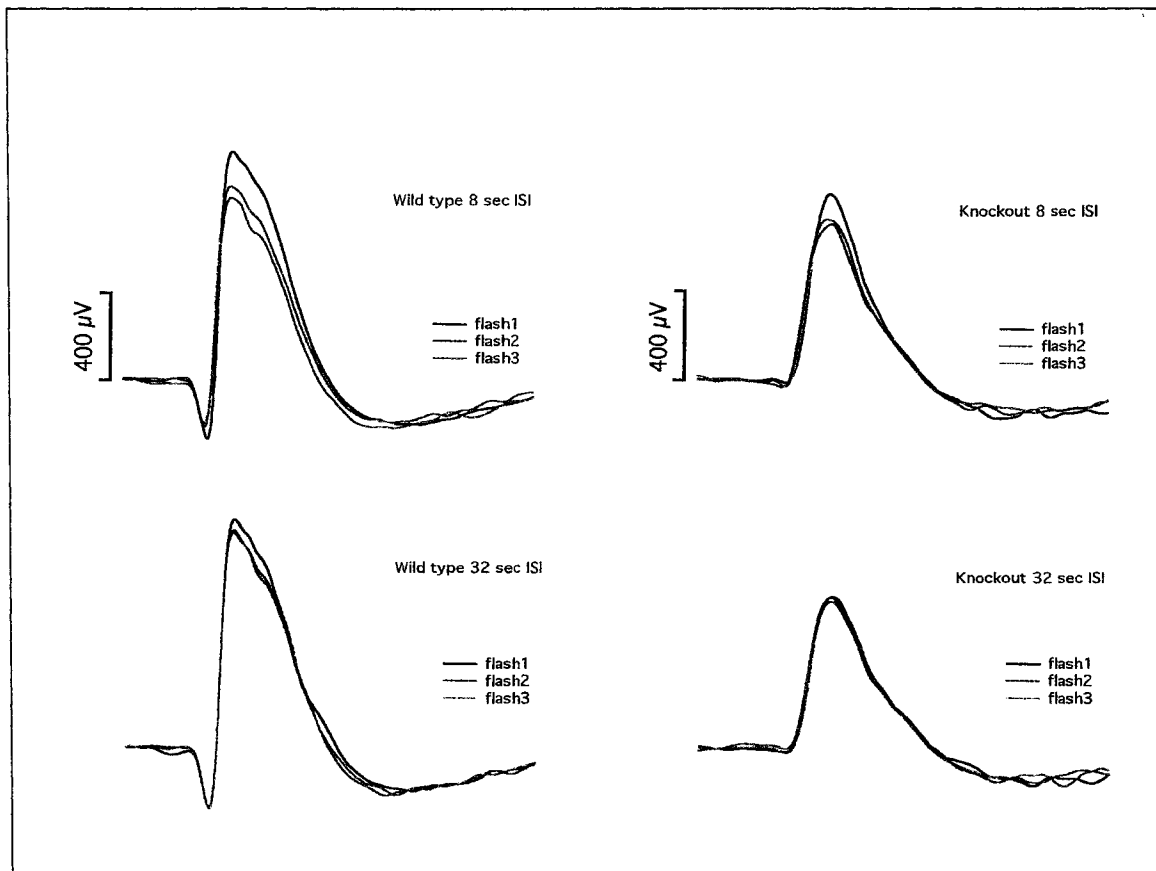


*Figure 16.* Dark-adapted ERG recovery under multiple flashes. WT and KO mice ERG recovery traces are shown. Each trace was elicited by 10 ms of 505-nm (ND 0.0, band width 35 nm) light with an intensity of  $1.7 \times 10^4$  R\*/rod. The traces are smooth because 70 Hz and above high-frequency components were filtered. The series of interstimulus interval (ISI) was as follows: 32, 16, 8, 4, and 2 s. Three flashes with a certain ISI were used in the experiment. Examples of 8- and 32-s ISI are shown above. The averaged second and third flashes are normalized as a percentage of the first flash for a specified ISI. The recovery is close to 95% in 32-s ISI in both genotypes; however, in 8-s ISI, KO mouse recovery is more complete than that of wild-type mice.

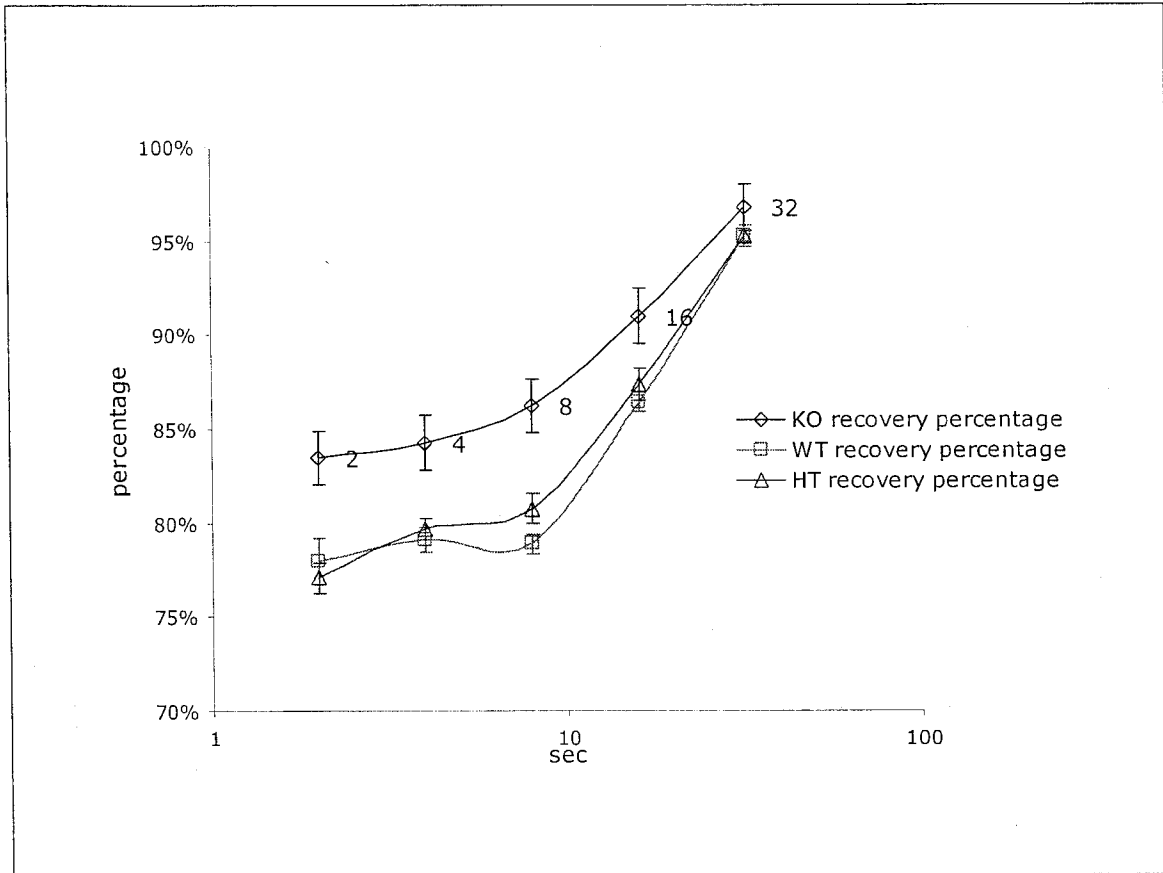


*Figure 17.* 1-month-old b-wave recovery by multiple flashes. Mice were divided into three groups, wild type (WT,  $n = 16$ ), heterozygote (HT,  $n = 17$ ), and knockout (KO,  $n = 15$ ). This figure is a semi-log curve that shows the average  $\pm$  SEM for each group and each specified ISI. Generally, all three genotypes of mice recover gradually from 2- to 32-s ISI. The recovery is close to 95% in 32-s ISI in all three genotypes. KO mice recover faster than WT and HT mice at all time points, at 2-, 4-, 8-, and 16-s ISI; the difference is significant statistically ( $P < 0.01$ ). On the other hand, there is no difference between WT and HT mice at different time points ( $p > 0.05$ )

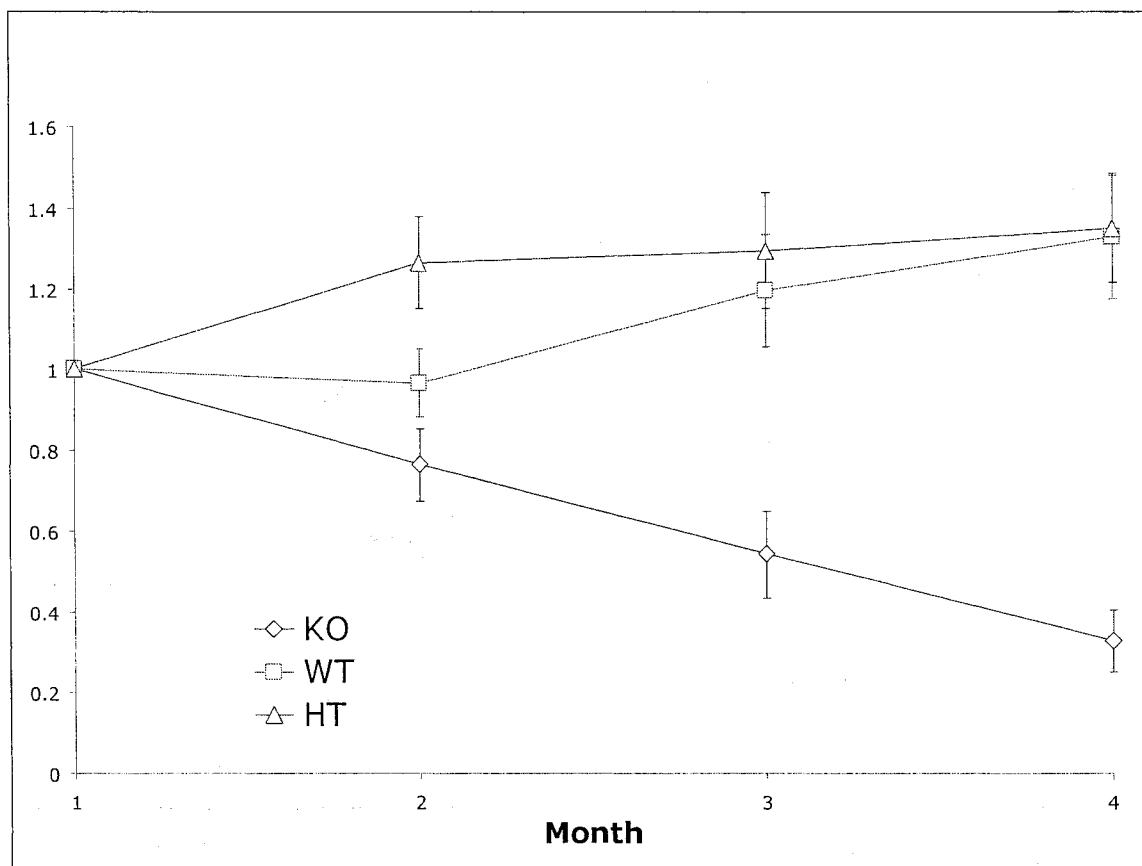


*Figure 18.* Normalized dark-adapted 1- to 4-month-old b-wave amplitudes. In dark-adapted conditions from 1- to 4-months, KO mice shows a linearized decreasing trend in b-wave amplitudes elicited by bright white flashes. WT and HT mice b-wave amplitudes were not decreased during a 4-month period. Error bars represent the SEM for each point.

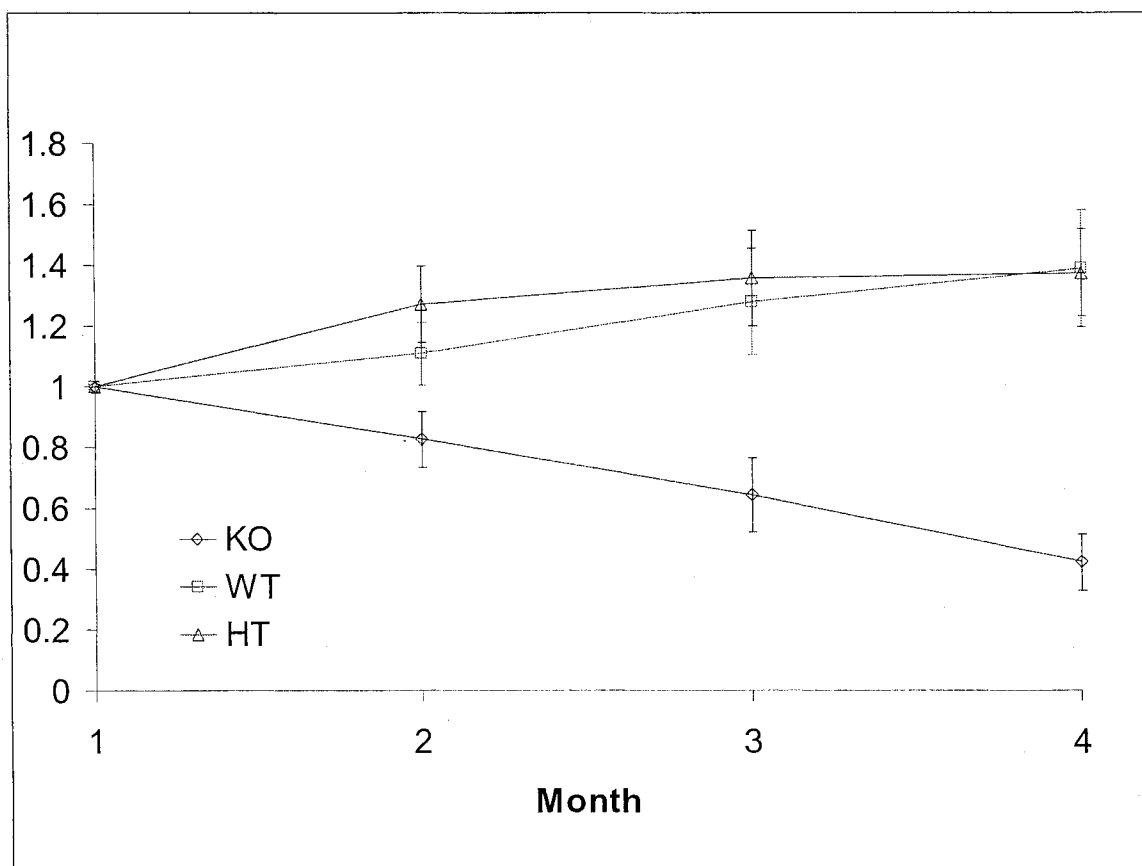


*Figure 19.* Normalized light-adapted 1- to 4-month-old b-wave amplitudes. In light-adapted conditions from 1- to 4-months, KO mice shows a linearized decrease trend in b-wave amplitudes elicited by bright white flashes. WT and HT mice b-wave amplitudes were not decreased during a 4-month period. Error bars represent the SEM for each point.

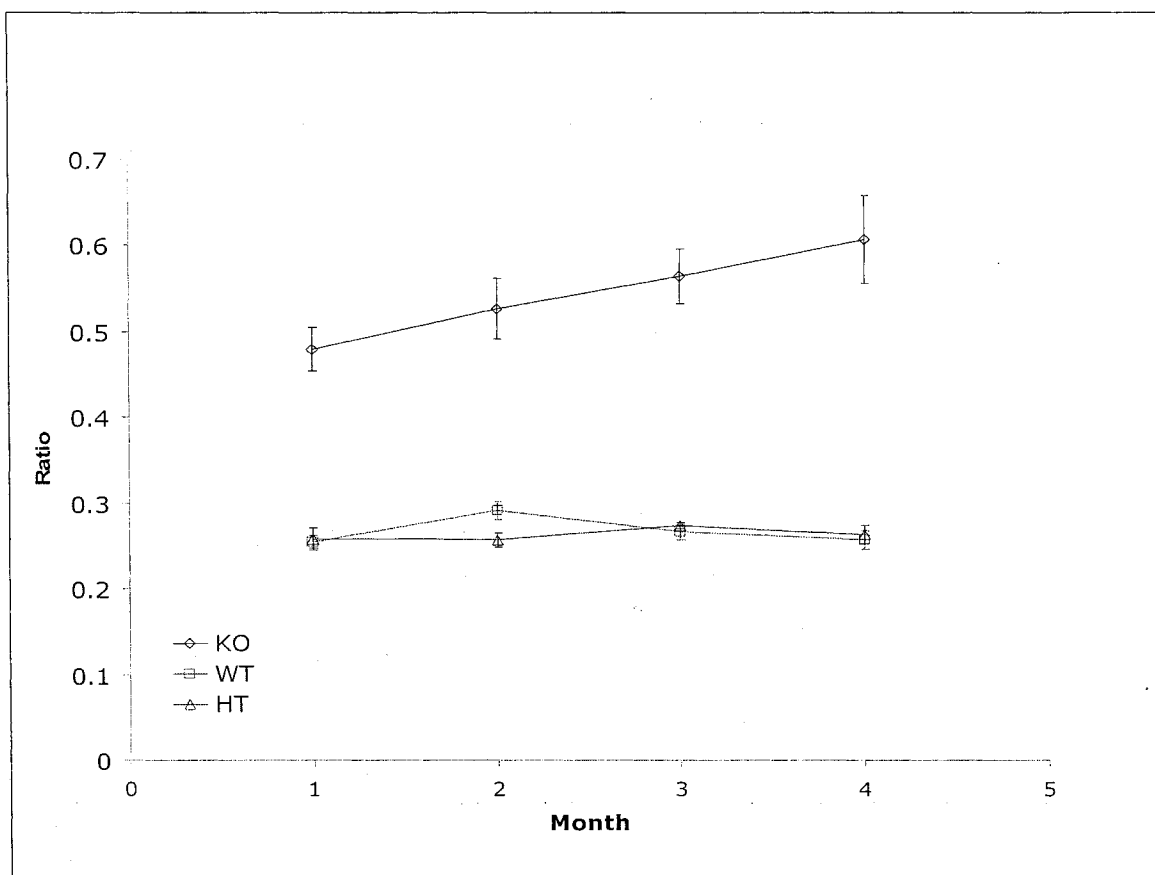


*Figure 20.* Light-/dark-adapted b-wave amplitudes over ageings. Both KO b-wave responses in dark-adapted (Fig. 18) and light-adapted conditions (Fig. 19) are decreased with ageings; in order to know the speed difference for both conditions, here we combined them in one curve. Each point shows the average ratio of light-adapted to dark-adapted b-wave amplitude elicited by bright white flashes. Generally, there is no change for the ratios of WT and HT mice; the curve is flat from 1- to 4-months-old. For knockout mice, the ratio is two times higher of that of WT mice in 1-month-old and also shows an increased trend over ageing. Error bars show standard error of mean. We find light-adapted b-wave's component is increasing in total b-wave. This means cone circuit is degenerating slower than the rod circuit.

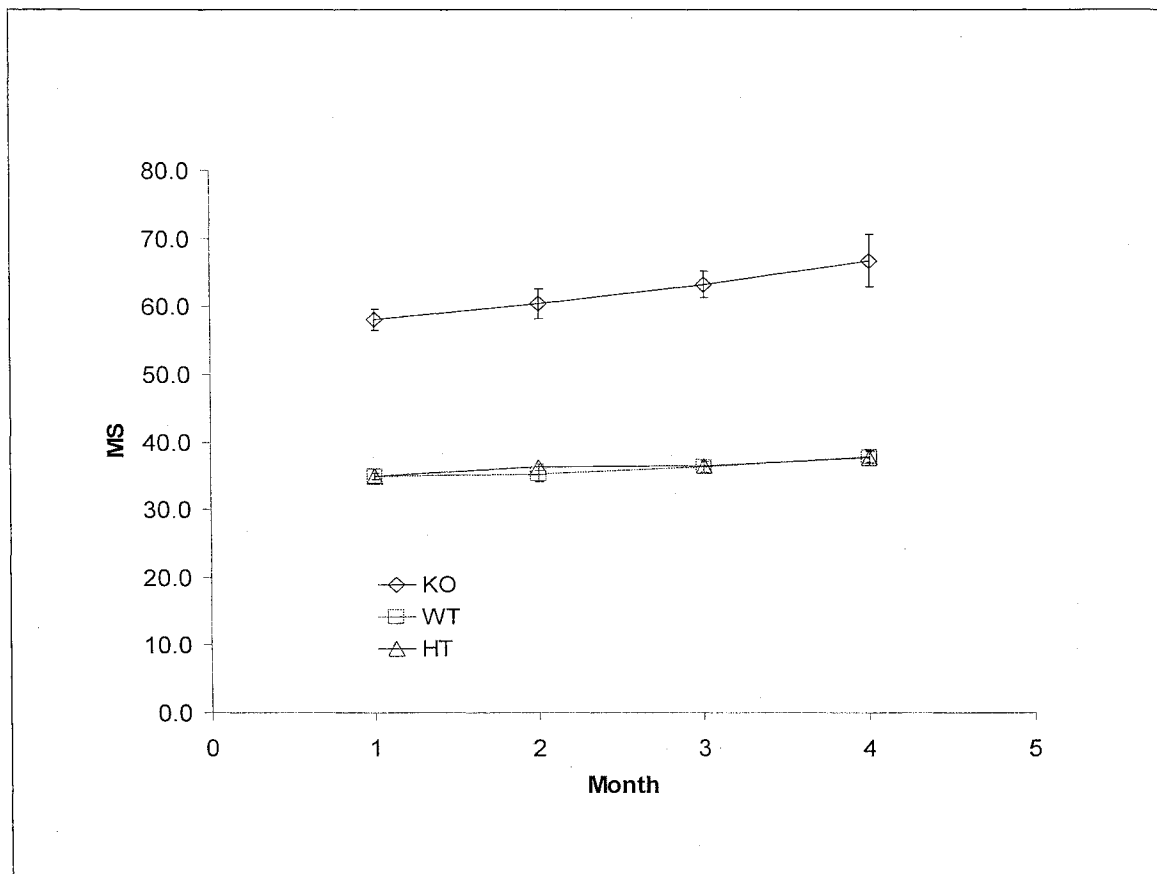


*Figure 21.* 1- to 4-month-old b-wave implicit times under dark-adapted conditions. WT, HT, and KO mice b-wave implicit times elicited by bright white flashes under dark-adapted conditions are shown by average. Error bars represent SEM. There is no difference between WT and HT for b-wave implicit times during a 4-month period, but between KO and WT, the difference is significant during a 4-month period ( $P < 0.0001$ ). Although there are increasing trends for all three genotypes, for KO mice this trend is more obvious. Significant differences can be found between 1- and 3- or 4-month ( $P = 0.044$  or  $P = 0.039$ ). In WT mice, between 1- and 4-month, the difference is significant ( $P = 0.0048$ ).

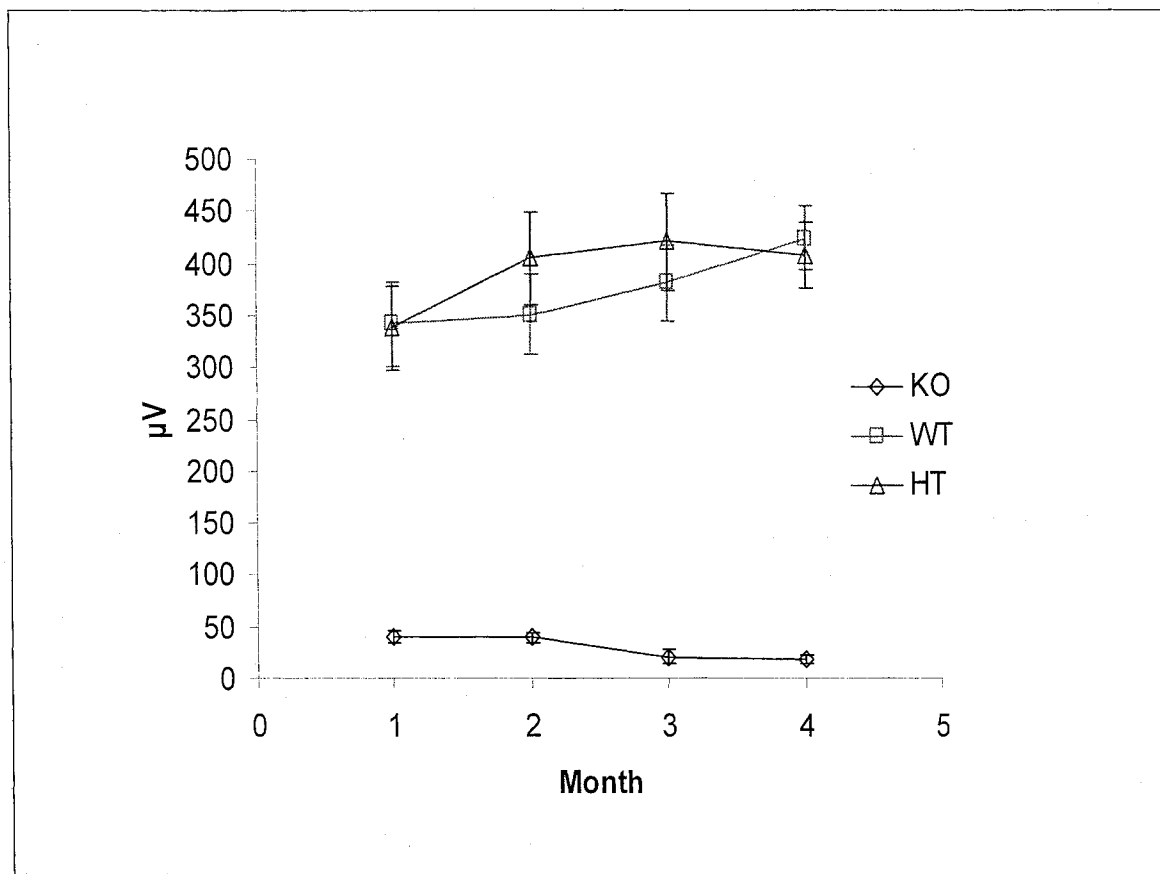
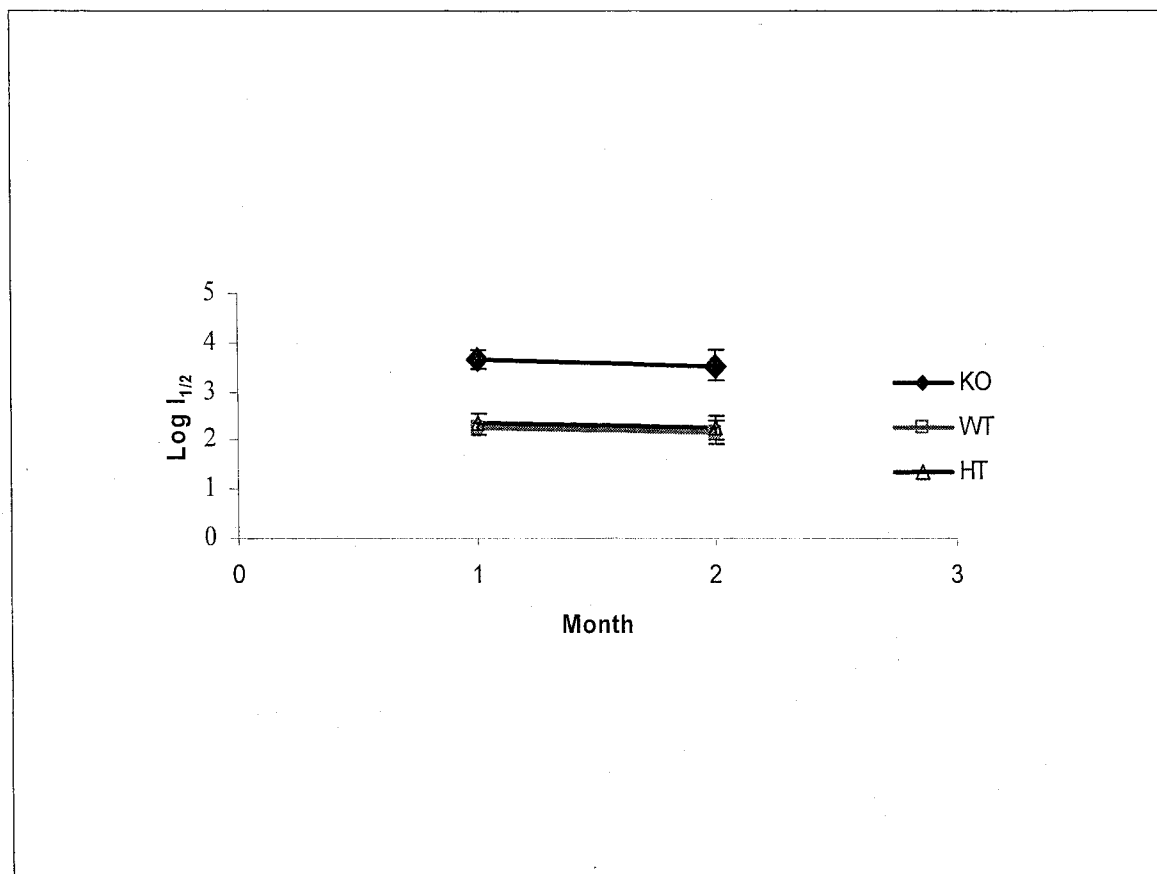


Figure 22. 1- to 4-month-old a-wave amplitudes under dark-adapted conditions. WT, HT, and KO mice a-wave amplitudes elicited by bright white flashes under light-adapted conditions are shown here. There is no significant difference for this parameter between WT and HT mice in a 4-month period. There is no a-wave decrease for WT (1- to 4-month,  $P > 0.05$ ), but in KO mice the decrease exists. In KO mice, the decrease trend is present (1- and 2-month to 3- and 4-month,  $P < 0.05$ ). Each point shows the average amplitude; the error bars represent standard error (SEM).



*Figure 23.* 1- and 2-month-old rod b-wave sensitivities ( $\log I_{1/2}$ ). 1- and 2-month-old  $\log I_{1/2}$  values are shown by an average at each time point. The error bars represent STDEV. There is no statistical difference between WT and HT mice at each time point ( $p > 0.05$ ). The differences between WT and KO mice are 1.41 and 1.37 log units at 1- and 2-month-old data,  $P < 0.001$ . No significant difference is found ( $p > 0.05$ ) between 1- and 2-month-old mice in all three genotypes. 3- and 4-month-old results are not plotted because some of rod b-wave amplitudes are less than  $70 \mu\text{V}$ .

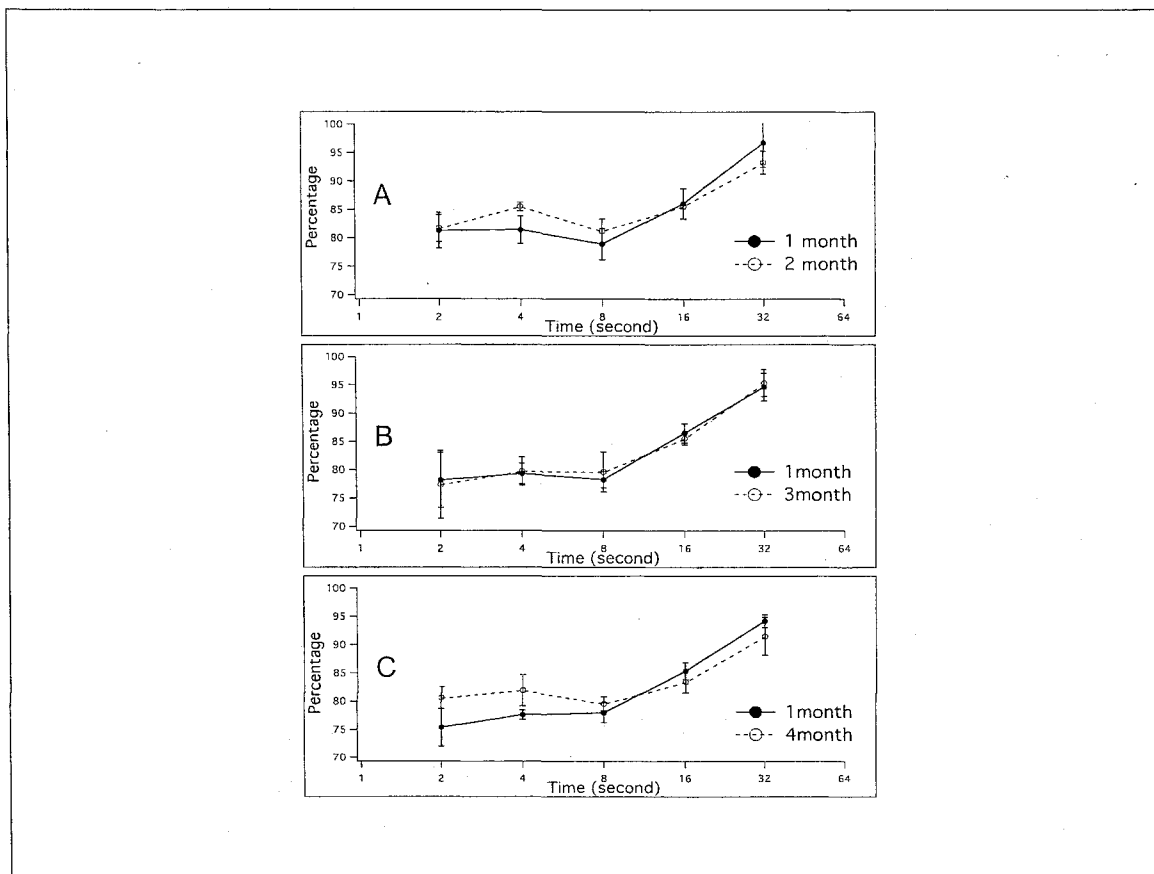


Figure 24. All 4-month b-wave recoveries by multiple flashes. Wild-type mice recoveries at different time points were recorded under dark-adapted conditions by three 505-nm (ND 0.0) flashes. Data from each panel are from same small group of mice. Upper panel (A) shows the recovery of 5 mice from 1- to 2-month. Middle panel (B) shows the recovery of 3 mice from 1- to 3-month. The lower panel (C) shows the recovery of 3 mice from 1- to 4-month (see table 12). We didn't see any difference in each time point during 4-month period, so we averaged all the recovery data (12 mice, 24 recordings) to set up a standard curve for KO and HT analysis in Figure 25. Error bars represent STDEV.

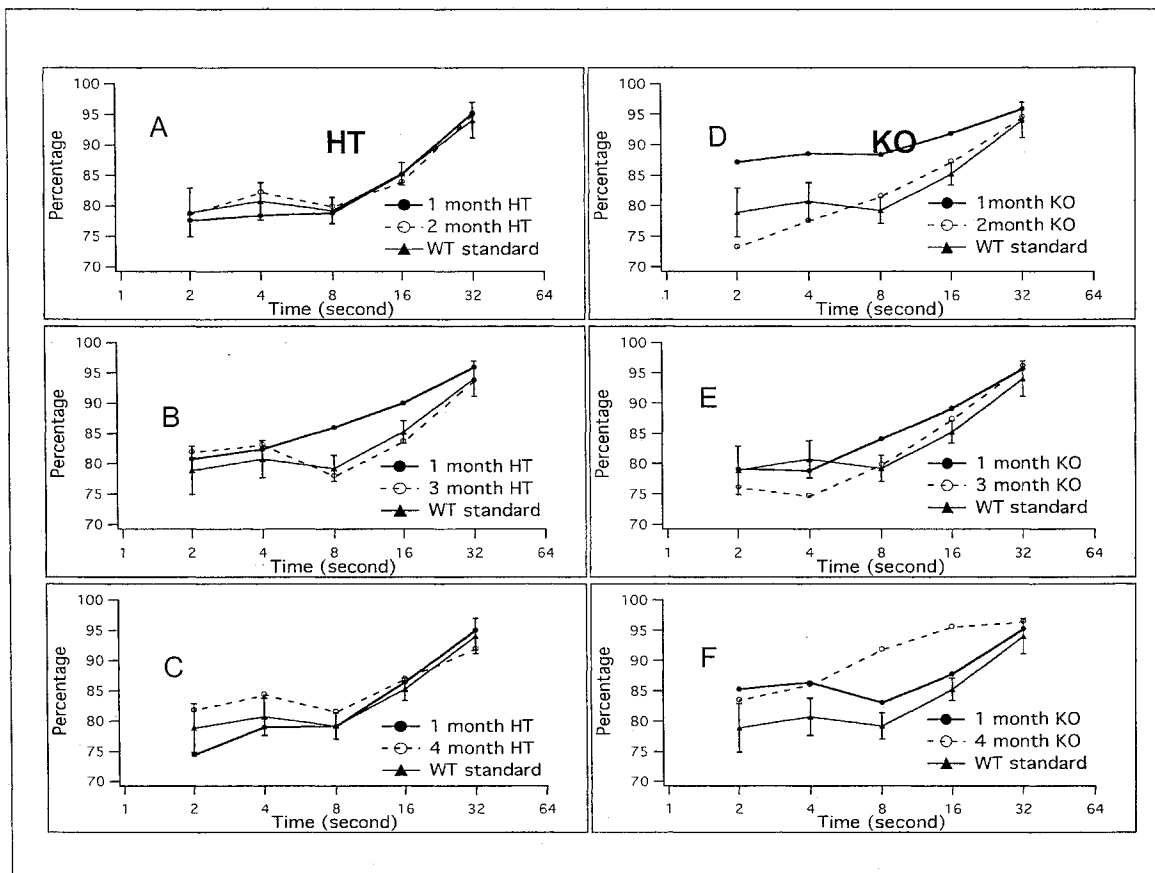


Figure 25. All 4-month HT and KO b-wave recoveries by multiple flashes. For HT mice, in panels A and C; 1- to 2- and 1- to 4-month recoveries are similar to standard WT. But in panel B, 1-month data at 8- and 16-s ISI shows larger variability. For KO mice in the right panels, 1-month recovery is faster than 2- and 3-month; 4-month recovery is faster than 1-month. Generally, KO recovery in a 4-month period is faster than the WT standard, consistent with 1-month recovery data in Figure 17, but at 2- and 4-s ISI, we can find that 2- and 3-month KO recoveries (panel D and E) are slower than the WT standard.

## CONCLUSION AND DISCUSSION

### *Cngb1* Gene Knockout Does not Affect Neighboring Genes

The murine *Cngb1* gene is located on chromosome 8 and spans ~68 kb of the genomic DNA sequence. The upstream gene TEPP is 5 kb from *Cngb1* and in a reverse orientation; therefore it is unlikely to affect the promoter region of TEPP (Figure 3). The downstream gene *kifc3* is in the same orientation and 127 kb away from *Cngb1*, including the length of *Cngb1* gene itself, the knockout region is about 200 kb from *Kifc3*; thus we can overlook the possibility that there are direct effects on *Kifc3* after the *Cngb1* gene knockout. The absence of the deleted region is unlikely to disturb the expression of other genes (Figure 3). In kidney, *Kifc3* functions in apical transport of annexin XIIIb-associated membranes (Noda et al., 2001). *Kifc3* can be expressed in brain and retina; in retina, it is expressed in the outer plexiform layer and RPE (Hoang, Whitehead, Dose, & Burnside, 1998; Yang et al., 2001). Although it is a candidate gene for Bardet–Biedl Syndrome (a disease that includes retinal degeneration as a cardinal feature) (Hoang et al., 1998), *kifc3* knockout mice do not show obvious abnormality in the retina (Yang et al., 2001). Therefore, *Kifc3* is of no concern in our studies. There is a pseudogene that maps to coordinate 11c3-ps6 that is very close (260 bp) to the deleted region, but by definition a pseudo-gene does not translate protein, so this also is not of concern for our KO model. The only gene to be considered is TEPP, because this gene is distributed in testis, prostate, and placenta; TEPP might have a role in reproductive biology (Bera et al., 2003). We found normal litter size variability (n = 4 to 11), normal body size of newborn mice, nor-

mal bodyweight at 1 month and 2 months, and normal lifespan in *Cngbl*<sup>-/-</sup> mice. We did not find any abnormal breeding, feeding, or mortality rates in the knockout mice, so the knockout design will likely not affect other genes that are close to the *Cngbl* locus. We have not found any systemic abnormalities and only retinal degeneration in the eye. Heterozygous breeding produced all three genotypes of mice (+/+, +/-, -/-) in expected Mendelian ratios. All of these phenomena indicate that this is a successful, single-gene knockout model.

#### The Effect of N-terminal Gene Knockout on *Cngblb*

In addition to expressing the channel  $\beta$ -subunit (*Cngb1a*), GARP-1, and GARP-2 in rod photoreceptors, the *Cngbl* gene also expresses a variant  $\beta$ -subunit (*Cngb1b*, without the GARP region) in olfactory, where it functions as a channel modulator (Kaupp & Seifert, 2002; Sautter et al., 1998). We summarize the gene transcripts of *Cngbl* in Figure 5. Huttl et al (2005) made a 3'-end *Cngbl* knockout mouse model deleted for exon 26 that encodes regions similar to the  $\alpha$ -subunit pore-forming region and S6 transmembrane segment. In addition to rod photoreceptor abnormality, Huttl et al. found a high mortality rate and low body weight in homozygous knockout mice, which were assumed to be caused by olfactory deficiency, because normal *Cngb1a* and *Cngb1b* subunits are disturbed in their knockout model. We did not find a high mortality of knockout mice, nor is there a significant difference ( $p < 0.01$ ) when comparing each pair of genotypes (see Table 2). We did not find similar effects in our 5' *Cngbl*<sup>-/-</sup> mouse, suggesting that *Cngb1a* and *Cngb1b* transcripts do not share common promoter regions upstream of exon 1; *Cngb1b* should have its own promoter inside the *Cngbl* gene.

### Complete *Cngbl* cDNA Sequence and Translated Protein Sequence Provide Basis for Further Study of *Cngbl*-Related Project

We were aware of CNGB1 cDNA sequences of bovine (Korschen et al., 1995), human (Colville & Molday, 1996), and rat in the Genbank database; however, there was not a complete murine *Cngbl* cDNA sequence. We found that the BAC clone BC016201 covers exons 1-12a and XM-286113 covers exons 15-33. We filled the 500-bp gap between exon 12 and exon 15 by RT-PCR amplification and sequencing. The complete murine *Cngbl* cDNA sequence is 6189 bp from exon 1 to exon 33, which translates to a 1325-amino acid residue  $\beta$ -subunit (Figure 4). Northern blot analysis reveals a 6.2-kb band corresponding to *Cngbl* mRNA in wild-type mice (Figure 8).

### Structure of Murine *Cngbl* Transcripts Exemplifies the Diversity of Transcription

Like the human gene (Ardell et al., 2000), the murine *Cngbl* locus consists of at least 36 exons and was undergone multiple modes of alternative splicing, generating transcript and encoded protein diversity (Figure 5). Except for the 33-exon full-length *Cngbl* transcript (*Cngbl*a), there are additional exons found in other transcripts, such as exon 12a in GARP-2, Exon 16a [Figure 6A(g)] in GARP-1 (Grunwald et al., 1998), and extended final exon 18 (18L) in GARP-1. In olfactory-expressed *Cngbl*b (Sautter et al., 1998), there is a predicted exon 14a in the *Cngbl* gene, which is the first exon of *Cngbl*b. Most likely, *Cngbl*b has its own promoter close to its first exon (14a in *Cngbl*a). Our knockout mice did not show a high mortality rate after birth, nor the low body weights which were observed in *Cngbl*b knockout mice (Huttl et al., 2005), indicating that the *Cngbl*b isoform uses an independent promoter that is downstream to exon 2 of the *Cngbl* gene (exon 1 and 2 are deleted in our model).

### Functional PGK Promoter for Part of *Cngb1* Gene Expression Can Be Avoided in Future Knockout Model Design

The Neo cassette consists of PGK promoter, neomycin resistance gene, and PGK polyA tail, so it is not surprising to see neomycin resistance gene transcripts in our KO model (Figure 7A). Since by RT-PCR [Figure 7 and Figure 6A(b)], we found a neomycin resistance gene and a *Cngb1* hybrid mRNA transcription of *Neo-Cngb1*. There is a stop codon in the PGK tail, and the stop codon disrupts the open reading frame of the remaining  $\beta$ -subunit. This result means that if the truncated  $\beta$ -subunit transcript is translated, it has to pass through the stop codon in the Neo gene, and therefore the hybrid mRNA cannot translate the truncated  $\beta$ -subunit protein unless there is alternative splicing to bypass through the stop codon. Because we could not rule out this possibility, we used Western blot analysis to identify any truncated protein expression. In future knockout construct design, we can reverse the direction of the Neo cassette or add conditional knockout inserts to delete the Neo cassette.

### Molecular Biology and Proteomics Confirm That Our Mouse Model Is a True $\beta$ -Subunit and GARP Knockout Model

RT-PCR in Figure 6A(a), (b) and Figure 7 show that exon 2 is deleted and that the *Neo-Cngb1* hybrid RNA is formed in KO mice. As noted above, although part of the *Cngb1* gene is transcribed (exon 3-33, in Figure 6 and Figure 7b), there is a stop codon in front of the remaining channel subunit sequence that will preclude continued translation into the  $\beta$ -subunit coding region. This means that no truncated channel sequence can be expressed. We found in our KO mice that the expression of a hybrid *Neo/Cngb1* and free GARP mRNA transcripts are undetectable in Northern blot analysis (Figure 8). Thus,

even if there was some expression, the transcript levels are too low to support any significant accumulation of protein. The Northern results are consistent with the expression level of GARPs and *Cngb1* seen by a Western blot of normal ROS homogenates where GARP-2 was the most abundant among the three proteins and GARP-1 was the least, about 1/10 of GARP-2 (Colville & Molday, 1996). Western blot and immunohistochemistry did not show the expression of truncated *Cngb1* or GARP in the KO (Figures 9 and 10), whereas control proteins are normally expressed, such as peripherin/rds, ABCA4, GC1, ROM1, Rhodopsin, and PDE6 $\alpha$ . These results together demonstrate that this mouse model is a true *Cngb1* null model.

#### The Channel $\beta$ -Subunit is Required for $\alpha$ -Subunit Transport to ROS

Surprisingly,  $\alpha$ -subunit in ROS is dramatically decreased in the Western blot and in immunohistochemistry. In Western blot, increasing the contrast revealed a minor band of the appropriate size that may represent the 63-kDa  $\alpha$ -subunit (not shown). Other ROS proteins, such as peripherin-2/rds, NCKX1, ABCA4, GC1, ROM1, Rhodopsin, and PDE6 $\alpha$  are not affected. Consistent with the protein levels, the transcriptions of the channel  $\alpha$ -subunit and other genes, such as peripherin-2, Rom-1, PDE6 $\gamma$ , and GC1, appear normal by RT-PCR. The expression of *Cngal* is greatly reduced in ROS and is not ectopically expressed elsewhere in the retina. This result implies that normal transport of the  $\alpha$ -subunit to the ROS requires the  $\beta$ -subunit and/or GARPs. This is in contrast to the heterologous expression of the  $\alpha$ -subunit, where the  $\beta$ -subunit is not required for transport to the membrane or channel function (Trudeau & Zagotta, 2002a). The difference between KO mice rod photoreceptors and the heterologous system used (*Xenopus* oo-

cytes) suggests that the channel proteins transporting to ROS plasma membrane use a different mechanism or pathway. The checkpoint that prevents the abnormal tetramerized proteins from incorporating into nascent disks is in the vicinity of the connecting cilium (Loewen et al., 2003). The connecting cilium may be involved in preventing or reducing  $\alpha$ -subunit-only homomeric channels from moving to the plasma membrane. This may also explain the 3'-end *Cngb1* knockout mice (Huttl et al., 2005), in which the  $\alpha$ -subunit in the ROS membrane was not detected by Western blot and was just barely detected by immunohistochemistry. The interaction of the  $\beta$ -subunit N-terminus and the  $\alpha$ -subunit C-terminus may be required for membrane targeting of wild-type heterotetrameric channels (Trudeau & Zagotta, 2002a, 2002b). This may explain why an interaction between the  $\alpha$ -subunit and  $\beta$ -subunit is required for  $\alpha$ -subunit transport to ROS. Both the N- and C-termini should join in the interaction, because 3'- and 5'-end  $\beta$ -subunit knockouts show dramatically decreased  $\alpha$ -subunit expression in ROS. The  $\beta$ -subunit may be required for assembly and/or transport of normal levels of  $\alpha$ -subunit to the ROS plasma membrane.

#### The $\beta$ -Subunit Does not Play a Critical Role in ROS Disk Morphogenesis but Has a Structural Role

The Western and histology results establish that ROS are formed and of sufficient integrity to remain relatively intact throughout the isolation procedures. This suggests that the  $\beta$ -subunit is not critical for the disk morphogenesis of ROS. Disk morphogenesis can be disrupted by different mechanisms, such as the disruption of actin cytoskeleton dynamics. Cytochalasin D interferes with F-actin filament polymerization, thereby inhibiting new disk formation by the cessation of the initiation of membrane evagination (Vaughan & Fisher, 1989). The retinitis pigmentosa GTPase regulator interacting protein

(RPGRIP) is located in the photoreceptor connecting cilium (CC). A defect in RPGRIP can cause Leber congenital amaurosis. In an RPGRIP<sup>-/-</sup> mouse model, oversized disks and quick degeneration can be found in ROS (Zhao et al., 2003). This model is thought to relate to disturbed cytoskeleton dynamics because of the C-terminal homology of RPGRIP<sup>-/-</sup> and actin-fragmin kinase. A second mechanism is classified as a structural disk protein gene abnormality. Genes involved in this class of disruption include peripherin/rds, ROM-1, and rhodopsin. Homozygous rhodopsin gene KO mice showed undeveloped ROS (Lem et al., 1999). The curved disk rim is formed by a tetrameric peripherin-rom-1 complex interaction on opposing membrane sides through disulfide bond formation (Boesze-Battaglia & Goldberg, 2002). Peripherin-2 is distributed not only in disk rims, but also in incisures (Arikawa et al., 1992; Loewen et al., 2003; Papermaster et al., 1978); this suggests that peripherin-2 also plays an important role for incisures formation. The rds mice homozygous for a disrupted peripherin-2 gene fail to develop outer segments; even heterozygous mice later develop highly disorganized disks (Hawkins et al., 1985; Sanyal & Jansen, 1981). Rom-1 knockout mice demonstrated a less severe phenotype (Clarke et al., 2000). Therefore, the proteins interacting with peripherin-2 must be important for the morphogenesis of ROS. The GARP part of the  $\beta$ -subunit and soluble GARPs were found to interact with peripherin-2 in vitro by immunoprecipitation. GARPs interact with peripherin-2 oligomers covalently, and also interact with peripherin-2 tetramer weakly (Poetsch et al., 2001). The  $\beta$ -subunit is localized in the plasma membrane, and its N-terminal GARP part is located in the cytoplasm (Colville & Molday, 1996). The other two soluble splicing variants, GARP-1 and GARP-2, are localized to the rim region and incisures of disks (Korschen et al., 1999). The gap between disk rims and

plasma membrane is about 10 nm; fibrous elements observed in the space between rim and plasma membrane by freeze fracture analysis may be comprised of proteins interacting to keep the shape of disks and plasma membrane (Roof & Heuser, 1982). Part of the 240-kDa  $\beta$ -subunit may be involved in the formation of this kind of filament (Wong & Molday, 1986). The interaction of the GARP part of the  $\beta$ -subunit and the peripherin-2 oligomers is the only known interaction that may comprise the structural scaffold between disks and plasma membrane. The interaction of free GARPs with peripherin-2 may play a critical role in keeping the tight stack of disks and space in incisures. The nonuniform stacks of ROS, as well as abnormal plasma membrane in 1-month *CNGB1*<sup>-/-</sup> mice, suggest that *CNGB1* gene products play an important role in maintaining ROS structural integrity.

#### Electrophysiological Change in 1-Month-Old KO Mice

Under dark-adapted and light-adapted conditions, although there are a couple of exceptions, such as b-wave amplitude and a-wave implicit time, under light-adapted conditions, we generally find significantly decreased a- and b-wave and delayed implicit time in the knockout mice. This means that the photoreceptors are degenerating in the 1-month retina after the *Cngbl* gene knockout.

An obvious question is whether the rod photoreceptors are still functional. There are several reasons why, from the ERG data alone that the answer to this question is yes, the rods are functional in the KO mice retina. First, the *Cngbl*<sup>-/-</sup> mice have a threshold light intensity 2.8 log units higher than WT mice, compared to 4.7 log units in the rhodopsin knockout mouse, which is devoid of rods due to the failure to develop ROS

(Toda et al., 1999). Based on the threshold study, our mouse is more sensitive to light, therefore some rod photoreceptors should remain in one month: Second, the b-wave amplitude is equal to 1/2 that of WT mice under the brightest flash; for WT mouse, the light-adapted b-wave amplitude extrapolated for a cone-only response is about 1/4 of dark-adapted b-wave in our experiments, and this result is close to the result of previous studies in which the cone b-wave ratio is 1/3 (Lyubarsky et al., 1999). This indicates that 50% of the b-wave must be driven by some functional rod photoreceptors in our knockout mice. In addition, significant change (>50% decrease) of a-wave amplitude in KO mice with or without background light means that impaired rod photoreceptors are still functional in knockout mice.

The photocurrent of the photoreceptors not only accounts for the ERG a-wave, but also is the driving force of the on-bipolar cell-originated b-wave. The decrease in amplitude of the a-wave (eight-fold) and the b-wave (two-fold) reflects the degeneration of the rod photoreceptors, because normally 97% of mouse photoreceptors are rods (Carter-Dawson & LaVail, 1979). The decreased a- and b-wave amplitudes and increased threshold could be caused by decreased photoreceptor numbers, shortened ROS, or decreased photoreceptor function. One-month histology shows a slight decrease in outer nuclear layer thickness and 1/3 shortened ROS. The 27-fold lower sensitivity (increased  $I_{1/2}$ ) suggests that the remaining photoreceptors are desensitized (Peachey, Alexander, Derlacki, & Fishman, 1992a). This result is also consistent with the abnormal morphology, such as the disorganization and apparent overgrowth of disks, as well as the single-cell recording that shows a 4.8-fold decrease in sensitivity (results not shown). The difference in reduced sensitivity of single rods compared to the reduction in the ERG response (27-

fold lower than wild type) in the *Cngb1*<sup>-/-</sup> retina is likely due to a selectivity bias for healthier rods in the single cell recording and the absence of downstream signaling with single-rod measurements.

The 85% reduced a-wave amplitude in the presence of the background light suggests decreased cone function, yet the b-wave amplitude in the presence of background was unchanged. Also in the dark, a-wave amplitude was decreased to a greater extent than that of the b-wave (8-fold to 2-fold). It is possible that there was some compensatory synaptic development amplifying the cone and rod signals within the bipolar layer, making up for the attenuated photoreceptor signals. As rod photoreceptors degenerate, rod bipolar cells establish synaptic contacts with cones in retinal degeneration (*rd1*) mouse and Royal College of Surgeon (RCS) rat (Peng, Hao, Petters, & Wong, 2000; Peng, Senda, Hao, Matsuno, & Wong, 2003). It is also possible that there was a higher convergence ratio of rods onto rod bipolar cells (Dacheux & Raviola, 1986; Freed, Smith, & Sterling, 1987) that would support a reduced number of rods can fully activate a rod bipolar-cell depolarization without background light.

Under both light- and dark-adapted conditions, the b-wave implicit times are delayed in knockout mice; the a-wave under dark-adapted conditions showed slightly longer time than wild type, indicating that the signal production in rods and the transduction kinetics in both rod and cone pathways are impaired in the knockout mice. Single cell recordings showed delayed time-to-peak in the rods, which could explain the delayed b-wave (single-cell results not shown).

### One to 4-Month-Old ERG Changes and Retinal Degeneration

We find that the KO mice b-wave amplitudes under both dark-adapted and light-adapted conditions show a linearized decreased trend from 1- to 4-month-old; WT and HT mice do not show a decreased trend in the same situation, but show slightly increased trends. Wild-type ERG showed the b-wave amplitude reaching maximum value at 2-month-old, and then showed a decreasing trend later on (Dalke et al., 2004; Li, Cheng, Yang, Peachey, & Naash, 2001). The continuously increasing trends in both HT and WT mice are most likely due to an improvement in my ERG technique, because we collected the data over an 8-month period. Regardless, the decreasing trends in both dark- and light-adapted conditions indicate a degeneration of the rods and cones, respectively. In order to know which type of photoreceptor is degenerating faster, we plotted the ratios of light/dark-adapted b-wave amplitude versus time, and found that WT and HT mice show flat and almost identical lines, but KO mice are represented by an increasing line. In addition, the initial ratio is higher than that for WT mice. This means that the cones are degenerating relatively more slowly than rods in KO mice and that the rod degeneration is apparent at one month. Morphometric analysis of the numbers of rods and cones in 1- to 4-month-old mice by histological staining may allow more definitive proof of this observation.

It is not a surprise that the b-wave implicit time increases with time under dark-adapted conditions in KO mice, because we find continuously progressive photoreceptor degeneration. We also find increased b-wave implicit times of WT mice between 1- and 4-month-old mice in the same condition as KO mice; this can be explained by age-related

changes. However, the implicit time is not changed in an age-dependent fashion in C57BL/6 mice (Li et al., 2001).

The changes of dark-adapted a-wave amplitudes in a 4-month period show similar trends to that seen for the b-wave in WT and HT mice; the trends are a relatively small a-wave amplitude at one month and stable or slightly increasing trends after 2 months. The relatively smaller a-wave amplitude in the first 2 months in KO mice (1/9 of WT) decreased significantly in 3-month and 4-month old mice (1/20 of WT), indicating that the number of functional rod photoreceptors decreased dramatically in 3-month-old KO mice. Since the 1-month light-adapted ERG shows only a 15- $\mu$ V a-wave which is equivalent to a cone-only photoreceptor photocurrent, we speculated that most if not all of the a-wave (18  $\mu$ V) is produced in cones in 4-month dark-adapted ERG. Other studies found that a cone-produced a-wave amplitude is around 21  $\mu$ V, which is comparable to our finding (Lyubarsky et al., 1999).

As noted above, rod b-wave sensitivity of 1-month-old KO mice decreased 1.41 log units (27-fold) compared to WT mice. In 2-month-old mice, the difference (1.37 log units) is not changed. In 3- and 4-month-old knockout mice, the ERG is noisier if compared to 1- and 2-month ERG, and about half of the responses are less than 70  $\mu$ V. We did not calculate the sensitivities ( $I_{1/2}$ ) at 3- and 4-months because of the advanced stage of retinal degeneration. The 2-month sensitivities results reflect the relatively slower degeneration of rod photoreceptor from 1- to 2-month-old mice or a compensation mechanism in rod bipolar cells.

### Recovery Kinetics and Retinal Degeneration

The 1-month recovery data show that the recoveries of KO mice are faster than those of WT and HT. At a 32-s ISI, the recoveries of three genotypes are around 95%, and there are no significant differences among them; however, at 2-, 4-, 8-, and 16-s ISI, the recoveries are faster in KO mice. Previous discussion indicated that cone response is about 1/4 in WT mice and 1/2 in KO mice in one month in light intensity ( $5.6 \times 10^4$  R\*/rod). Although the cones are not fully excited in this light intensity ( $1.7 \times 10^4$  R\*/rod) for the recovery kinetics study, the cone response still exists and occupies a relatively large ratio in KO mice because of the ongoing rod degeneration. Cones are not easily saturated and have faster recovery kinetics than that of rods (Burkhardt, 1994; Normann & Werblin, 1974), so the photoreceptors recovery is faster in KO mice. I propose that in rod photoreceptors the recovery is close to WT mice. At least we can say, after the *Cngb1* gene knockout, that the recovery of rods is not delayed. The undelayed recovery kinetics exclude the potential activating interactions of GARPs and channel subunits with other ROS proteins, such as RK, arrestin, ABCR, RGS9-1, G $\beta$ 5L, R9AP, and PDE6 $\gamma$  which activate R\* phosphorylation, increases opsin concentration, or T $\alpha$ -GTPase function. Both of the activation processes lead to slow recovery kinetics (Krispel, Chen, Simon, & Burns, 2003; Lyubarsky et al., 2000; Nishiguchi et al., 2004). The inhibiting interactions seem not to exist, since the actual recovery may not be faster in rods. The 2- to 4-month studies generally show the faster recovery of KO mice but could not give us consistent results in some ISI. Also, the recoveries of different age groups in KO mice are variable. A possible reason is the smaller sample size at each age ( $n = 3$  to  $6$ ) for each genotype; which could increase the variability of the data.

### Comparison of the 3' and Our 5' *Cngb1* Knockout Mouse Models

Recently, a targeted deletion of exon 26 at the 3' end of the *cngb1* locus was reported; this knockout region covers the pore-forming and transmembrane segment 6 encoding regions (Huttl et al., 2005). There are a number of significant differences between this 3' KO and our 5' KO. Comparison of these two models will benefit further *Cngb1* research. In our 5' KO all three retinal products from the *Cngb1* locus are knocked out (GARP-1, GARP-2, and the  $\beta$ -subunit), but in their 3' KO only the  $\beta$ -subunit is disrupted and GARP expression remains intact. For general phenotypes, Huttl et al. observed a lower weight during early postnatal development and high postnatal mortality of KO mice, presumably due to a loss of olfaction, which is not observed in our 5'-KO mice (Table 2). The alternatively spliced  $\beta$ -subunit variant (*Cngb1b*) (Bonigk et al., 1999; Kaupp & Seifert, 2002; Sautter et al., 1998) used in the olfactory CNG channel as a modulatory subunit is likely to use a different promoter just upstream of the first exon of *Cngb1b* (14a in Figure 5) (Ardell et al., 2000). Curiously, the 3' KO shows a slower retinal degeneration, but the rods are not functional. In our 5'-KO mice, most of the rods recorded from gave a measurable response from which a sensitivity curve is readily generated. There are two major differences in the 5'- and 3'- KO mice that may account for the functional properties observed: (a)  $\alpha$ -subunit levels are significantly lower in the 3'-KO mouse, which retains normal GARPs expression. It is possible that GARPs, in the absence of the  $\beta$ -subunit, inhibit  $\alpha$ -subunit transport to the outer segment leading to an even greater reduction of the  $\alpha$ -subunit in ROS and other part of rods. This also correlates with a critical role for the  $\beta$ -subunit in transport of the channel complex to plasma membrane. (b) In the 3'-KO the authors noted that disk stacks are mainly intact, in contrast to disk

stacks reported here that show signs of disruption and abnormal extension. This is consistent with a role for the GARP proteins in maintaining the structural integrity of the disks. In vitro studies showed that the disk rim and incisure-associated protein, peripherin-2, interacts with soluble GARPs and the  $\beta$ -subunit (Poetsch et al., 2001). According to the location where all three GARP proteins are distributed in ROS, we speculate that the GARP part of the  $\beta$ -subunit interacting with peripherin-2 plays a role in maintaining ROS structure, perhaps by preventing plasma-disk membrane fusion, and also could serve to restrict free disk rotation or side-to-side movement. Free GARPs interacting with peripherin-2 are postulated to play an important role in maintaining disk spacing and incisure alignment. A model for the structural roles of are distributed in ROS, we speculate that the GARP part of the  $\beta$ -subunit interacting with peripherin-2 plays a role in maintaining ROS structure perhaps by preventing plasma-disk membrane fusion, and also could serve to restrict free disk rotation or side to side movement. Free GARPs interacting with peripherin-2 are postulated to play an important role to maintain disk spacing and incisure alignment. A model for the structural roles of soluble GARPs and the  $\beta$ -subunit is shown in Figure 26. Physical interaction of the GARP extension of the  $\beta$ -subunit and the peripherin-2 oligomer or the peripherin-2/Rom-1 oligomer creates a physical link between the disks and the plasma membrane. The model also proposes a physical link between disks in the stack mediated by the interaction of GARP-2 and peripherin-2 or P2/ROM-1 oligomers. Both plasma/disk and disk/disk membrane physical links have been observed by freeze fracture analysis (Roof & Heuser, 1982); in addition, part of the 240-kDa  $\beta$ -subunit may be involved in the formation of this kind of filament (Wong & Molday, 1986).

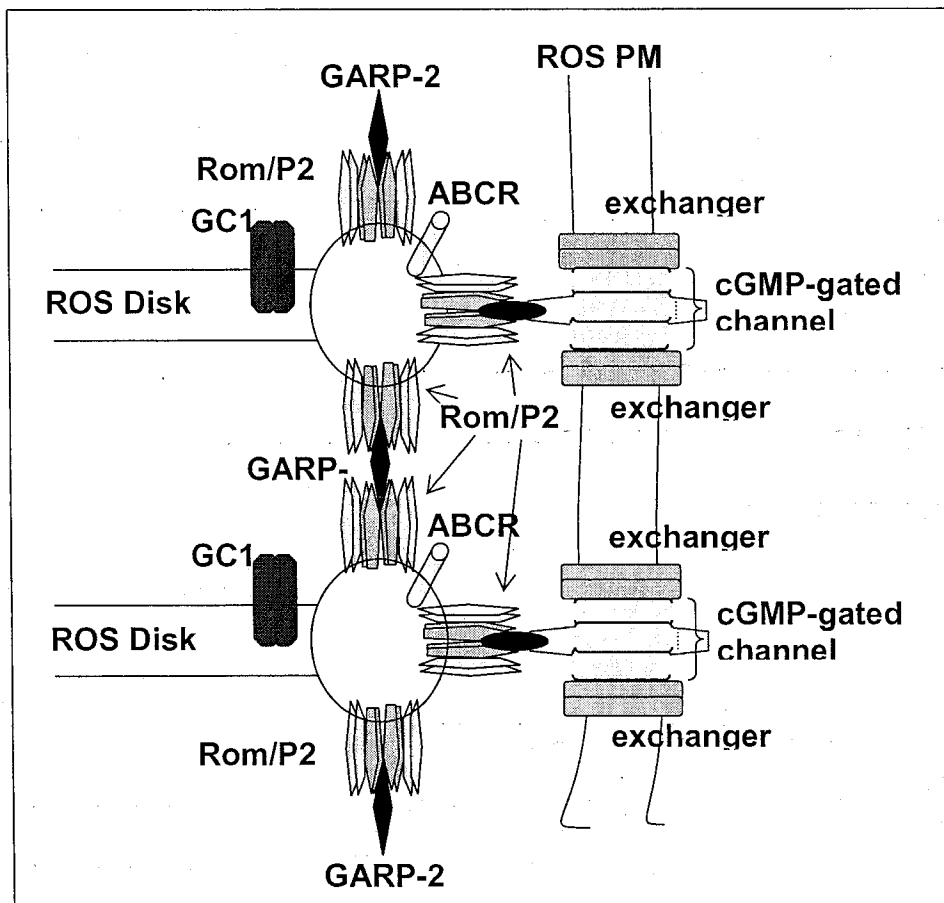


*Figure 26* A structural role for GARP-2 and the  $\beta$ -subunit in ROS. The GARP part of the  $\beta$ -subunit interacts with rim protein peripherin-2 oligomeric complex horizontally; GARP-2 interacts with peripherin-2 oligomeric complex vertically. Both interactions maintain the stability of disks and the plasma membrane in the rod outer segment.

### Retinal Degeneration Model

*Cngb1* knockout mice have slightly decreased (1/10) but close to normal  $\text{Ca}^{2+}$  concentration (unpublished data); therefore the degeneration could not be attributed to  $\text{Ca}^{2+}$  concentration changes. Single-cell ERG shows normal dominant time in KO rods, suggesting that PDE6 deactivation occurs with normal kinetics. The recovery of the rod photoreceptor does not show a delay in 1-month-old mice, indicating that the *Cngb1* gene knockout does not affect the function of other proteins, such as arrestin, RK, ABCR, RGS9-1, G $\beta$ 5L, or R9AP. It is well known that RK, arrestin, and ABCR knockout lead to retinal degeneration that may be evoked according to the equivalent-light hypothesis. Therefore, the retinal degeneration is not caused by equivalent light, but is more likely due to structural abnormalities after *Cngb1* knockout (see Figure 26). The GARP part of the  $\beta$ -subunit interacts with rim protein peripherin-2 oligomeric complex horizontally; GARP-2 interacts with peripherin-2 oligomeric complex vertically. Both interactions maintain the stability of the disks and the plasma membrane in the rod ROS. The 5' knockout of the *Cngb1* locus eliminates the expression of free GARPs (GARP-1 and GARP-2) and the  $\beta$ -subunit; therefore, the ROS loses the vertical and horizontal forces to keep its stability. This is proposed to be the primary reason for degeneration of rod photoreceptors in our knockout model.

## REFERENCES

- Alpern, M. (1971). Rhodopsin kinetics in the human eye. *The Journal of Physiology*, 217(2), 447-471.
- Ames, J. B., Dizhoor, A. M., Ikura, M., Palczewski, K., & Stryer, L. (1999). Three-dimensional structure of guanylyl cyclase activating protein-2, a calcium-sensitive modulator of photoreceptor guanylyl cyclases. *The Journal of Biological Chemistry*, 274(27), 19329-19337.
- Ames, J. B., Ishima, R., Tanaka, T., Gordon, J. I., Stryer, L., & Ikura, M. (1997). Molecular mechanics of calcium-myristoyl switches. *Nature*, 389(6647), 198-202.
- Anderson, D. H., Fisher, S. K., & Steinberg, R. H. (1978). Mammalian cones: disc shedding, phagocytosis, and renewal. *Investigative Ophthalmology & Visual Science*, 17(2), 117-133.
- Angleton, J. K., & Wensel, T. G. (1994). Enhancement of rod outer segment GTPase accelerating protein activity by the inhibitory subunit of cGMP phosphodiesterase. *The Journal of Biological Chemistry*, 269(23), 16290-16296.
- Ardell, M. D., Aragon, I., Oliveira, L., Porche, G. E., Burke, E., & Pittler, S. J. (1996). The beta subunit of human rod photoreceptor cGMP-gated cation channel is generated from a complex transcription unit. *FEBS Letters*, 389(2), 213-218.
- Ardell, M. D., Bedsole, D. L., Schoborg, R. V., & Pittler, S. J. (2000). Genomic organization of the human rod photoreceptor cGMP-gated cation channel beta-subunit gene. *Gene*, 245(2), 311-318.
- Ardell, M. D., Makhija, A. K., Oliveira, L., Miniou, P., Viegas-Pequignot, E., & Pittler, S. J. (1995). cDNA, gene structure, and chromosomal localization of human GAR1 (CNCG3L), a homolog of the third subunit of bovine photoreceptor cGMP-gated channel. *Genomics*, 28(1), 32-38.
- Arikawa, K., Molday, L. L., Molday, R. S., & Williams, D. S. (1992). Localization of peripherin/rds in the disk membranes of cone and rod photoreceptors: relationship to disk membrane morphogenesis and retinal degeneration. *The Journal of Cell Biology*, 116(3), 659-667.
- Armington, J.C. (1974). *The electroretinogram*. New York: Academic Press.

- Arshavsky, V., & Bownds, M. D. (1992). Regulation of deactivation of photoreceptor G protein by its target enzyme and cGMP. *Nature*, 357(6377), 416-417.
- Arshavsky, V. Y., Lamb, T. D., & Pugh, E. N., Jr. (2002). G proteins and phototransduction. *Annual Review of Physiology*, 64, 153-187.
- Asi, H., & Perlman, I. (1992). Relationships between the electroretinogram a-wave, b-wave and oscillatory potentials and their application to clinical diagnosis. *Documenta Ophthalmologica*, 79(2), 125-139.
- Awatramani, G., Wang, J., & Slaughter, M. M. (2001). Amacrine and ganglion cell contributions to the electroretinogram in amphibian retina. *Visual Neuroscience*, 18(1), 147-156.
- Baehr, W., Devlin, M. J., & Applebury, M. L. (1979). Isolation and characterization of cGMP phosphodiesterase from bovine rod outer segments. *The Journal of Biological Chemistry*, 254(22), 11669-11677.
- Bareil, C., Hamel, C. P., Delague, V., Arnaud, B., Demaille, J., & Claustres, M. (2001). Segregation of a mutation in CNGB1 encoding the beta-subunit of the rod cGMP-gated channel in a family with autosomal recessive retinitis pigmentosa. *Human Genetics*, 108(4), 328-334.
- Barnes, S. (1994). After transduction: response shaping and control of transmission by ion channels of the photoreceptor inner segments. *Neuroscience*, 58(3), 447-459.
- Bascom, R. A., Manara, S., Collins, L., Molday, R. S., Kalnins, V. I., & McInnes, R. R. (1992). Cloning of the cDNA for a novel photoreceptor membrane protein (rom-1) identifies a disk rim protein family implicated in human retinopathies. *Neuron*, 8(6), 1171-1184.
- Bauer, P. J., & Drechsler, M. (1992). Association of cyclic GMP-gated channels and Na(+)-Ca(2+)-K+ exchangers in bovine retinal rod outer segment plasma membranes. *The Journal of Physiology*, 451, 109-131.
- Baylor, D. A. (1987). Photoreceptor signals and vision. Proctor lecture. *Investigative Ophthalmology & Visual Science*, 28(1), 34-49.
- Baylor, D. A., Lamb, T. D., & Yau, K. W. (1979). Responses of retinal rods to single photons. *The Journal of Physiology*, 288, 613-634.
- Baylor, D. A., Nunn, B. J., & Schnapf, J. L. (1984). The photocurrent, noise and spectral sensitivity of rods of the monkey *Macaca fascicularis*. *The Journal of Physiology*, 357, 575-607.

- Beavo, J. A. (1995). Cyclic nucleotide phosphodiesterases: functional implications of multiple isoforms. *Physiological Reviews*, 75(4), 725-748.
- Beech, P. L., Pagh-Roehl, K., Noda, Y., Hirokawa, N., Burnside, B., & Rosenbaum, J. L. (1996). Localization of kinesin superfamily proteins to the connecting cilium of fish photoreceptors. *Journal of Cell Science*, 109 (Pt. 4), 889-897.
- Ben-Shabat, S., Parish, C. A., Vollmer, H. R., Itagaki, Y., Fishkin, N., Nakanishi, K., et al. (2002). Biosynthetic studies of A2E, a major fluorophore of retinal pigment epithelial lipofuscin. *The Journal of Biological Chemistry*, 277(9), 7183-7190.
- Bera, T. K., Hahn, Y., Lee, B., & Pastan, I. H. (2003). TEPP, a new gene specifically expressed in testis, prostate, and placenta and well conserved in chordates. *Biochemical Biophysical Research Communications*, 312(4), 1209-1215.
- Biel, M., Seeliger, M., Pfeifer, A., Kohler, K., Gerstner, A., Ludwig, A., et al. (1999). Selective loss of cone function in mice lacking the cyclic nucleotide-gated channel CNG3. *Proceedings of the National Academy of Science, USA*, 96(13), 7553-7557.
- Birch, D. G., & Fish, G. E. (1987). Rod ERGs in retinitis pigmentosa and cone-rod degeneration. *Investigative Ophthalmology & Visual Science*, 28(1), 140-150.
- Birch, D. G., Peters, A. Y., Locke, K. L., Spencer, R., Megarity, C. F., & Travis, G. H. (2001). Visual function in patients with cone-rod dystrophy (CRD) associated with mutations in the ABCA4(ABCR) gene. *Experimental Eye Research*, 73(6), 877-886.
- Boesze-Battaglia, K., & Goldberg, A. F. (2002). Photoreceptor renewal: a role for peripherin/rds. *International Review of Cytology*, 217, 183-225.
- Bonigk, W., Bradley, J., Muller, F., Sesti, F., Boekhoff, I., Ronnett, G. V., et al. (1999). The native rat olfactory cyclic nucleotide-gated channel is composed of three distinct subunits. *The Journal of Neuroscience*, 19(13), 5332-5347.
- Bowmaker, J. K., & Dartnall, H. J. (1980). Visual pigments of rods and cones in a human retina. *The Journal of Physiology*, 298, 501-511.
- Bradley, J., Frings, S., Yau, K. W., & Reed, R. (2001). Nomenclature for ion channel subunits. *Science*, 294(5549), 2095-2096.
- Brown, B. M., Carlson, B. L., Zhu, X., Lolley, R. N., & Craft, C. M. (2002). Light-driven translocation of the protein phosphatase 2A complex regulates light/dark dephosphorylation of phosphodiesterase and rhodopsin. *Biochemistry*, 41(46), 13526-13538.

- Brown, K. T. (1968). The electroretinogram: its components and their origins. *Vision Research*, 8(6), 633-677.
- Brown, R. L., & Stryer, L. (1989). Expression in bacteria of functional inhibitory subunit of retinal rod cGMP phosphodiesterase. *Proceedings of the National Academy of Science, USA*, 86(13), 4922-4926.
- Burkhardt, D. A. (1994). Light adaptation and photopigment bleaching in cone photoreceptors in situ in the retina of the turtle. *The Journal of Neuroscience*, 14(3, Pt. 1), 1091-1105.
- Calvert, P. D., Krasnoperova, N. V., Lyubarsky, A. L., Isayama, T., Nicolo, M., Kosaras, B., et al. (2000). Phototransduction in transgenic mice after targeted deletion of the rod transducin alpha-subunit. *Proceedings of the National Academy of Science, USA*, 97(25), 13913-13918.
- Carter-Dawson, L. D., & LaVail, M. M. (1979). Rods and cones in the mouse retina. I. Structural analysis using light and electron microscopy. *The Journal of Comparative Neurology*, 188(2), 245-262.
- Cervetto, L., Lagnado, L., Perry, R. J., Robinson, D. W., & McNaughton, P. A. (1989). Extrusion of calcium from rod outer segments is driven by both sodium and potassium gradients. *Nature*, 337(6209), 740-743.
- Chattopadhyaya, R., Meador, W. E., Means, A. R., & Quijcho, F. A. (1992). Calmodulin structure refined at 1.7 Å resolution. *Journal of Molecular Biology*, 228(4), 1177-1192.
- Chen, C. K., Burns, M. E., He, W., Wensel, T. G., Baylor, D. A., & Simon, M. I. (2000). Slowed recovery of rod photoresponse in mice lacking the GTPase accelerating protein RGS9-1. *Nature*, 403(6769), 557-560.
- Chen, C. K., Burns, M. E., Spencer, M., Niemi, G. A., Chen, J., Hurley, J. B., et al. (1999). Abnormal photoresponses and light-induced apoptosis in rods lacking rhodopsin kinase. *Proceedings of the National Academy of Science, USA*, 96(7), 3718-3722.
- Chen, J., Simon, M. I., Matthes, M. T., Yasumura, D., & LaVail, M. M. (1999). Increased susceptibility to light damage in an arrestin knockout mouse model of Oguchi disease (stationary night blindness). *Investigative Ophthalmology & Visual Science*, 40(12), 2978-2982.
- Chen, J., Yoshida, T., Nakano, K., & Bitensky, M. W. (2005). Subcellular localization of phosducin in rod photoreceptors. *Visual Neuroscience*, 22(1), 19-25.

- Chen, T. Y., Illing, M., Molday, L. L., Hsu, Y. T., Yau, K. W., & Molday, R. S. (1994). Subunit 2 (or beta) of retinal rod cGMP-gated cation channel is a component of the 240-kDa channel-associated protein and mediates Ca(2+)-calmodulin modulation. *Proceedings of the National Academy of Science, USA*, 91(24), 11757-11761.
- Chen, T. Y., Peng, Y. W., Dhallan, R. S., Ahamed, B., Reed, R. R., & Yau, K. W. (1993). A new subunit of the cyclic nucleotide-gated cation channel in retinal rods. *Nature*, 362(6422), 764-767.
- Clarke, G., Goldberg, A. F., Vidgen, D., Collins, L., Ploder, L., Schwarz, L., et al. (2000). Rom-1 is required for rod photoreceptor viability and the regulation of disk morphogenesis. *Nature Genetics*, 25(1), 67-73.
- Cohen, A. I. (1965). New details of the ultrastructure of the outer segments and ciliary connectives of the rods of human and macaque retinas. *The Anatomical Record*, 152, 63-79.
- Colville, C. A., & Molday, R. S. (1996). Primary structure and expression of the human beta-subunit and related proteins of the rod photoreceptor cGMP-gated channel. *The Journal of Biological Chemistry*, 271(51), 32968-32974.
- Connell, G., Bascom, R., Molday, L., Reid, D., McInnes, R. R., & Molday, R. S. (1991). Photoreceptor peripherin is the normal product of the gene responsible for retinal degeneration in the rds mouse. *Proceedings of the National Academy of Science, USA*, 88(3), 723-726.
- Conner, J. D., & MacLeod, D. I. (1977). Rod photoreceptors detect rapid flicker. *Science*, 195(4279), 698-699.
- Cook, N. J., Hanke, W., & Kaupp, U. B. (1987). Identification, purification, and functional reconstitution of the cyclic GMP-dependent channel from rod photoreceptors. *Proceedings of the National Academy of Science, USA*, 84(2), 585-589.
- Cook, N. J., & Kaupp, U. B. (1988). Solubilization, purification, and reconstitution of the sodium-calcium exchanger from bovine retinal rod outer segments. *The Journal of Biological Chemistry*, 263(23), 11382-11388.
- Cook, N. J., Molday, L. L., Reid, D., Kaupp, U. B., & Molday, R. S. (1989). The cGMP-gated channel of bovine rod photoreceptors is localized exclusively in the plasma membrane. *The Journal of Biological Chemistry*, 264(12), 6996-6999.
- Cornwall, M. C., & Fain, G. L. (1994). Bleached pigment activates transduction in isolated rods of the salamander retina. *The Journal of Physiology*, 480 (Pt. 2), 261-279.

- Cote, R. H., Bownds, M. D., & Arshavsky, V. Y. (1994). cGMP binding sites on photoreceptor phosphodiesterase: role in feedback regulation of visual transduction. *Proceedings of the National Academy of Science, USA*, 91(11), 4845-4849.
- Cowan, C. W., Fariss, R. N., Sokal, I., Palczewski, K., & Wensel, T. G. (1998). High expression levels in cones of RGS9, the predominant GTPase accelerating protein of rods. *Proceedings of the National Academy of Science, USA*, 95(9), 5351-5356.
- Cremers, F. P., van de Pol, D. J., van Driel, M., den Hollander, A. I., van Haren, F. J., Knoers, N. V., et al. (1998). Autosomal recessive retinitis pigmentosa and cone-rod dystrophy caused by splice site mutations in the Stargardt's disease gene ABCR. *Human Molecular Genetics*, 7(3), 355-362.
- Curcio, C. A., Sloan, K. R., Kalina, R. E., & Hendrickson, A. E. (1990). Human photoreceptor topography. *The Journal of Comparative Neurology*, 292(4), 497-523.
- Dacheux, R. F., & Raviola, E. (1986). The rod pathway in the rabbit retina: a depolarizing bipolar and amacrine cell. *The Journal of Neuroscience*, 6(2), 331-345.
- Dalke, C., Loster, J., Fuchs, H., Gailus-Durner, V., Soewarto, D., Favor, J., et al. (2004). Electroretinography as a screening method for mutations causing retinal dysfunction in mice. *Investigative Ophthalmology & Visual Science*, 45(2), 601-609.
- Deterre, P., Bigay, J., Forquet, F., Robert, M., & Chabre, M. (1988). cGMP phosphodiesterase of retinal rods is regulated by two inhibitory subunits. *Proceedings of the National Academy of Science, USA*, 85(8), 2424-2428.
- Dhallan, R. S., Macke, J. P., Eddy, R. L., Shows, T. B., Reed, R. R., Yau, K. W., et al. (1992). Human rod photoreceptor cGMP-gated channel: amino acid sequence, gene structure, and functional expression. *The Journal of Neuroscience*, 12(8), 3248-3256.
- Dizhoor, A. M., & Hurley, J. B. (1996). Inactivation of EF-hands makes GCAP-2 (p24) a constitutive activator of photoreceptor guanylyl cyclase by preventing a Ca<sup>2+</sup>-induced "activator-to-inhibitor" transition. *The Journal of Biological Chemistry*, 271(32), 19346-19350.
- Dizhoor, A. M., & Hurley, J. B. (1999). Regulation of photoreceptor membrane guanylyl cyclases by guanylyl cyclase activator proteins. *Methods*, 19(4), 521-531.

- Dizhoor, A. M., Lowe, D. G., Olshevskaya, E. V., Laura, R. P., & Hurley, J. B. (1994). The human photoreceptor membrane guanylyl cyclase, RetGC, is present in outer segments and is regulated by calcium and a soluble activator. *Neuron*, 12(6), 1345-1352.
- Dizhoor, A. M., Ray, S., Kumar, S., Niemi, G., Spencer, M., Brolley, D., et al. (1991). Recoverin: a calcium sensitive activator of retinal rod guanylate cyclase. *Science*, 251(4996), 915-918.
- Dong, C. J., & Hare, W. A. (2000). Contribution to the kinetics and amplitude of the electroretinogram b-wave by third-order retinal neurons in the rabbit retina. *Vision Research*, 40(6), 579-589.
- Dowling, J. E. (1960). Chemistry of visual adaptation in the rat. *Nature*, 188, 114-118.
- Dowling J.E. (1987). *The retina: An approachable part of the brain*. Cambridge, MA: Belknap Press.
- Dratz, E. A., Lewis, J. W., Schaechter, L. E., Parker, K. R., & Kliger, D. S. (1987). Retinal rod GTPase turnover rate increases with concentration: a key to the control of visual excitation? *Biochemical Biophysical Research Communications*, 146(2), 379-386.
- Driessen, C. A., Winkens, H. J., Hoffmann, K., Kuhlmann, L. D., Janssen, B. P., Van Vugt, A. H., et al. (2000). Disruption of the 11-cis-retinol dehydrogenase gene leads to accumulation of cis-retinols and cis-retinyl esters. *Molecular and Cellular Biology*, 20(12), 4275-4287.
- Dryer, S. E., & Henderson, D. (1991). A cyclic GMP-activated channel in dissociated cells of the chick pineal gland. *Nature*, 353(6346), 756-758.
- Dryja, T. P., Finn, J. T., Peng, Y. W., McGee, T. L., Berson, E. L., & Yau, K. W. (1995). Mutations in the gene encoding the alpha subunit of the rod cGMP-gated channel in autosomal recessive retinitis pigmentosa. *Proceedings of the National Academy of Science, USA*, 92(22), 10177-10181.
- Dryja, T. P., Hahn, L. B., Kajiwarra, K., & Berson, E. L. (1997). Dominant and digenic mutations in the peripherin/RDS and ROM1 genes in retinitis pigmentosa. *Investigative Ophthalmology & Visual Science*, 38(10), 1972-1982.
- Dryja, T. P., Hahn, L. B., Reboul, T., & Arnaud, B. (1996). Missense mutation in the gene encoding the alpha subunit of rod transducin in the Nougaret form of congenital stationary night blindness. *Nature genetics*, 13(3), 358-360.

- Dryja, T. P., McGee, T. L., Reichel, E., Hahn, L. B., Cowley, G. S., Yandell, D. W., et al. (1990). A point mutation of the rhodopsin gene in one form of retinitis pigmentosa. *Nature*, *343*(6256), 364-366.
- Eckmiller, M. S. (2000). Microtubules in a rod-specific cytoskeleton associated with outer segment incisures. *Visual Neuroscience*, *17*(5), 711-722.
- Eismann, E., Muller, F., Heinemann, S. H., & Kaupp, U. B. (1994). A single negative charge within the pore region of a cGMP-gated channel controls rectification, Ca<sup>2+</sup> blockage, and ionic selectivity. *Proceedings of the National Academy of Science, USA*, *91*(3), 1109-1113.
- Ekesten, B., Gouras, P., & Moschos, M. (1998). Cone properties of the light-adapted murine ERG. *Documenta Ophthalmologica*, *97*(1), 23-31.
- Fain, G. L., & Lisman, J. E. (1993). Photoreceptor degeneration in vitamin A deprivation and retinitis pigmentosa: the equivalent light hypothesis. *Experimental Eye Research*, *57*(3), 335-340.
- Fain, G. L., & Lisman, J. E. (1999). Light, Ca<sup>2+</sup>, and photoreceptor death: new evidence for the equivalent-light hypothesis from arrestin knockout mice. *Investigative Ophthalmology & Visual Science*, *40*(12), 2770-2772.
- Fain, G. L., Matthews, H. R., Cornwall, M. C., & Koutalos, Y. (2001). Adaptation in vertebrate photoreceptors. *Physiological Reviews*, *81*(1), 117-151.
- Fan, J., Woodruff, M. L., Cilluffo, M. C., Crouch, R. K., & Fain, G. (2005). Opsin activation of transduction in the rods of dark-reared rpe65 knockout Mice. *The Journal of Physiology*, *568*(Pt. 1), 83-95.
- Farber, D. B. (1995). From mice to men: the cyclic GMP phosphodiesterase gene in vision and disease. The Proctor Lecture. *Investigative Ophthalmology & Visual Science*, *36*(2), 263-275.
- Farber, D. B., Heckenlively, J. R., Sparkes, R. S., & Bateman, J. B. (1991). Molecular genetics of retinitis pigmentosa. *Western Journal of Medicine*, *155*(4), 388-399.
- Fesenko, E. E., Kolesnikov, S. S., & Lyubarsky, A. L. (1985). Induction by cyclic GMP of cationic conductance in plasma membrane of retinal rod outer segment. *Nature*, *313*(6000), 310-313.
- Finn, J. T., Grunwald, M. E., & Yau, K. W. (1996). Cyclic nucleotide-gated ion channels: an extended family with diverse functions. *Annual Review of Physiology*, *58*, 395-426.

- Flaherty, K. M., Zozulya, S., Stryer, L., & McKay, D. B. (1993). Three-dimensional structure of recoverin, a calcium sensor in vision. *Cell*, *75*(4), 709-716.
- Frasson, M., Sahel, J. A., Fabre, M., Simonutti, M., Dreyfus, H., & Picaud, S. (1999). Retinitis pigmentosa: rod photoreceptor rescue by a calcium-channel blocker in the rd mouse. *Nature Medicine*, *5*(10), 1183-1187.
- Frederick, J., Bronson, J. D., & Baehr, W. (2000). Animal models of inherited retinal diseases. *Methods in Enzymology*, *316*, 515-526.
- Freed, M. A., Smith, R. G., & Sterling, P. (1987). Rod bipolar array in the cat retina: pattern of input from rods and GABA-accumulating amacrine cells. *The Journal of Comparative Neurology*, *266*(3), 445-455.
- Frishman, L. J., & Steinberg, R. H. (1989). Light-evoked increases in  $[K^+]_o$  in proximal portion of the dark-adapted cat retina. *Journal of Neurophysiology*, *61*(6), 1233-1243.
- Fulton, A. B., & Hansen, R. M. (2003). Recovery of the rod photoresponse in infant rats. *Vision Research*, *43*(28), 3081-3085.
- Fulton, A. B., & Rushton, W. A. (1978). The human rod ERG: correlation with psychophysical responses in light and dark adaptation. *Vision Research*, *18*(7), 793-800.
- Fung, B. K. (1983). Characterization of transducin from bovine retinal rod outer segments. I. Separation and reconstitution of the subunits. *The Journal of Biological Chemistry*, *258*(17), 10495-10502.
- Fung, B. K., Hurley, J. B., & Stryer, L. (1981). Flow of information in the light-triggered cyclic nucleotide cascade of vision. *Proceedings of the National Academy of Science, USA*, *78*(1), 152-156.
- Fung, B. K., Young, J. H., Yamane, H. K., & Griswold-Prenner, I. (1990). Subunit stoichiometry of retinal rod cGMP phosphodiesterase. *Biochemistry*, *29*(11), 2657-2664.
- Furman, R. E., & Tanaka, J. C. (1990). Monovalent selectivity of the cyclic guanosine monophosphate-activated ion channel. *The Journal of General Physiology*, *96*(1), 57-82.
- Gaudet, R., Bohm, A., & Sigler, P. B. (1996). Crystal structure at 2.4 angstroms resolution of the complex of transducin betagamma and its regulator, phosducin. *Cell*, *87*(3), 577-588.

- GeneBee Server. (n.d.). Retrieved April 8, 2005, from [http://www.genebee.msu.su/services/malign\\_reduced.html/](http://www.genebee.msu.su/services/malign_reduced.html/)
- Genome blat. (n.d.). Retrieved April 8, 2005, from <http://www.genome.ucsc.edu/cgi-bin/hgBlat/>
- Gerstner, A., Zong, X., Hofmann, F., & Biel, M. (2000). Molecular cloning and functional characterization of a new modulatory cyclic nucleotide-gated channel subunit from mouse retina. *The Journal of Neuroscience*, 20(4), 1324-1332.
- Gillespie, P. G., & Beavo, J. A. (1988). Characterization of a bovine cone photoreceptor phosphodiesterase purified by cyclic GMP-sepharose chromatography. *The Journal of Biological Chemistry*, 263(17), 8133-8141.
- Gillespie, P. G., Prusti, R. K., Apel, E. D., & Beavo, J. A. (1989). A soluble form of bovine rod photoreceptor phosphodiesterase has a novel 15-kDa subunit. *The Journal of Biological Chemistry*, 264(21), 12187-12193.
- Goldberg, A. F., & Molday, R. S. (1996). Subunit composition of the peripherin/rds-rom-1 disk rim complex from rod photoreceptors: hydrodynamic evidence for a tetrameric quaternary structure. *Biochemistry*, 35(19), 6144-6149.
- Gorczyca, W. A., Gray-Keller, M. P., Detwiler, P. B., & Palczewski, K. (1994). Purification and physiological evaluation of a guanylate cyclase activating protein from retinal rods. *Proceedings of the National Academy of Science, USA*, 91(9), 4014-4018.
- Gorczyca, W. A., Polans, A. S., Surgucheva, I. G., Subbaraya, I., Baehr, W., & Palczewski, K. (1995). Guanylyl cyclase activating protein. A calcium-sensitive regulator of phototransduction. *The Journal of Biological Chemistry*, 270(37), 22029-22036.
- Gordon, S. E., Brautigan, D. L., & Zimmerman, A. L. (1992). Protein phosphatases modulate the apparent agonist affinity of the light-regulated ion channel in retinal rods. *Neuron*, 9(4), 739-748.
- Gordon, S. E., Downing-Park, J., Tam, B., & Zimmerman, A. L. (1995). Diacylglycerol analogs inhibit the rod cGMP-gated channel by a phosphorylation-independent mechanism. *Biophysical Journal*, 69(2), 409-417.
- Gordon, S. E., Downing-Park, J., & Zimmerman, A. L. (1995). Modulation of the cGMP-gated ion channel in frog rods by calmodulin and an endogenous inhibitory factor. *The Journal of Physiology*, 486 (Pt. 3), 533-546.

- Goto, Y., Peachey, N. S., Ripps, H., & Naash, M. I. (1995). Functional abnormalities in transgenic mice expressing a mutant rhodopsin gene. *Investigative Ophthalmology & Visual Science*, 36(1), 62-71.
- Green, D. G., & Kapousta-Bruneau, N. V. (1999). A dissection of the electroretinogram from the isolated rat retina with microelectrodes and drugs. *Visual Neuroscience*, 16(4), 727-741.
- Grunwald, M. E., Yu, W. P., Yu, H. H., & Yau, K. W. (1998). Identification of a domain on the beta-subunit of the rod cGMP-gated cation channel that mediates inhibition by calcium-calmodulin. *The Journal of Biological Chemistry*, 273(15), 9148-9157.
- Gurevich, L., & Slaughter, M. M. (1993). Comparison of the waveforms of the ON bipolar neuron and the b-wave of the electroretinogram. *Vision Research*, 33(17), 2431-2435.
- Hagins, W. A., Penn, R. D., & Yoshikami, S. (1970). Dark current and photocurrent in retinal rods. *Biophysical Journal*, 10(5), 380-412.
- Haider, N. B., Ikeda, A., Naggert, J. K., & Nishina, P. M. (2002). Genetic modifiers of vision and hearing. *Human Molecular Genetics*, 11(10), 1195-1206.
- Hamm, H. E. (1998). The many faces of G protein signaling. *The Journal of Biological Chemistry*, 273(2), 669-672.
- Hanke, W., Cook, N. J., & Kaupp, U. B. (1988). cGMP-dependent channel protein from photoreceptor membranes: single-channel activity of the purified and reconstituted protein. *Proceedings of the National Academy of Science, USA*, 85(1), 94-98.
- Hansen, R. M., & Fulton, A. B. (2005). Recovery of the rod photoresponse in infants. *Investigative Ophthalmology & Visual Science*, 46(2), 764-768.
- Hargrave, P. A., McDowell, J. H., Curtis, D. R., Wang, J. K., Juszczak, E., Fong, S. L., et al. (1983). The structure of bovine rhodopsin. *Biophysics of Structure and Mechanism*, 9(4), 235-244.
- Hawkins, R. K., Jansen, H. G., & Sanyal, S. (1985). Development and degeneration of retina in rds mutant mice: photoreceptor abnormalities in the heterozygotes. *Experimental Eye Research*, 41(6), 701-720.
- Haynes, L., & Yau, K. W. (1985). Cyclic GMP-sensitive conductance in outer segment membrane of catfish cones. *Nature*, 317(6032), 61-64.

- Haynes, L. W., Kay, A. R., & Yau, K. W. (1986). Single cyclic GMP-activated channel activity in excised patches of rod outer segment membrane. *Nature*, *321*(6065), 66-70.
- He, W., Cowan, C. W., & Wensel, T. G. (1998). RGS9, a GTPase accelerator for phototransduction. *Neuron*, *20*(1), 95-102.
- He, W., Lu, L., Zhang, X., El-Hodiri, H. M., Chen, C. K., Slep, K. C., et al. (2000). Modules in the photoreceptor RGS9-1.Gbeta 5L GTPase-accelerating protein complex control effector coupling, GTPase acceleration, protein folding, and stability. *The Journal of Biological Chemistry*, *275*(47), 37093-37100.
- He, Y., Ruiz, M., & Karpen, J. W. (2000). Constraining the subunit order of rod cyclic nucleotide-gated channels reveals a diagonal arrangement of like subunits. *Proceedings of the National Academy of Science, USA*, *97*(2), 895-900.
- Heck, M., & Hofmann, K. P. (2001). Maximal rate and nucleotide dependence of rhodopsin-catalyzed transducin activation: initial rate analysis based on a double displacement mechanism. *The Journal of Biological Chemistry*, *276*(13), 10000-10009.
- Heynen, H., Wachtmeister, L., & van Norren, D. (1985). Origin of the oscillatory potentials in the primate retina. *Vision Research*, *25*(10), 1365-1373.
- Higgins, M. K., Weitz, D., Warne, T., Schertler, G. F., & Kaupp, U. B. (2002). Molecular architecture of a retinal cGMP-gated channel: the arrangement of the cytoplasmic domains. *The Embo Journal*, *21*(9), 2087-2094.
- Hoang, E. H., Whitehead, J. L., Dose, A. C., & Burnside, B. (1998). Cloning of a novel C-terminal kinesin (KIFC3) that maps to human chromosome 16q13-q21 and thus is a candidate gene for Bardet-Biedl syndrome. *Genomics*, *52*(2), 219-222.
- Hofmann, F., Biel, M., & Kaupp, U. B. (2003). International Union of Pharmacology. XLII. Compendium of voltage-gated ion channels: cyclic nucleotide-modulated channels. *Pharmacological Reviews*, *55*(4), 587-589.
- Hood, D. C. (1998). Lower-level visual processing and models of light adaptation. *Annual Review Psychology*, *49*, 503-535.
- Hood, D. C., & Birch, D. G. (1990a). A quantitative measure of the electrical activity of human rod photoreceptors using electroretinography. *Visual Neuroscience*, *5*(4), 379-387.
- Hood, D. C., & Birch, D. G. (1990b). The A-wave of the human electroretinogram and rod receptor function. *Investigative Ophthalmology & Visual Science*, *31*(10), 2070-2081.

- Hood, D. C., & Birch, D. G. (1992). A computational model of the amplitude and implicit time of the b-wave of the human ERG. *Visual Neuroscience*, 8(2), 107-126.
- Howes, K. A., Pennesi, M. E., Sokal, I., Church-Kopish, J., Schmidt, B., Margolis, D., et al. (2002). GCAP1 rescues rod photoreceptor response in GCAP1/GCAP2 knockout mice. *The Embo Journal*, 21(7), 1545-1554.
- Hsu, S. C., & Molday, R. S. (1991). Glycolytic enzymes and a GLUT-1 glucose transporter in the outer segments of rod and cone photoreceptor cells. *The Journal of Biological Chemistry*, 266(32), 21745-21752.
- Hsu, Y. T., & Molday, R. S. (1993). Modulation of the cGMP-gated channel of rod photoreceptor cells by calmodulin. *Nature*, 361(6407), 76-79.
- Hsu, Y. T., & Molday, R. S. (1994). Interaction of calmodulin with the cyclic GMP-gated channel of rod photoreceptor cells. Modulation of activity, affinity purification, and localization. *The Journal of Biological Chemistry*, 269(47), 29765-29770.
- Hu, G., & Wensel, T. G. (2002). R9AP, a membrane anchor for the photoreceptor GTPase accelerating protein, RGS9-1. *Proceedings of the National Academy of Science, USA*, 99(15), 9755-9760.
- Hu, G., Zhang, Z., & Wensel, T. G. (2003). Activation of RGS9-1GTPase acceleration by its membrane anchor, R9AP. *The Journal of Biological Chemistry*, 278(16), 14550-14554.
- Huang, S. H., Pittler, S. J., Huang, X., Oliveira, L., Berson, E. L., & Dryja, T. P. (1995). Autosomal recessive retinitis pigmentosa caused by mutations in the alpha subunit of rod cGMP phosphodiesterase. *Nature genetics*, 11(4), 468-471.
- Humphries, M. M., Kiang, S., McNally, N., Donovan, M. A., Sieving, P. A., Bush, R. A., et al. (2001). Comparative structural and functional analysis of photoreceptor neurons of Rho<sup>-/-</sup> mice reveal increased survival on C57BL/6J in comparison to 129Sv genetic background. *Visual Neuroscience*, 18(3), 437-443.
- Humphries, M. M., Rancourt, D., Farrar, G. J., Kenna, P., Hazel, M., Bush, R. A., et al. (1997). Retinopathy induced in mice by targeted disruption of the rhodopsin gene. *Nature genetics*, 15(2), 216-219.
- Hurley, J. B., & Stryer, L. (1982). Purification and characterization of the gamma regulatory subunit of the cyclic GMP phosphodiesterase from retinal rod outer segments. *The Journal of Biological Chemistry*, 257(18), 11094-11099.

- Huttl, S., Michalakis, S., Seeliger, M., Luo, D. G., Acar, N., Geiger, H., et al. (2005). Impaired channel targeting and retinal degeneration in mice lacking the cyclic nucleotide-gated channel subunit CNGB1. *The Journal of Neuroscience*, 25(1), 130-138.
- Illing, M., Molday, L. L., & Molday, R. S. (1997). The 220-kDa rim protein of retinal rod outer segments is a member of the ABC transporter superfamily. *The Journal of Biological Chemistry*, 272(15), 10303-10310.
- Imanishi, Y., Li, N., Sokal, I., Sowa, M. E., Lichtarge, O., Wensel, T. G., et al. (2002). Characterization of retinal guanylate cyclase-activating protein 3 (GCAP3) from zebrafish to man. *The European Journal of Neuroscience*, 15(1), 63-78.
- Jacobs, G. H., Neitz, J., & Deegan, J. F., 2nd. (1991). Retinal receptors in rodents maximally sensitive to ultraviolet light. *Nature*, 353(6345), 655-656.
- Jan, L. Y., & Jan, Y. N. (1990). A superfamily of ion channels. *Nature*, 345(6277), 672.
- Jeon, C. J., Strettoi, E., & Masland, R. H. (1998). The major cell populations of the mouse retina. *The Journal of Neuroscience*, 18(21), 8936-8946.
- Kachi, S., Nishizawa, Y., Olshevskaya, E., Yamazaki, A., Miyake, Y., Wakabayashi, T., et al. (1999). Detailed localization of photoreceptor guanylate cyclase activating protein-1 and -2 in mammalian retinas using light and electron microscopy. *Experimental Eye Research*, 68(4), 465-473.
- Kajimura, N., Yamazaki, M., Morikawa, K., Yamazaki, A., & Mayanagi, K. (2002). Three-dimensional structure of non-activated cGMP phosphodiesterase 6 and comparison of its image with those of activated forms. *Journal of Structural Biology*, 139(1), 27-38.
- Kajiwara, K., Berson, E. L., & Dryja, T. P. (1994). Digenic retinitis pigmentosa due to mutations at the unlinked peripherin/RDS and ROM1 loci. *Science*, 264(5165), 1604-1608.
- Kajiwara, K., Hahn, L. B., Mukai, S., Travis, G. H., Berson, E. L., & Dryja, T. P. (1991). Mutations in the human retinal degeneration slow gene in autosomal dominant retinitis pigmentosa. *Nature*, 354(6353), 480-483.
- Kameni Tcheudji, J. F., Lebeau, L., Virmaux, N., Maffei, C. G., Cote, R. H., Lugnier, C., et al. (2001). Molecular organization of bovine rod cGMP-phosphodiesterase 6. *Journal of Molecular Biology*, 310(4), 781-791.
- Kamps, K. M., De Grip, W. J., & Daemen, F. J. (1982). Use of a density modification technique for isolation of the plasma membrane of rod outer segments. *Biochimica et Biophysica Acta*, 687(2), 296-302.

- Kapousta-Bruneau, N. V. (2000). Opposite effects of GABA(A) and GABA(C) receptor antagonists on the b-wave of ERG recorded from the isolated rat retina. *Vision Research*, 40(13), 1653-1665.
- Karwoski, C. J., Lu, H. K., & Newman, E. A. (1989). Spatial buffering of light-evoked potassium increases by retinal Muller (glial) cells. *Science*, 244(4904), 578-580.
- Katz, M. L., & Redmond, T. M. (2001). Effect of Rpe65 knockout on accumulation of lipofuscin fluorophores in the retinal pigment epithelium. *Investigative Ophthalmology & Visual Science*, 42(12), 3023-3030.
- Kaupp, U. B., Niidome, T., Tanabe, T., Terada, S., Bonigk, W., Stuhmer, W., et al. (1989). Primary structure and functional expression from complementary DNA of the rod photoreceptor cyclic GMP-gated channel. *Nature*, 342(6251), 762-766.
- Kaupp, U. B., & Seifert, R. (2002). Cyclic nucleotide-gated ion channels. *Physiological Reviews*, 82(3), 769-824.
- Kawamura, S. (1993). Rhodopsin phosphorylation as a mechanism of cyclic GMP phosphodiesterase regulation by S-modulin. *Nature*, 362(6423), 855-857.
- Kelsell, R. E., Gregory-Evans, K., Payne, A. M., Perrault, I., Kaplan, J., Yang, R. B., et al. (1998). Mutations in the retinal guanylate cyclase (RETGC-1) gene in dominant cone-rod dystrophy. *Human Molecular Genetics*, 7(7), 1179-1184.
- Keresztes, G., Martemyanov, K. A., Krispel, C. M., Mutai, H., Yoo, P. J., Maison, S. F., et al. (2004). Absence of the RGS9.Gbeta5 GTPase-activating complex in photoreceptors of the R9AP knockout mouse. *The Journal of Biological Chemistry*, 279(3), 1581-1584.
- Khew-Goodall, Y., Mayer, R. E., Maurer, F., Stone, S. R., & Hemmings, B. A. (1991). Structure and transcriptional regulation of protein phosphatase 2A catalytic subunit genes. *Biochemistry*, 30(1), 89-97.
- Kim, T. S., Reid, D. M., & Molday, R. S. (1998). Structure-function relationships and localization of the Na/Ca-K exchanger in rod photoreceptors. *The Journal of Biological Chemistry*, 273(26), 16561-16567.
- King, A. J., Andjelkovic, N., Hemmings, B. A., & Akhtar, M. (1994). The phospho-opsin phosphatase from bovine rod outer segments. An insight into the mechanism of stimulation of type-2A protein phosphatase activity by protamine. *European Journal of Biochemistry*, 225(1), 383-394.
- Klenchin, V. A., Calvert, P. D., & Bownds, M. D. (1995). Inhibition of rhodopsin kinase by recoverin. Further evidence for a negative feedback system in phototransduction. *The Journal of Biological Chemistry*, 270(27), 16147-16152.

- Koch, K. W. (1992). Biochemical mechanism of light adaptation in vertebrate photoreceptors. *Trends in Biochemical Sciences*, 17(8), 307-311.
- Kohl, S., Baumann, B., Broghammer, M., Jagle, H., Sieving, P., Kellner, U., et al. (2000). Mutations in the CNGB3 gene encoding the beta-subunit of the cone photoreceptor cGMP-gated channel are responsible for achromatopsia (ACHM3) linked to chromosome 8q21. *Human Molecular Genetics*, 9(14), 2107-2116.
- Kohl, S., Marx, T., Giddings, I., Jagle, H., Jacobson, S. G., Apfelstedt-Sylla, E., et al. (1998). Total colour blindness is caused by mutations in the gene encoding the alpha-subunit of the cone photoreceptor cGMP-gated cation channel. *Nature genetics*, 19(3), 257-259.
- Kolesnikov, A. V., Golobokova, E. Y., & Govardovskii, V. I. (2003). The identity of metarhodopsin III. *Visual Neuroscience*, 20(3), 249-265.
- Kondo, H., Qin, M., Mizota, A., Kondo, M., Hayashi, H., Hayashi, K., et al. (2004). A homozygosity-based search for mutations in patients with autosomal recessive retinitis pigmentosa, using microsatellite markers. *Investigative Ophthalmology & Visual Science*, 45(12), 4433-4439.
- Korschen, H. G., Beyermann, M., Muller, F., Heck, M., Vantler, M., Koch, K. W., et al. (1999). Interaction of glutamic-acid-rich proteins with the cGMP signalling pathway in rod photoreceptors. *Nature*, 400(6746), 761-766.
- Korschen, H. G., Illing, M., Seifert, R., Sesti, F., Williams, A., Gotzes, S., et al. (1995). A 240 kDa protein represents the complete beta subunit of the cyclic nucleotide-gated channel from rod photoreceptor. *Neuron*, 15(3), 627-636.
- Krispel, C. M., Chen, C. K., Simon, M. I., & Burns, M. E. (2003). Prolonged photoresponses and defective adaptation in rods of Gbeta5<sup>-/-</sup> mice. *The Journal of Neuroscience*, 23(18), 6965-6971.
- Kuhn, H., Hall, S. W., & Wilden, U. (1984). Light-induced binding of 48-kDa protein to photoreceptor membranes is highly enhanced by phosphorylation of rhodopsin. *FEBS Letters*, 176(2), 473-478.
- Kuhn, H., & Wilden, U. (1987). Deactivation of photoactivated rhodopsin by rhodopsin-kinase and arrestin. *Journal of Receptor Research*, 7(1-4), 283-298.
- Lamb, T. D., & Pugh, E. N., Jr. (2004). Dark adaptation and the retinoid cycle of vision. *Progress in Retinal and Eye Research*, 23(3), 307-380.
- Langlois, G., Chen, C. K., Palczewski, K., Hurley, J. B., & Vuong, T. M. (1996). Responses of the phototransduction cascade to dim light. *Proceedings of the National Academy of Science, USA*, 93(10), 4677-4682.

- Lee, R. H., Brown, B. M., & Lolley, R. N. (1990). Protein kinase A phosphorylates retinal phosphodiacylglycerol on serine 73 in situ. *The Journal of Biological Chemistry*, 265(26), 15860-15866.
- Lee, R. H., Lieberman, B. S., & Lolley, R. N. (1987). A novel complex from bovine visual cells of a 33,000-dalton phosphoprotein with beta- and gamma-transducin: purification and subunit structure. *Biochemistry*, 26(13), 3983-3990.
- Lei, B., & Perlman, I. (1999). The contributions of voltage- and time-dependent potassium conductances to the electroretinogram in rabbits. *Visual Neuroscience*, 16(4), 743-754.
- Lem, J., Krasnoperova, N. V., Calvert, P. D., Kosaras, B., Cameron, D. A., Nicolo, M., et al. (1999). Morphological, physiological, and biochemical changes in rhodopsin knockout mice. *Proceedings of the National Academy of Science, USA*, 96(2), 736-741.
- Li, C., Cheng, M., Yang, H., Peachey, N. S., & Naash, M. I. (2001). Age-related changes in the mouse outer retina. *Optometry and Vision Science*, 78(6), 425-430.
- Li, N., Fariss, R. N., Zhang, K., Otto-Bruc, A., Haeseleer, F., Bronson, D., et al. (1998). Guanylate-cyclase-inhibitory protein is a frog retinal Ca<sup>2+</sup>-binding protein related to mammalian guanylate-cyclase-activating proteins. *European Journal of Biochemistry*, 252(3), 591-599.
- Liebman, P. A., Parker, K. R., & Dratz, E. A. (1987). The molecular mechanism of visual excitation and its relation to the structure and composition of the rod outer segment. *Annual Review of Physiology*, 49, 765-791.
- Linn, D. M., Solessio, E., Perlman, I., & Lasater, E. M. (1998). The role of potassium conductance in the generation of light responses in Muller cells of the turtle retina. *Visual Neuroscience*, 15(3), 449-458.
- Lisman, J., & Fain, G. (1995). Support for the equivalent light hypothesis for RP. *Nature Medicine*, 1(12), 1254-1255.
- Liu, D. T., Tibbs, G. R., & Siegelbaum, S. A. (1996). Subunit stoichiometry of cyclic nucleotide-gated channels and effects of subunit order on channel function. *Neuron*, 16(5), 983-990.
- Liu, X., Seno, K., Nishizawa, Y., Hayashi, F., Yamazaki, A., Matsumoto, H., et al. (1994). Ultrastructural localization of retinal guanylate cyclase in human and monkey retinas. *Experimental Eye Research*, 59(6), 761-768.

- Loewen, C. J., & Molday, R. S. (2000). Disulfide-mediated oligomerization of Peripherin/Rds and Rom-1 in photoreceptor disk membranes. Implications for photoreceptor outer segment morphogenesis and degeneration. *The Journal of Biological Chemistry*, 275(8), 5370-5378.
- Loewen, C. J., Moritz, O. L., & Molday, R. S. (2001). Molecular characterization of peripherin-2 and rom-1 mutants responsible for digenic retinitis pigmentosa. *The Journal of Biological Chemistry*, 276(25), 22388-22396.
- Loewen, C. J., Moritz, O. L., Tam, B. M., Papermaster, D. S., & Molday, R. S. (2003). The role of subunit assembly in peripherin-2 targeting to rod photoreceptor disk membranes and retinitis pigmentosa. *Molecular Biology of the Cell*, 14(8), 3400-3413.
- Lyubarsky, A. L., Chen, C., Simon, M. I., & Pugh, E. N., Jr. (2000). Mice lacking G-protein receptor kinase 1 have profoundly slowed recovery of cone-driven retinal responses. *The Journal of Neuroscience*, 20(6), 2209-2217.
- Lyubarsky, A. L., Daniele, L. L., & Pugh, E. N., Jr. (2004). From candelas to photoisomerizations in the mouse eye by rhodopsin bleaching in situ and the light-rearing dependence of the major components of the mouse ERG. *Vision Research*, 44(28), 3235-3251.
- Lyubarsky, A. L., Falsini, B., Pennesi, M. E., Valentini, P., & Pugh, E. N., Jr. (1999). UV- and midwave-sensitive cone-driven retinal responses of the mouse: a possible phenotype for coexpression of cone photopigments. *The Journal of Neuroscience*, 19(1), 442-455.
- Lyubarsky, A. L., Naarendorp, F., Zhang, X., Wensel, T., Simon, M. I., & Pugh, E. N., Jr. (2001). RGS9-1 is required for normal inactivation of mouse cone phototransduction. *Molecular Vision*, 7, 71-78.
- Lyubarsky, A. L., & Pugh, E. N., Jr. (1996). Recovery phase of the murine rod photoresponse reconstructed from electroretinographic recordings. *The Journal of Neuroscience*, 16(2), 563-571.
- MacLeod, D. I. A. (1972) Rods cancel cones in flicker. *Nature* 235, 173-174.
- Makino, E. R., Handy, J. W., Li, T., & Arshavsky, V. Y. (1999). The GTPase activating factor for transducin in rod photoreceptors is the complex between RGS9 and type 5 G protein beta subunit. *Proceedings of the National Academy of Science, USA*, 96(5), 1947-1952.
- Map Viewer. (n.d.). Retrieved May 8, 2005, from <http://www.ncbi.nlm.nih.gov/mapview/>

- Marmor, M.F. & Wolfensberger, T.J. (1998). *The retinal pigment epithelium*. New York: Oxford University Press.
- Marszalek, J. R., Liu, X., Roberts, E. A., Chui, D., Marth, J. D., Williams, D. S., et al. (2000). Genetic evidence for selective transport of opsin and arrestin by kinesin-II in mammalian photoreceptors. *Cell*, 102(2), 175-187.
- Martinez-Mir, A., Vilela, C., Bayes, M., Valverde, D., Dain, L., Beneyto, M., et al. (1997). Putative association of a mutant ROM1 allele with retinitis pigmentosa. *Human Genetics*, 99(6), 827-830.
- Masu, M., Iwakabe, H., Tagawa, Y., Miyoshi, T., Yamashita, M., Fukuda, Y., et al. (1995). Specific deficit of the ON response in visual transmission by targeted disruption of the mGluR6 gene. *Cell*, 80(5), 757-765.
- Matthews, R. G., Hubbard, R., Brown, P. K., & Wald, G. (1963). Tautomeric Forms of Metarhodopsin. *The Journal of General Physiology*, 47, 215-240.
- McDowell, J. H., Nawrocki, J. P., & Hargrave, P. A. (1993). Phosphorylation sites in bovine rhodopsin. *Biochemistry*, 32(18), 4968-4974.
- McLaughlin, M. E., Sandberg, M. A., Berson, E. L., & Dryja, T. P. (1993). Recessive mutations in the gene encoding the beta-subunit of rod phosphodiesterase in patients with retinitis pigmentosa. *Nature genetics*, 4(2), 130-134.
- Mendez, A., Burns, M. E., Sokal, I., Dizhoor, A. M., Baehr, W., Palczewski, K., et al. (2001). Role of guanylate cyclase-activating proteins (GCAPs) in setting the flash sensitivity of rod photoreceptors. *Proceedings of the National Academy of Science, USA*, 98(17), 9948-9953.
- Mendez, A., Lem, J., Simon, M., & Chen, J. (2003). Light-dependent translocation of arrestin in the absence of rhodopsin phosphorylation and transducin signaling. *The Journal of Neuroscience*, 23(8), 3124-3129.
- Menini, A. (1990). Currents carried by monovalent cations through cyclic GMP-activated channels in excised patches from salamander rods. *The Journal of Physiology*, 424, 167-185.
- Milam, A. H., Dacey, D. M., & Dizhoor, A. M. (1993). Recoverin immunoreactivity in mammalian cone bipolar cells. *Visual Neuroscience*, 10(1), 1-12.
- Molday, L. L., Cook, N. J., Kaupp, U. B., & Molday, R. S. (1990). The cGMP-gated cation channel of bovine rod photoreceptor cells is associated with a 240-kDa protein exhibiting immunochemical cross-reactivity with spectrin. *The Journal of Biological Chemistry*, 265(30), 18690-18695.

- Molday, R. S., Hicks, D., & Molday, L. (1987). Peripherin. A rim-specific membrane protein of rod outer segment discs. *Investigative Ophthalmology & Visual Science*, 28(1), 50-61.
- Molday, R. S., & Molday, L. L. (1987). Differences in the protein composition of bovine retinal rod outer segment disk and plasma membranes isolated by a ricin-gold-dextran density perturbation method. *The Journal of Cell Biology*, 105(6, Pt. 1), 2589-2601.
- Molday, R. S., & Molday, L. L. (1998). Molecular properties of the cGMP-gated channel of rod photoreceptors. *Vision Research*, 38(10), 1315-1323.
- Molday, R. S., Molday, L. L., Dose, A., Clark-Lewis, I., Illing, M., Cook, N. J., et al. (1991). The cGMP-gated channel of the rod photoreceptor cell characterization and orientation of the amino terminus. *The Journal of Biological Chemistry*, 266(32), 21917-21922.
- Molokanova, E., Maddox, F., Luetje, C. W., & Kramer, R. H. (1999). Activity-dependent modulation of rod photoreceptor cyclic nucleotide-gated channels mediated by phosphorylation of a specific tyrosine residue. *The Journal of Neuroscience*, 19(12), 4786-4795.
- Molokanova, E., Trivedi, B., Savchenko, A., & Kramer, R. H. (1997). Modulation of rod photoreceptor cyclic nucleotide-gated channels by tyrosine phosphorylation. *The Journal of Neuroscience*, 17(23), 9068-9076.
- Moritz, O. L., & Molday, R. S. (1996). Molecular cloning, membrane topology, and localization of bovine rom-1 in rod and cone photoreceptor cells. *Investigative Ophthalmology & Visual Science*, 37(2), 352-362.
- Murakami, M., & Pak, W. L. (1970). Intracellularly recorded early receptor potential of the vertebrate photoreceptors. *Vision Research*, 10(10), 965-975.
- Nakamura, T., & Gold, G. H. (1987). A cyclic nucleotide-gated conductance in olfactory receptor cilia. *Nature*, 325(6103), 442-444.
- Nakano, K., Chen, J., Tarr, G. E., Yoshida, T., Flynn, J. M., & Bitensky, M. W. (2001). Rethinking the role of phosphodiesterase: light-regulated binding of phosphodiesterase to 14-3-3 in rod inner segments. *Proceedings of the National Academy of Science, USA*, 98(8), 4693-4698.
- Nakatani, K., & Yau, K. W. (1988a). Calcium and magnesium fluxes across the plasma membrane of the toad rod outer segment. *The Journal of Physiology*, 395, 695-729.

- Nakatani, K., & Yau, K. W. (1988b). Guanosine 3',5'-cyclic monophosphate-activated conductance studied in a truncated rod outer segment of the toad. *The Journal of Physiology*, 395, 731-753.
- Nathans, J. (1992). Rhodopsin: structure, function, and genetics. *Biochemistry*, 31(21), 4923-4931.
- Newman, E. A. (1989). Potassium conductance block by barium in amphibian Muller cells. *Brain Research*, 498(2), 308-314.
- Nishiguchi, K. M., Sandberg, M. A., Kooijman, A. C., Martemyanov, K. A., Pott, J. W., Hagstrom, S. A., et al. (2004). Defects in RGS9 or its anchor protein R9AP in patients with slow photoreceptor deactivation. *Nature*, 427(6969), 75-78.
- Noda, Y., Okada, Y., Saito, N., Setou, M., Xu, Y., Zhang, Z., et al. (2001). KIF3C, a microtubule minus end-directed motor for the apical transport of annexin XIIIb-associated Triton-insoluble membranes. *The Journal of Cell Biology*, 155(1), 77-88.
- Noell, W. K., Walker, V. S., Kang, B. S., & Berman, S. (1966). Retinal damage by light in rats. *Investigative Ophthalmology*, 5(5), 450-473.
- Normann, R. A., & Werblin, F. S. (1974). Control of retinal sensitivity. I. Light and dark adaptation of vertebrate rods and cones. *The Journal of General Physiology*, 63(1), 37-61.
- Nucleotide Entre. (n.d.). Retrived May 8, 2005, from <http://www.ncbi.nlm.nih.gov/>
- Nusinowitz, S., Nguyen, L., Radu, R., Kashani, Z., Farber, D., & Danciger, M. (2003). Electroretinographic evidence for altered phototransduction gain and slowed recovery from photobleaches in albino mice with a MET450 variant in RPE65. *Expimental Eye Research*, 77(5), 627-638.
- Oakley, B., 2nd. (1977). Potassium and the photoreceptor-dependent pigment epithelial hyperpolarization. *The Journal of General Physiology*, 70(4), 405-425.
- Oakley, B., 2nd, & Green, D. G. (1976). Correlation of light-induced changes in retinal extracellular potassium concentration with c-wave of the electroretinogram. *Journal of Neurophysiology*, 39(5), 1117-1133.
- O'Brien, D. F. (1982). The chemistry of vision. *Science*, 218(4576), 961-966.
- Ohguro, H., Van Hooser, J. P., Milam, A. H., & Palczewski, K. (1995). Rhodopsin phosphorylation and dephosphorylation in vivo. *The Journal of Biological Chemistry*, 270(24), 14259-14262.

- Pacione, L. R., Szego, M. J., Ikeda, S., Nishina, P. M., & McInnes, R. R. (2003). Progress toward understanding the genetic and biochemical mechanisms of inherited photoreceptor degenerations. *Annual Review of Neuroscience*, 26, 657-700.
- Palczewski, K., Hargrave, P. A., McDowell, J. H., & Ingebritsen, T. S. (1989). The catalytic subunit of phosphatase 2A dephosphorylates phosphopsin. *Biochemistry*, 28(2), 415-419.
- Palczewski, K., Kumasaka, T., Hori, T., Behnke, C. A., Motoshima, H., Fox, B. A., et al. (2000). Crystal structure of rhodopsin: A G protein-coupled receptor. *Science*, 289(5480), 739-745.
- Palczewski, K., Polans, A. S., Baehr, W., & Ames, J. B. (2000). Ca(2+)-binding proteins in the retina: structure, function, and the etiology of human visual diseases. *Bioessays*, 22(4), 337-350.
- Palczewski, K., Sokal, I., & Baehr, W. (2004). Guanylate cyclase-activating proteins: structure, function, and diversity. *Biochemical Biophysical Research Communications*, 322(4), 1123-1130.
- Papermaster, D. S., Schneider, B. G., Zorn, M. A., & Kraehenbuhl, J. P. (1978). Immunocytochemical localization of a large intrinsic membrane protein to the incisures and margins of frog rod outer segment disks. *The Journal of Cell Biology*, 78(2), 415-425.
- Peachey, N. S., Alexander, K. R., Derlacki, D. J., & Fishman, G. A. (1992a). Light adaptation and the luminance-response function of the cone electroretinogram. *Documenta Ophthalmologica*, 79(4), 363-369.
- Peachey, N. S., Alexander, K. R., Derlacki, D. J., & Fishman, G. A. (1992b). Light adaptation, rods, and the human cone flicker ERG. *Visual Neuroscience*, 8(2), 145-150.
- Peachey, N. S., Alexander, K. R., & Fishman, G. A. (1989). The luminance-response function of the dark-adapted human electroretinogram. *Vision Research*, 29(3), 263-270.
- Peachey, N. S., Goto, Y., al-Ubaidi, M. R., & Naash, M. I. (1993). Properties of the mouse cone-mediated electroretinogram during light adaptation. *Neuroscience Letters*, 162(1-2), 9-11.
- Pedler, C. M., & Tilly, R. (1967). The fine structure of photoreceptor discs. *Vision Research*, 7(11), 829-836.
- Peng, C., Rich, E. D., & Varnum, M. D. (2004). Subunit configuration of heteromeric cone cyclic nucleotide-gated channels. *Neuron*, 42(3), 401-410.

- Peng, Y. W., Hao, Y., Petters, R. M., & Wong, F. (2000). Ectopic synaptogenesis in the mammalian retina caused by rod photoreceptor-specific mutations. *Nature Neuroscience*, 3(11), 1121-1127.
- Peng, Y. W., Senda, T., Hao, Y., Matsuno, K., & Wong, F. (2003). Ectopic synaptogenesis during retinal degeneration in the royal college of surgeons rat. *Nature Neuroscience*, 119(3), 813-820.
- Penn, R. D., & Hagins, W. A. (1969). Signal transmission along retinal rods and the origin of the electroretinographic a-wave. *Nature*, 223(202), 201-204.
- Pennesi, M. E., Howes, K. A., Baehr, W., & Wu, S. M. (2003). Guanylate cyclase-activating protein (GCAP) 1 rescues cone recovery kinetics in GCAP1/GCAP2 knockout mice. *Proceedings of the National Academy of Science, USA*, 100(11), 6783-6788.
- Pepperberg, D. R., Brown, P. K., Lurie, M., & Dowling, J. E. (1978). Visual pigment and photoreceptor sensitivity in the isolated skate retina. *The Journal of General Physiology*, 71(4), 369-396.
- Petersen-Jones, S. M., Entz, D. D., & Sargan, D. R. (1999). cGMP phosphodiesterase-alpha mutation causes progressive retinal atrophy in the Cardigan Welsh corgi dog. *Investigative Ophthalmology & Visual Science*, 40(8), 1637-1644.
- Peterson, J. J., Tam, B. M., Moritz, O. L., Shelamer, C. L., Dugger, D. R., McDowell, J. H., et al. (2003). Arrestin migrates in photoreceptors in response to light: a study of arrestin localization using an arrestin-GFP fusion protein in transgenic frogs. *Experimental Eye Research*, 76(5), 553-563.
- Pittler, S. J., Fliesler, S. J., Fisher, P. L., Keller, P. K., & Rapp, L. M. (1995). In vivo requirement of protein prenylation for maintenance of retinal cytoarchitecture and photoreceptor structure. *The Journal of Cell Biology*, 130(2), 431-439.
- Pittler, S. J., Keeler, C. E., Sidman, R. L., & Baehr, W. (1993). PCR analysis of DNA from 70-year-old sections of rodless retina demonstrates identity with the mouse rd defect. *Proceedings of the National Academy of Science, USA*, 90(20), 9616-9619.
- Pittler, S. J., Lee, A. K., Altherr, M. R., Howard, T. A., Seldin, M. F., Hurwitz, R. L., et al. (1992). Primary structure and chromosomal localization of human and mouse rod photoreceptor cGMP-gated cation channel. *The Journal of Biological Chemistry*, 267(9), 6257-6262.

- Poetsch, A., Molday, L. L., & Molday, R. S. (2001). The cGMP-gated channel and related glutamic acid-rich proteins interact with peripherin-2 at the rim region of rod photoreceptor disc membranes. *The Journal of Biological Chemistry*, 276(51), 48009-48016.
- Polans, A., Baehr, W., & Palczewski, K. (1996). Turned on by Ca<sup>2+</sup>! The physiology and pathology of Ca(2+)-binding proteins in the retina. *Trends in Neurosciences*, 19(12), 547-554.
- Prinsen, C. F., Szerencsei, R. T., & Schnetkamp, P. P. (2000). Molecular cloning and functional expression of the potassium-dependent sodium-calcium exchanger from human and chicken retinal cone photoreceptors. *The Journal of Neuroscience*, 20(4), 1424-1434.
- Pugh, E. N., Jr., Duda, T., Sitaramayya, A., & Sharma, R. K. (1997). Photoreceptor guanylate cyclases: a review. *Bioscience Reports*, 17(5), 429-473.
- Rando, R. R. (1992). Molecular mechanisms in visual pigment regeneration. *Photochemistry and Photobiology*, 56(6), 1145-1156.
- Ray, S., Zozulya, S., Niemi, G. A., Flaherty, K. M., Brolley, D., Dizhoor, A. M., et al. (1992). Cloning, expression, and crystallization of recoverin, a calcium sensor in vision. *Proceedings of the National Academy of Science, USA*, 89(13), 5705-5709.
- Reid, D. M., Friedel, U., Molday, R. S., & Cook, N. J. (1990). Identification of the sodium-calcium exchanger as the major ricin-binding glycoprotein of bovine rod outer segments and its localization to the plasma membrane. *Biochemistry*, 29(6), 1601-1607.
- Retinal Information Network. (n.d.). Retrived May 8, 2005, from <http://www.sph.uth.tmc.edu/RetNet/>
- Ridge, K. D., Abdulaev, N. G., Sousa, M., & Palczewski, K. (2003). Phototransduction: crystal clear. *Trends in Biochemical Sciences*, 28(9), 479-487.
- Roof, D. J., & Heuser, J. E. (1982). Surfaces of rod photoreceptor disk membranes: integral membrane components. *The Journal of Cell Biology*, 95(2, Pt. 1), 487-500.
- Root, M. J., & MacKinnon, R. (1993). Identification of an external divalent cation-binding site in the pore of a cGMP-activated channel. *Neuron*, 11(3), 459-466.
- Ross, E. M., & Wilkie, T. M. (2000). GTPase-activating proteins for heterotrimeric G proteins: regulators of G protein signaling (RGS) and RGS-like proteins. *Annual Review of Biochemistry*, 69, 795-827.

- Sampath, A. P., Matthews, H. R., Cornwall, M. C., Bandarchi, J., & Fain, G. L. (1999). Light-dependent changes in outer segment free-Ca<sup>2+</sup> concentration in salamander cone photoreceptors. *The Journal of General Physiology*, 113(2), 267-277.
- Sanyal, S., & Jansen, H. G. (1981). Absence of receptor outer segments in the retina of rds mutant mice. *Neuroscience Letters*, 21(1), 23-26.
- Sautter, A., Zong, X., Hofmann, F., & Biel, M. (1998). An isoform of the rod photoreceptor cyclic nucleotide-gated channel beta subunit expressed in olfactory neurons. *Proceedings of the National Academy of Science, USA*, 95(8), 4696-4701.
- Schadel, S. A., Heck, M., Marezki, D., Filipek, S., Teller, D. C., Palczewski, K., et al. (2003). Ligand channeling within a G-protein-coupled receptor. The entry and exit of retinals in native opsin. *The Journal of Biological Chemistry*, 278(27), 24896-24903.
- Schertler, G. F., Villa, C., & Henderson, R. (1993). Projection structure of rhodopsin. *Nature*, 362(6422), 770-772.
- Schnetkamp, P. P., Basu, D. K., & Szerencsei, R. T. (1989). Na<sup>+</sup>-Ca<sup>2+</sup> exchange in bovine rod outer segments requires and transports K<sup>+</sup>. *American Journal of Physiology*, 257(1, Pt. 1), C153-157.
- Schoenlein, R. W., Peteanu, L. A., Mathies, R. A., & Shank, C. V. (1991). The first step in vision: femtosecond isomerization of rhodopsin. *Science*, 254(5030), 412-415.
- Schwarzer, A., Kim, T. S., Hagen, V., Molday, R. S., & Bauer, P. J. (1997). The Na/Ca-K exchanger of rod photoreceptor exists as dimer in the plasma membrane. *Biochemistry*, 36(44), 13667-13676.
- Schwarzer, A., Schauf, H., & Bauer, P. J. (2000). Binding of the cGMP-gated channel to the Na/Ca-K exchanger in rod photoreceptors. *The Journal of Biological Chemistry*, 275(18), 13448-13454.
- Semple-Rowland, S. L., Lee, N. R., Van Hooser, J. P., Palczewski, K., & Baehr, W. (1998). A null mutation in the photoreceptor guanylate cyclase gene causes the retinal degeneration chicken phenotype. *Proceedings of the National Academy of Science, USA*, 95(3), 1271-1276.
- Shammat, I. M., & Gordon, S. E. (1999). Stoichiometry and arrangement of subunits in rod cyclic nucleotide-gated channels. *Neuron*, 23(4), 809-819.
- Sharon, D., Yamamoto, H., McGee, T. L., Rabe, V., Szerencsei, R. T., Winkfein, R. J., et al. (2002). Mutated alleles of the rod and cone Na-Ca<sup>+</sup>K-exchanger genes in patients with retinal diseases. *Investigative Ophthalmology & Visual Science*, 43(6), 1971-1979.

- Shichi, H., & Somers, R. L. (1978). Light-dependent phosphorylation of rhodopsin. Purification and properties of rhodopsin kinase. *The Journal of Biological Chemistry*, 253(19), 7040-7046.
- Sieving, P. A., Murayama, K., & Naarendorp, F. (1994). Push-pull model of the primate photopic electroretinogram: a role for hyperpolarizing neurons in shaping the b-wave. *Visual Neuroscience*, 11(3), 519-532.
- Slaughter, M. M., & Miller, R. F. (1981). 2-amino-4-phosphonobutyric acid: a new pharmacological tool for retina research. *Science*, 211(4478), 182-185.
- Smith, W. C., Milam, A. H., Dugger, D., Arendt, A., Hargrave, P. A., & Palczewski, K. (1994). A splice variant of arrestin. Molecular cloning and localization in bovine retina. *The Journal of Biological Chemistry*, 269(22), 15407-15410.
- Sokal, I., Li, N., Surgucheva, I., Warren, M. J., Payne, A. M., Bhattacharya, S. S., et al. (1998). GCAP1 (Y99C) mutant is constitutively active in autosomal dominant cone dystrophy. *Molecular Cell*, 2(1), 129-133.
- Steinberg, R. H., Fisher, S. K., & Anderson, D. H. (1980). Disc morphogenesis in vertebrate photoreceptors. *The Journal of Comparative Neurology*, 190(3), 501-508.
- Steinberg, R. H., Schmidt, R., & Brown, K. T. (1970). Intracellular responses to light from cat pigment epithelium: origin of the electroretinogram c-wave. *Nature*, 227(5259), 728-730.
- Stern, J. H., Kaupp, U. B., & MacLeish, P. R. (1986). Control of the light-regulated current in rod photoreceptors by cyclic GMP, calcium, and 1-cis-diltiazem. *Proceedings of the National Academy of Science, USA*, 83(4), 1163-1167.
- Stockman, A., Sharpe, L. T., Ruther, K., & Nordby, K. (1995). Two signals in the human rod visual system: a model based on electrophysiological data. *Visual Neuroscience*, 12(5), 951-970.
- Stryer, L. (1986). Cyclic GMP cascade of vision. *Annual Review of Neuroscience*, 9, 87-119.
- Stryer, L. (1991). Visual excitation and recovery. *The Journal of Biological Chemistry*, 266(17), 10711-10714.
- Sugimoto, Y., Yatsunami, K., Tsujimoto, M., Khorana, H. G., & Ichikawa, A. (1991). The amino acid sequence of a glutamic acid-rich protein from bovine retina as deduced from the cDNA sequence. *Proceedings of the National Academy of Science, USA*, 88(8), 3116-3119.

- Sun, H., Macke, J. P., & Nathans, J. (1997). Mechanisms of spectral tuning in the mouse green cone pigment. *Proceedings of the National Academy of Science, USA*, 94(16), 8860-8865.
- Sun, Z. P., Akabas, M. H., Goulding, E. H., Karlin, A., & Siegelbaum, S. A. (1996). Exposure of residues in the cyclic nucleotide-gated channel pore: P region structure and function in gating. *Neuron*, 16(1), 141-149.
- Tam, B. M., Moritz, O. L., & Papermaster, D. S. (2004). The C terminus of peripherin/rds participates in rod outer segment targeting and alignment of disk incisures. *Molecular Biology of the Cell*, 15(4), 2027-2037.
- Tanaka, J. C., Eccleston, J. F., & Furman, R. E. (1989). Photoreceptor channel activation by nucleotide derivatives. *Biochemistry*, 28(7), 2776-2784.
- Tanaka, T., Ames, J. B., Harvey, T. S., Stryer, L., & Ikura, M. (1995). Sequestration of the membrane-targeting myristoyl group of recoverin in the calcium-free state. *Nature*, 376(6539), 444-447.
- Taylor, W. R., & Baylor, D. A. (1995). Conductance and kinetics of single cGMP-activated channels in salamander rod outer segments. *The Journal of Physiology*, 483 (Pt. 3), 567-582.
- Toda, K., Bush, R. A., Humphries, P., & Sieving, P. A. (1999). The electroretinogram of the rhodopsin knockout mouse. *Visual Neuroscience*, 16(2), 391-398.
- Torre, V., Straforini, M., Sesti, F., & Lamb, T. D. (1992). Different channel-gating properties of two classes of cyclic GMP-activated channel in vertebrate photoreceptors. *Proceedings. Biological Sciences*, 250(1329), 209-215.
- Travis, G. H. (1998). Mechanisms of cell death in the inherited retinal degenerations. *American Journal of Human Genetics*, 62(3), 503-508.
- Travis, G. H., Brennan, M. B., Danielson, P. E., Kozak, C. A., & Sutcliffe, J. G. (1989). Identification of a photoreceptor-specific mRNA encoded by the gene responsible for retinal degeneration slow (rds). *Nature*, 338(6210), 70-73.
- Trudeau, M. C., & Zagotta, W. N. (2002a). An intersubunit interaction regulates trafficking of rod cyclic nucleotide-gated channels and is disrupted in an inherited form of blindness. *Neuron*, 34(2), 197-207.
- Trudeau, M. C., & Zagotta, W. N. (2002b). Mechanism of calcium/calmodulin inhibition of rod cyclic nucleotide-gated channels. *Proceedings of the National Academy of Science, USA*, 99(12), 8424-8429.

- Tsang, S. H., Burns, M. E., Calvert, P. D., Gouras, P., Baylor, D. A., Goff, S. P., et al. (1998). Role for the target enzyme in deactivation of photoreceptor G protein in vivo. *Science*, 282(5386), 117-121.
- Tsang, S. H., Gouras, P., Yamashita, C. K., Kjeldbye, H., Fisher, J., Farber, D. B., et al. (1996). Retinal degeneration in mice lacking the gamma subunit of the rod cGMP phosphodiesterase. *Science*, 272(5264), 1026-1029.
- Tucker, J. E., Winkfein, R. J., Cooper, C. B., & Schnetkamp, P. P. (1998). cDNA cloning of the human retinal rod Na-Ca + K exchanger: comparison with a revised bovine sequence. *Investigative Ophthalmology & Visual Science*, 39(2), 435-440.
- Tucker, M. A., Chang, P. L., Prince, C. W., Gillespie, G. Y., & Mapstone, T. B. (1998). TPA-mediated regulation of osteopontin in human malignant glioma cells. *Anticancer Research*, 18(2A), 807-812.
- Varnum, M. D., & Zagotta, W. N. (1996). Subunit interactions in the activation of cyclic nucleotide-gated ion channels. *Biophysical Journal*, 70(6), 2667-2679.
- Vaughan, D. K., & Fisher, S. K. (1989). Cytochalasin D disrupts outer segment disc morphogenesis in situ in rabbit retina. *Investigative Ophthalmology & Visual Science*, 30(2), 339-342.
- Wachtmeister, L., & Dowling, J. E. (1978). The oscillatory potentials of the mudpuppy retina. *Investigative Ophthalmology & Visual Science*, 17(12), 1176-1188.
- Wagner, R., Ryba, N., & Uhl, R. (1988). Sub-second turnover of transducin GTPase in bovine rod outer segments. A light scattering study. *FEBS Letters*, 234(1), 44-48.
- Weitz, D., Ficek, N., Kremmer, E., Bauer, P. J., & Kaupp, U. B. (2002). Subunit stoichiometry of the CNG channel of rod photoreceptors. *Neuron*, 36(5), 881-889.
- Weitz, D., Zoche, M., Muller, F., Beyermann, M., Korschen, H. G., Kaupp, U. B., et al. (1998). Calmodulin controls the rod photoreceptor CNG channel through an unconventional binding site in the N-terminus of the beta-subunit. *The Embo Journal*, 17(8), 2273-2284.
- Weng, J., Mata, N. L., Azarian, S. M., Tzekov, R. T., Birch, D. G., & Travis, G. H. (1999). Insights into the function of Rim protein in photoreceptors and etiology of Stargardt's disease from the phenotype in abcr knockout mice. *Cell*, 98(1), 13-23.
- Wilden, U., Hall, S. W., & Kuhn, H. (1986). Phosphodiesterase activation by photoexcited rhodopsin is quenched when rhodopsin is phosphorylated and binds the intrinsic 48-kDa protein of rod outer segments. *Proceedings of the National Academy of Science, USA*, 83(5), 1174-1178.

- Wilden, U., & Kuhn, H. (1982). Light-dependent phosphorylation of rhodopsin: number of phosphorylation sites. *Biochemistry*, *21*(12), 3014-3022.
- Wilkins, J. F., Bitensky, M. W., & Willardson, B. M. (1996). Regulation of the kinetics of phosphodiesterase phosphorylation in retinal rods. *The Journal of Biological Chemistry*, *271*(32), 19232-19237.
- Witkovsky, P., Dudek, F. E., & Ripps, H. (1975). Slow PIII component of the carp electroretinogram. *The Journal of General Physiology*, *65*(2), 119-134.
- Wolf, G. (2005). Function of the protein RPE65 in the visual cycle. *Nutrition Reviews*, *63*(3), 97-100.
- Womack, K. B., Gordon, S. E., He, F., Wensel, T. G., Lu, C. C., & Hilgemann, D. W. (2000). Do phosphatidylinositides modulate vertebrate phototransduction? *The Journal of Neuroscience*, *20*(8), 2792-2799.
- Wong, S., & Molday, R. S. (1986). A spectrin-like protein in retinal rod outer segments. *Biochemistry*, *25*(20), 6294-6300.
- Woodruff, M. L., & Bownds, M. D. (1979). Amplitude, kinetics, and reversibility of a light-induced decrease in guanosine 3',5'-cyclic monophosphate in frog photoreceptor membranes. *The Journal of General Physiology*, *73*(5), 629-653.
- Woodruff, M. L., Sampath, A. P., Matthews, H. R., Krasnoperova, N. V., Lem, J., & Fain, G. L. (2002). Measurement of cytoplasmic calcium concentration in the rods of wild-type and transducin knock-out mice. *The Journal of Physiology*, *542*(Pt. 3), 843-854.
- Xu, J., Dodd, R. L., Makino, C. L., Simon, M. I., Baylor, D. A., & Chen, J. (1997). Prolonged photoresponses in transgenic mouse rods lacking arrestin. *Nature*, *389*(6650), 505-509.
- Xu, X., & Karwoski, C. (1995). Current source density analysis of the electroretinographic d wave of frog retina. *Journal of Neurophysiology*, *73*(6), 2459-2469.
- Xue, L., Gollapalli, D. R., Maiti, P., Jahng, W. J., & Rando, R. R. (2004). A palmitoylation switch mechanism in the regulation of the visual cycle. *Cell*, *117*(6), 761-771.
- Yamazaki, A., Bartucca, F., Ting, A., & Bitensky, M. W. (1982). Reciprocal effects of an inhibitory factor on catalytic activity and noncatalytic cGMP binding sites of rod phosphodiesterase. *Proceedings of the National Academy of Science, USA*, *79*(12), 3702-3706.

- Yang, R. B., Foster, D. C., Garbers, D. L., & Fulle, H. J. (1995). Two membrane forms of guanylyl cyclase found in the eye. *Proceedings of the National Academy of Science, USA*, 92(2), 602-606.
- Yang, R. B., Robinson, S. W., Xiong, W. H., Yau, K. W., Birch, D. G., & Garbers, D. L. (1999). Disruption of a retinal guanylyl cyclase gene leads to cone-specific dystrophy and paradoxical rod behavior. *The Journal of Neuroscience*, 19(14), 5889-5897.
- Yang, Z., Xia, C., Roberts, E. A., Bush, K., Nigam, S. K., & Goldstein, L. S. (2001). Molecular cloning and functional analysis of mouse C-terminal kinesin motor KifC3. *Molecular and Cellular Biology*, 21(3), 765-770.
- Yau, K. W. (1994). Phototransduction mechanism in retinal rods and cones. The Friedenwald Lecture. *Investigative Ophthalmology & Visual Science*, 35(1), 9-32.
- Yau, K. W., & Baylor, D. A. (1989). Cyclic GMP-activated conductance of retinal photoreceptor cells. *Annual Review of Neuroscience*, 12, 289-327.
- Yau, K. W., & Nakatani, K. (1985). Light-suppressible, cyclic GMP-sensitive conductance in the plasma membrane of a truncated rod outer segment. *Nature*, 317(6034), 252-255.
- Yokoyama, S. (2000). Molecular evolution of vertebrate visual pigments. *Progress in Retinal and Eye Research*, 19(4), 385-419.
- Yoshida, T., Willardson, B. M., Wilkins, J. F., Jensen, G. J., Thornton, B. D., & Bitensky, M. W. (1994). The phosphorylation state of phosducin determines its ability to block transducin subunit interactions and inhibit transducin binding to activated rhodopsin. *The Journal of Biological Chemistry*, 269(39), 24050-24057.
- Young, R. W. (1967). The renewal of photoreceptor cell outer segments. *The Journal of Cell Biology*, 33(1), 61-72.
- Young, R. W. (1971). Shedding of discs from rod outer segments in the rhesus monkey. *Journal of Ultrastructure Research*, 34(1), 190-203.
- Young, R. W., & Bok, D. (1969). Participation of the retinal pigment epithelium in the rod outer segment renewal process. *The Journal of Cell Biology*, 42(2), 392-403.
- Young, R. W., & Droz, B. (1968). The renewal of protein in retinal rods and cones. *The Journal of Cell Biology*, 39(1), 169-184.

- Zhao, Y., Hong, D. H., Pawlyk, B., Yue, G., Adamian, M., Grynberg, M., et al. (2003). The retinitis pigmentosa GTPase regulator (RPGR)- interacting protein: subserving RPGR function and participating in disk morphogenesis. *Proceedings of the National Academy of Science, USA*, 100(7), 3965-3970.
- Zheng, J., Trudeau, M. C., & Zagotta, W. N. (2002). Rod cyclic nucleotide-gated channels have a stoichiometry of three CNGA1 subunits and one CNGB1 subunit. *Neuron*, 36(5), 891-896.
- Zhong, H., Molday, L. L., Molday, R. S., & Yau, K. W. (2002). The heteromeric cyclic nucleotide-gated channel adopts a 3A:1B stoichiometry. *Nature*, 420(6912), 193-198.

APPENDIX

INSTITUTIONAL ANIMAL CARE AND USE COMMITTEE APPROVAL FORM



Office of the Provost

**NOTICE OF APPROVAL**

**DATE:** September 16, 2005

**TO:** Steven J. Pittler, Ph.D.  
WORB 658 4390  
FAX: 934-5725

**FROM:** Judith A. Kapp, Ph.D., Chair   
Institutional Animal Care and Use Committee

**SUBJECT:** Title: Structure and Regulation of Retinal cGMP PDE Alpha Gene  
Sponsor: NIH  
Animal Project Number: 050904662

On September 16, 2005, the University of Alabama at Birmingham Institutional Animal Care and Use Committee (IACUC) reviewed the animal use proposed in the above referenced application. It approved the use of the following species and numbers of animals:

Species	Use Category	Number in Category
Mice	B	500

Animal use is scheduled for review one year from September 2005. Approval from the IACUC must be obtained before implementing any changes or modifications in the approved animal use.

**Please keep this record for your files, and forward the attached letter to the appropriate granting agency.**

Refer to Animal Protocol Number (APN) 050904662 when ordering animals or in any correspondence with the IACUC or Animal Resources Program (ARP) offices regarding this study. If you have concerns or questions regarding this notice, please call the IACUC office at 934-7692.

Institutional Animal Care and Use Committee  
B10 Volker Hall  
1717 7th Avenue South  
205.934.7692 • Fax 205.934.1188  
iacuc@uab.edu  
www.uab.edu/iacuc

The University of  
Alabama at Birmingham  
Mailing Address:  
VH B10  
1530 3RD AVE S  
BIRMINGHAM AL 35294-0019

**GRADUATE SCHOOL  
UNIVERSITY OF ALABAMA AT BIRMINGHAM  
DISSERTATION APPROVAL FORM  
DOCTOR OF PHILOSOPHY**

**Name of Candidate**           Youwen Zhang            
**Graduate Program**           Vision Science            
**Title of Dissertation**           Characterization of a Rod Photoreceptor cGMP-gated  
          Cation Channel Beta-Subunit Knockout Mouse          

**I certify that I have read this document and examined the student regarding its content. In my opinion, this dissertation conforms to acceptable standards of scholarly presentation and is adequate in scope and quality, and the attainments of this student are such that he may be recommended for the degree of Doctor of Philosophy.**

**Dissertation Committee:**

Name	Signature
<u>          Shu-Zhen Wang          </u> , <b>Chair</b>	<u>          S. Z. Wang          </u>
<u>          Franklin R. Amthor          </u>	<u>          Franklin R. Amthor          </u>
<u>          Kent T. Keyser          </u>	<u>          Kent T. Keyser          </u>
<u>          Timothy W. Kraft          </u>	<u>          Timothy W. Kraft          </u>
<u>          Steven J. Pittler          </u>	<u>          S. J. Pittler          </u>

**Director of Graduate Program**           Kent T. Keyser            
**Dean, UAB Graduate School**           Bryan D. Nee            
**Date**           JAN 06 2006